1985-09

Variation of the drag coefficient with wind and wave state

Byars, Beverly J.

NAVAL POSTGRADUATE SCHOOL
Monterey, California

THESIS

VARIATION OF THE DRAG COEFFICIENT
WITH
WIND AND WAVE STATE

by

Beverly J. Byars

September 1985

Thesis Advisor: K. L. Davidson

Approved for public release; distribution unlimited

REPORT DOCUMENTATION PAGE

READ INSTRUCTIONS BEFORE COMPLETING FORM

1. REPORT NUMBER

2. GOVT ACCESSION NO.

3. RECIPIENT'S CATALOG NUMBER

4. TITLE (and Subtitle)
Variation of the Drag Coefficient with Wind and Wave State

5. TYPE OF REPORT & PERIOD COVERED
Master's thesis
September 1985

6. PERFORMING ORG. REPORT NUMBER

7. AUTHOR(s)
Beverly J. Byars

8. CONTRACT OR GRANT NUMBER(s)

9. PERFORMING ORGANIZATION NAME AND ADDRESS
Naval Postgraduate School
Monterey, California 93943-5100

10. PROGRAM ELEMENT, PROJECT, TASK AREA & WORK UNIT NUMBERS

11. CONTROLLING OFFICE NAME AND ADDRESS
Naval Postgraduate School
Monterey, California 93943-5100

12. REPORT DATE
September 1985

13. NUMBER OF PAGES
110

14. MONITORING AGENCY NAME & ADDRESS(if different from Controlling Office)

15. SECURITY CLASS. (of this report)
Unclassified

15a. DECLASSIFICATION/DOWNGRADING SCHEDULE

16. DISTRIBUTION STATEMENT (of this Report)
Approved for public release; distribution unlimited.

17. DISTRIBUTION STATEMENT (of the abstract entered in Block 20, if different from Report)

18. SUPPLEMENTARY NOTES

19 KEY WORDS (Continue on reverse side if necessary and identify by block number)
marine atmospheric boundary layer
neutral drag coefficient
drag coefficient
diurnal variations
dissipation method

20. ABSTRACT (Continue on reverse side if necessary and identify by block number)
The dissipation method is used to obtain estimates for the friction velocity, U_*, as well as values for the neutral drag coefficient, C_{DN}, for data collected from a coastal tower off San Diego, California. C_{DN} is found to be independent of the ten-meter height windspeed, U_{10}, for velocities between 4-9 m/sec. Its value is estimated to be $(0.94+0.4)10^3$ which compares well with values by Smith (1980) and Large and Pond (1981). Definite

trends in C_{DN} with fetch and sea state are also observed. Drag coefficient estimates are found to be higher for short fetch than for long fetch conditions. C_{DN} is also seen to increase sharply just before frontal passages and during sea breeze conditions when the waves are actively growing. With the windspeed and wave field reaching equilibrium, C_{DN} is found to decrease with time to a smaller and more constant value.

Approved for public release; distribution is unlimited.

Variation of the Drag Coefficient with Wind and Wave State

by

Beverly J. Byars
Lieutenant Commander, United States Navy
B.S., Kansas University, 1976

Submitted in partial fulfillment of the
requirements for the degree of

MASTER OF SCIENCE IN METEOROLOGY AND OCEANOGRAPHY

from the

NAVAL POSTGRADUATE SCHOOL
September 1985

ABSTRACT

The dissipation method is used to obtain estimates for the friction velocity, U_*, as well as values for the neutral drag coefficient, C_{DN}, for data collected from a coastal tower off San Diego, California. C_{DN} is found to be independent of the ten-meter height windspeed, U_{10}, for velocities between 4-9 m/sec. Its value is estimated to be $(0.94 \pm 0.4)10^3$ which compares well with values by Smith (1980) and Large and Pond (1981). Definite trends in C_{DN} with fetch and sea state are also observed. Drag coeffcient estimates are found to be higher for short fetch than for long fetch conditions. C_{DN} is also seen to increase sharply just before frontal passages and during sea breeze conditions when the waves are actively growing. With the windspeed and wave field reaching equilibrium, C_{DN} is found to decrease with time to a smaller and more constant value.

TABLE OF CONTENTS

LIST OF TABLES

LIST OF FIGURES

I. INTRODUCTION

The Marine Atmospheric Boundary Layer (MABL) is the region adjacent to the air-sea interface where the vertical variation of the mean stresses is large compared to the horizontal gradients (Holton, 1979). In this layer, turbulent shear stresses due to both molecular properties (viscosity and diffusion) and turbulent eddies coexist. These eddies are very effective mixing agents which serve to transfer momentum, heat and other quantities to and from the earth's surface, at a rate much faster than that for molecular diffusion. Frictional forces due to molecular viscosity are usually neglected by means of scale analysis (Holton, 1979), and the emphasis has been placed on parameterizing the fluxes resulting from the turbulent eddies.

The mean vertical fluxes of momentum, sensible heat and latent heat are (Fleagle and Businger, 1980):

$$\tau = -\rho_a \overline{u'w'} \qquad (1a)$$

$$H = C_p \overline{\theta'w'} \qquad (1b)$$

$$E = L_f \overline{w'q'} \qquad (1c)$$

where τ, H and E are the momentum flux (wind stress), sensible heat flux and latent heat flux, respectively. u' and w' are the horizontal and vertical turbulent wind components, while θ' and q' represent the turbulent fluctuations of potential temperature and specific humidity. L_f is the latent heat of vaporization, ρ_a is the air density and C_p is the specific heat of air at constant pressure.

In order to estimate these fluxes using routine surface layer observations, bulk transfer formulae were developed (see Fleagle and Businger, 1980):

$$\tau = \rho_a C_D (U_z - U_o)^2 \qquad (2a)$$

$$H = \rho_a C_p C_H (U_z - U_o)(T_o - T_z) \quad (2b)$$

$$E = \rho_a L_f C_E (U_z - U_o)(q_o - q_z) \quad (2c)$$

where U_z, T_z and q_z represent the windspeed, temperature and humidity specified, by convention, for a reference height, z. U_o, T_o and q_o are the same quantities measured at the surface. C_D, C_H and C_E are dimensionless quantities representing bulk transfer coefficients for momentum, sensible heat and latent heat, and are for the height, z. These are known as the drag coefficient, the Stanton Number, and the Dalton Number, respectively.

The turbulent exchange processes greatly influence the general circulation of the atmosphere and thus have tremendous impact on countless social and environmental concerns. Central to their understanding is a determination of the nature of the bulk transfer coefficients, particularly the drag coefficient, C_D. This quantity encompasses the mechanism responsible for the wind stress at the surface. Since most of the parameters used to describe the bulk formulae are routinely measured, ascertaining a reliable value for C_D based on these quantities is essential for accurately defining the surface stress, τ. Further, C_D is an important factor driving many of the current ocean wave, acoustic and boundary layer models (Geernaert, 1985a).

Considerable effort has gone into examining the overwater drag coefficient. It has been shown to be windspeed and stability dependent, and may also vary with factors such as fetch and depth (Geernaert, 1983). Studies also indicate that the overwater drag coefficient tends to have a magnitude on the order of 10^{-3}. Its value exhibits considerable scatter under varying environmental conditions. Higher values are usually associated with an unstable atmosphere, short fetch and/or shallow seas, implying a wave dependence (Geernaert, 1983). The more recent use of remote sensing to

study winds over the ocean requires an understanding of this wave dependence since it assumes that the wave structure is related to the wind stress. Clearly, the processes affecting the drag coefficient merit considerable further study. This thesis will investigate the dependence of the drag coefficient on windspeed, fetch and wave state.

An important scaling parameter, based on the wind stress, is the friction velocity , U_*, which may be defined as:

$$\tau = \rho_a U_*^2 \qquad (3)$$

The quantity U_* is related to most air-sea exchange processes such as heat and moisture fluxes (Businger, 1973), the surface drift (Hicks, 1972) and ocean mixed layer dynamics (Kraus, 1972).

Data considered in this investigation were from the Tower Ocean Wave and Radar Dependence (TOWARD) experiment. Located offshore of Mission Beach at San Diego, California, the Naval Ocean Systems Center (NOSC) tower provided a stable platform with a capability for mounting a variety of sensors to measure the variables needed to parameterize the bulk formulae. Naval Postgraduate School (NPS) personnel made atmospheric surface layer measurements of both mean and fluctuating velocity, temperature and humidity. The NPS measurements are listed in Table I. Wave information based on radar signal returns was collected through investigations from the Naval Research Laboratory, the Jet Propulsion Laboratory and the University of Kansas. The Scripps Institute of Oceanography measured tower frequency wave spectra with an array of sub-surface pressure transducers.

The measurement strategy for the TOWARD Experiment was originally composed of two intensive data collection periods: September/October 1984 and January/ February 1985. These periods were chosen because of their differing average

windspeeds and resultant sea states. With its relatively low average windspeeds, the fall measurement period had calm to moderate sea state conditions. The winter period, with its higher average windspeeds, was designed to focus on more active sea states. Equipment problems, however, forced the postponement of Phase I to October/November 1984 and Phase II to March/April 1985.

Figs. 1.1 and 1.2 provide two views of the NOSC tower. Located in 17-18 meters water depth, the tower provided a stable platform for data collection. A structural extension of the tower from the south side allowed wave rider sensors to be placed away from the main tower structure.

Measurements of wind speed and direction, wave height, tide level and near surface currents were recorded routinely during intensive measurement periods. Air and sea-surface temperatures were also recorded, along with wind stress data that was obtained with a sonic anemometer and a hot film sensor.

TABLE I

NPS Measurements

Measurement	Sensor
Sea-Surface Temperature	Floating platinum thermometer
Mean Surface Layer:	
Wind (speed and direction)	Cup anemometer, vane
Temperature	Aspirated platinum thermometer
Humidity	Dew cell (cooled mirror)
Radiation (solar and IR)	Eppleys (up and down), Total
Turbulent Surface Layer:	
Wind stress: direct	Sonic anemometer
Wind stress: indirect	Hot films
K. E. dissipation rates	Hot films
Sensible heat flux	Platinum thermometer and sonic anemometer
Latent heat flux	Lyman-alpha and sonic anemometer
Spectra: windspeed	sonic anemometer
temperature	Platinum thermometer
humidity	Lyman-alpha

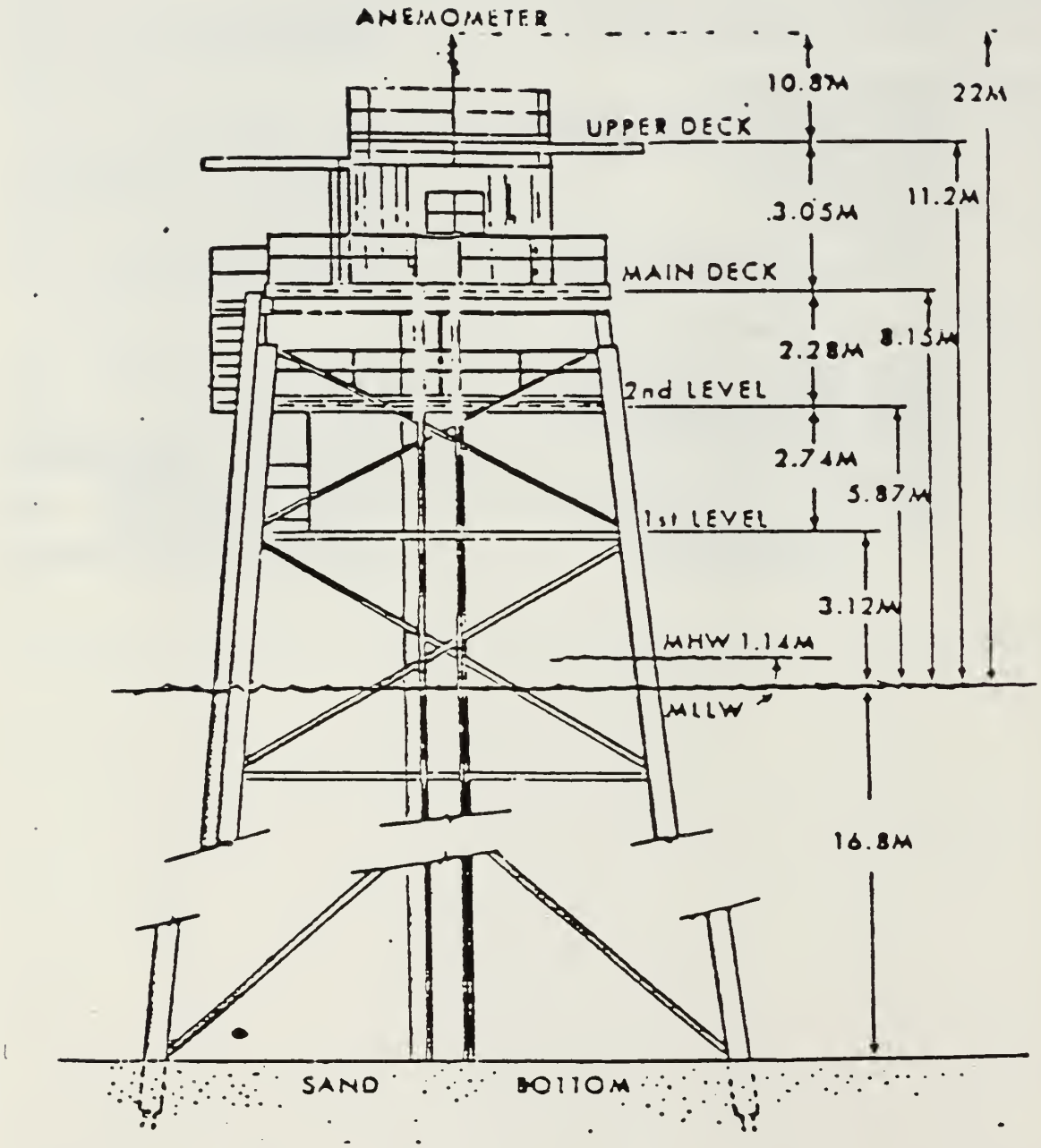

Figure 1.1 The NOSC Tower.

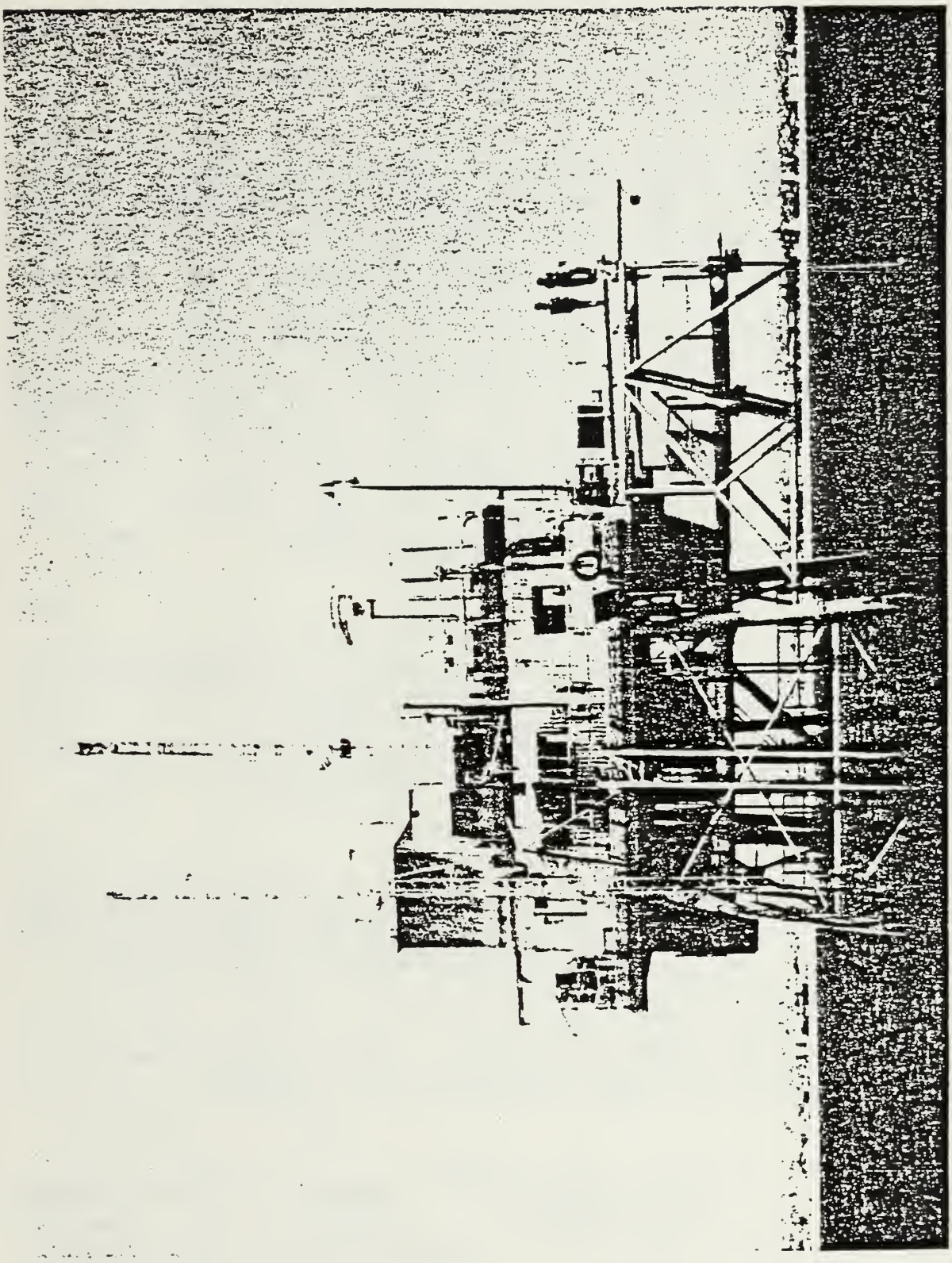

Figure 1.2 The NOSC Tower.

II. REVIEW OF EXISTING SURFACE LAYER THEORY

The surface layer comprises approximately the lowest ten per cent of the MABL and is defined as the layer of air nearest the ground where atmospheric parameters may be scaled with surface fluxes. Within this layer, an approximation adopted is that the fluxes are independent of height (Businger, 1973).

In Eqn. (2a), the surface speed, U_o, is a parameter necessary for estimation of the drag coefficient. However, because U_o is very small compared to U_{10}, U_o is assumed to be zero in the bulk definitions. With this assumption, Eqns. (2a) and (3) may be combined into the form:

$$C_{D10} = (U_*/U_{10})^2 \qquad (4)$$

Note that the drag coefficient in Eqn. (4) is defined for a height of 10 meters and is denoted as C_{D10}.

The similarity theory which described the mean surface layer wind profile is (Monin and Obukhov, 1954):

$$\partial\bar{U}/\partial z = (U_*/kz)\phi_m(z/L) \qquad (5)$$

where $\partial\bar{U}/\partial z$ represents the vertical gradient of the wind speed and k is the von Karman constant, which ranges in value from .35 to .43 (Panofsky and Dutton, 1984). This study assumes a value of 0.4 for this constant. $\phi_m(z/L)$ is a dimensionless stability function. One parameterization of this function is that presented by Businger, et. al., (1971):

$$\phi_m = [1 - \alpha(z/L)]^{-1/4} \quad (z/L<0) \qquad (6a)$$

$$\phi_m = [1 + \beta(z/L)] \quad (z/L>0) \qquad (6b)$$

where α and β are diabatic profile constants, with approximate values of 15±1 and 5±0.5, respectively (Geernaert, 1983). z is the measurement height and L is the Monin-Obukhov length, defined as the height at which the buoyant energy production equals the shear production (Businger, 1973). z/L is defined as:

$$z/L = -gkz\overline{w'T_v'}/T_o'(U_*^3) \quad (7)$$

The virtual temperature fluctuation, T_v', is related to the air temperature fluctuation, T', and specific humidity fluctuation, q', by:

$$T_v' = T'(1 + .61q) + .61Tq' \quad (8)$$

Thus:

$$\overline{w'T_v'} = \overline{w'T'}(1 + .61q) + .61T\overline{w'q'} \quad (9)$$

where g is the gravitational acceleration. The first term on the right hand side of Eqn. (9) represents the temperature flux and the second term describes the humidity flux. These terms are further estimated by bulk equations where:

$$\overline{w'T'} = C_H U_{10}(T_o - T_z) \quad (10a)$$

$$\overline{w'q'} = C_E U_{10}(q_o - q_z) \quad (10b)$$

Both C_E and C_H are on the order of 10^{-3}, but are less well defined than the drag coefficient (Geernaert, 1983).

Under neutral or adiabatic conditions,

$$\phi_m(z/L) = 1 \quad (11)$$

and Eqn. (5) reduces to:

$$\partial\bar{U}/\partial z = U_*/kz \quad (12)$$

Integrating Eqn. (12):

$$\int_{U(z_o)}^{U(z)} dU = (U_*/k)\int_{z_o}^{z} dz/z \quad (13)$$

yields the well known logarithmic wind profile:

$$U = (U_*/k)\ln(z/z_o) \quad (14)$$

where the roughness length, z_o, is a measure of the effective surface roughness.

For non-neutral (diabatic) conditions, the stability parameter must be included. Integrating Eqn. (5) yields the stability dependent logarithmic wind profile (Paulson, 1970):

$$U = (U_*/k)[\ln(z/z_o) - \psi] \quad (15)$$

where ψ represents the stability parameter.

For unstable stratifications ($z/L<0$):

$$\psi = 2\ln[(1+x)/2] + \ln[(1+x^2)/2] - 2(\tan)^{-1}x + (\pi/2) \quad (16)$$

where:

$$x = [(1 - \alpha(z/L)]^{1/4} \quad (16a)$$

For stable conditions ($z/L>0$):

$$\psi = - \beta(z/L) \quad (17)$$

The logarithmic wind profile is important primarily for two reasons. First, it can be used to estimate the ten meter height wind speed, U_{10}. Beginning with Eqn. (14), the wind speed at a particular height, z, may be described as:

$$U_z = (U_*/k)[\ln(z/z_o) - \psi_z] \quad (18)$$

At ten meters elevation:

$$U_{10} = (U_*)/k[\ln(10/z_o) - \psi_{10}] \quad (19)$$

Combining Eqns. (18) and (19) yields the following relationship:

$$U_{10} = U_z + (U_*/k)[\ln(10/z) - \psi_z + \psi_{10}] \quad (20)$$

This particular equation is important because it is not always possible to place sensors on ships or platforms at

the required ten meter height. As a result, U_{10} can be estimated regardless of the height of the instrument.

Second, the log wind profile is important in determining the neutral drag coefficient, C_{DN}, which may be defined as the wind stress exerted on the surface for neutral stratifications. Estimation of the neutral drag coefficient is important because it eliminates variations in C_D parameterizations due to differing stability conditions. Many modellers prefer to be provided with C_{DN} instead of C_D because the in-situ bulk weather data may be used to estimate a stability correction. Eqn. (24) may then be applied to a given C_{DN} and ψ.

A. GENERAL DRAG COEFFICIENT REPRESENTATIONS

Eqns. (4) and (15) yield:

$$C_D = (U_*/U_z)^2[k/[\ln(z/z_o) - \psi_m(z/L)]]^2 \quad (21)$$

Under neutral conditions, where $\psi=0$:

$$C_{DN} = [k/\ln(z/z_{on})]^2 \quad (22)$$

where C_{DN} and z_{on} are the drag coefficient and roughness length under neutral conditions. Rearranging Eqn. (22) yields:

$$kC_{DN}^{-1/2} = \ln(z/z_{on}) \quad (23)$$

Combining Eqns. (21) and (23) produces the following general result (Geernaert, 1983):

$$C_D = [C_{DN}^{-1/2} - \psi/k + (1/k)\ln(z_{on}/z_o)]^{-2} \quad (24)$$

The drag coefficient is known to vary under differing environmental conditions. Studies have indicated that C_D increases more rapidly with increasing winds over water than over land (Hsu, 1974). Geerneart (1983) discussed the application of Eqn. (24) to both land and water cases. Over

land, the roughness length is assumed to be largely independent of the surface stress. Thus, $z_{on} = z_o$ and Eqn. (24) is reduced to:

$$C_D = (C_{DN}^{-1/2} - \psi/k)^{-2} \quad (25)$$

Over water, both the drag coefficient and, hence, the roughness length show considerable windspeed and stress dependence (Kitaigorodskii, 1973). Charnock (1955) was among the first to recognize that C_D increases considerably with windspeed over the sea. He postulated that the roughness length, and hence, the neutral drag coefficient was proportional to the wind stress through the following scaling argument:

$$z_o = \alpha' U_*^2/g \quad (26)$$

where α' is the Charnock constant with a typical value of .015-.020 (Geernaert, 1983). Charnock's work served as a basis for subsequent parameterizations of the drag coefficient and the roughness length in terms of sea state elements.

Kitaigorodskii (1973) further described z_o based on wave spectral densities. Since that time, z_o and C_D have been shown to be dependent on a variety of other factors that are linked to the character of surface waves such as fetch, depth and wave age. C_D, therefore, can be evaluated as:

$$C_D = C_{DN}(U_{10}, z/L, \text{waves}) \quad (27)$$

As a result, a different relationship is often used to estimate the drag coefficient over the ocean. Applying Charnock's relation to Eqn. (24) yields (Geernaert, 1983):

$$C_D = [C_{DN}^{-1/2} - \psi/k + (1/k)\ln(C_{DN}/C_D)]^{-2} \quad (28)$$

B. DETERMINING THE WIND STRESS BY THE DISSIPATION METHOD

Since estimation of the drag coefficient requires values for the friction velocity, it is important to examine how the momentum flux is measured. Two primary methods for obtaining τ are the eddy correlation technique and the dissipation method. The former method involves measurement of the turbulent wind components u', v' and w', and ideally requires a steady platform. Because of the low frequency motions inherent in sea-going vessels on which most marine studies are conducted, the dissipation method is often substituted for oceanic wind stress experiments.

The dissipation method is an indirect approach in which the rate of dissipation of turbulent kinetic energy is used to determine U_*. This method requires application of the turbulent kinetic equation:

$$\partial\bar{e}/\partial t = U_*^2\partial\bar{U}/\partial z + (g\overline{w'T_v'})/T_o - \partial/\partial z[\overline{w'e} + (1/\rho_a)\overline{w'p'}] - \epsilon \qquad (29)$$

where $\partial\bar{e}/\partial t$ is the local time rate of change of turbulent kinetic energy (TKE), $U_*^2\partial\bar{U}/\partial z$ is the wind shear production, $(g\overline{w'T_v'})/T_o$ represents the buoyancy forces, $\partial/\partial z[\overline{w'e} + (1/\rho_a)\overline{w'p'}]$ is the redistribution of the flux of TKE and work done by pressure fluctuations and ϵ is epsilon, the rate of dissipation of turbulent kinetic energy.

Steady state conditions are assumed. The divergence term is small relative to the remaining terms in the equation and is therefore neglected (Large and Pond, 1981). Eqn. (29) then simplifies to:

$$U_*^2\partial\bar{U}/\partial z + [(g\overline{w'T_v'})/T_o] - \epsilon = 0 \qquad (30)$$

After combining Eqns. (5), (7) and (30), and rearranging, an expression for the friction velocity is obtained:

$$U_* = [\epsilon kz/[\phi_m(z/L) - (z/L)]]^{1/3} \qquad (31)$$

For unstable conditions, the denominator is often replaced by:

$$\phi_\epsilon(z/L) = \phi_m(z/L) - (z/L) \quad (32)$$

Eqn. (31) may then be written as:

$$U_* = [\epsilon kz/\phi_\epsilon(z/L)]^{1/3} \quad (33)$$

with stability corrections for dissipation scaling (Wyngaard and Cote', 1971):

$$\phi_\epsilon = (1 + 0.5|z/L|^{3/5})^{3/2} \quad z/L<0 \quad (34a)$$

$$\phi_\epsilon = (1 + 2.5|z/L|^{2/3})^{3/2} \quad z/L>0 \quad (34b)$$

The friction velocity, U_*, can therefore be estimated in terms of the dissipation rate, ϵ. Kolmogoroff theory is then employed to determine a value for ϵ based on high frequency wind fluctuations. All spectra can be divided into three portions: the energy producing subrange, the inertial subrange and the dissipation subrange (Panofsky and Dutton, 1984). Large eddies from the energy containing subrange cascade kinetic energy and momentum down to smaller eddies, eventually reaching the dissipation region where molecular viscosity converts the kinetic energy to heat. Between these two regions is the inertial subrange. In this region, energy is neither produced nor dissipated. Kolmogoroff theory states that in the inertial subrange of isotropic turbulence, the high frequency fluctuations of the wind velocity, u' can be expressed by a one-dimensional power spectrum (Schacher, et. al., 1981):

$$Su(k_*) = \alpha_* \epsilon^{2/3} k_*^{-5/3} \quad (35)$$

where Su is the energy density spectrum of the horizontal windspeed, is a coefficient of magnitude 0.50 (Champagne, et. al., 1977), and k_* is the wavenumber.

Applying Taylor's frozen turbulence hypothesis:

$$k_* = 2\pi f/\bar{U} \tag{36}$$

equation (35) becomes:

$$Su(k_*) = \alpha_* \epsilon^{2/3}(2\pi f/\bar{U})^{-5/3} \tag{37}$$

The Kolmogoroff Spectrum can now be integrated between two wavenumbers, designated k_{*1} and k_{*h} to give the energy, $\sigma^2_{\Delta k_*}$ interval (Schacher, et. al., 1981):

$$\sigma^2_{\Delta k_*} = \int_{k*1}^{k*h} Su(k_*)dk_* \tag{38}$$

$$= 1.5\alpha_* \epsilon^{2/3}(k_{*1}^{-2/3} - k_{*h}^{-2/3}) \tag{38a}$$

Combining Eqns. (36) and (38) yields:

$$\sigma^2_{\Delta f} = 0.230(\epsilon\bar{U})^{2/3}(f_1^{-2/3} - f_h^{-2/3}) \tag{39}$$

where $f_1=(k_{*1}\bar{U})/2$ and $f_h=(k_{*h}\bar{U})/2$. Rearranging Eqn. (39) by using Eqn. (35) produces:

$$U_* = 2.65\sigma_{U\Delta f}[z/[\bar{U}\phi_\epsilon(z/L)]]^{1/3}(f_1^{-2/3} - f_h^{-2/3})^{1/2} \tag{40}$$

For the TOWARD Experiment, f_1 = 5 Hz and f_h = 50 Hz, and z=22 meters. Substituting these values reduces Eqn. (40) to:

$$U_* = 7.81\sigma_{U\Delta f}[\bar{U}\phi_\epsilon(z/L)]^{-1/3} \tag{41}$$

Because $\phi_\epsilon(z/L)$ also depends on U_*, Eqn. (41) must be solved iteratively.

C. IN-SITU HOT FILM CALIBRATION

Calibration of the hot film sensor was accomplished by recording the changes in voltage produced by the winds passing over the sensor. The relationship may be expressed by:

$$V^2 = V_o^2 + B\bar{U}rel^{1/2} \tag{42}$$

where V is the voltage, V_o is the plotted calibration intercept and $\bar{U}rel$ is the relative windspeed. B represents a calibration factor that must be continuously determined for each data collection period.

B may be estimated either through the dynamic or the regression methods. The dynamic method begins by differentiating Eqn. (42):

$$B = 4V\bar{U}rel^{1/2}(dV/d\bar{U}) \quad (43)$$

Over each data collection period, $dV/d\bar{U}$ is estimated by $\sigma_V/\sigma_{\bar{U}}$, where $\sigma_{\bar{U}}$ and σ_V are the standard deviations of $\bar{U}$ and V, respectively. Averaging V and $\bar{U}rel$ and solving for B yields:

$$B = 4V\bar{U}rel^{1/2}(\sigma_V/\sigma_{\bar{U}}) \quad (44)$$

Rearranging Eqn. (44) and substituting into Eqn. (40) produces the following estimate for U_*:

$$U_* = 2.81[(4V/B)\bar{U}rel^{1/2}]\sigma_{V\Delta f}[z/\bar{U}\phi_\epsilon(z/L)]^{1/3}(f_l^{-2/3} - f_h^{-2/3}) \quad (45)$$

The regression method is based on values of V and Urel over several time periods with varying average relative windspeeds. V is then usually plotted as a function of $\bar{U}rel$. According to Eqn. (42), the points should fall along a line with a slope, B, where V_o represents the y-intercept.

Measurement-relative scatter in both $\bar{U}rel$ and V can cause errors in the slope. Therefore, it is sometimes advantageous to choose V as the independent variable if it shows less scatter. In cases where it is difficult to determine which variable is the least reliable, two regressions are calculated, with Urel and V alternated as independent variables. B is then determined from the average of the two slopes.

D. WIND-WAVE COUPLING DYNAMICS

The total wave field energy is divided into swell and wind wave components:

$$\sigma^2_T = \sigma^2_s + \sigma^2_{ww} \quad (46)$$

where σ^2_T represents the total energy in the wave field and σ^2_s and σ^2_{ww} are the energies contained by the swell and wind waves, respectively. σ^2_{ww} cannot be predicted based on local scaling. σ^2_{ww} has received considerable study and a great deal of theory exists concerning this parameter. The approach currently is to describe σ^2_{ww} in terms of a local equilibrium spectrum. This theory assumes that wind forcing controls the dynamics of every wave component of the wind wave spectrum. Each wave is characterized by an angular frequency, n', where:

$$n' = 2\pi f \quad (47)$$

Gravity is the primary restoring force for these waves.

The local equilibrium energy density spectrum, S(n'), is defined as:

$$\sigma^2_{ww} = \int_{n'}^{\infty} S(n')dn' \quad (48)$$

and S(n') may be parameterized in terms of Phillips scaling arguments (Phillips, 1980):

$$S(n') = \beta g(n')^{-5} \qquad n'>n_o' \quad (49)$$

Beta is the Phillips coefficient which can vary from .006 to .020 (Geernaert, 1983). n_o' represents both the wind-wave peak frequency and the boundary between the swell and equilibrium ranges. Waves of frequency $n'<n_o'$ represent swell. Wind waves are defined to be those with frequencies of $n'>n_o'$. n_o' is usually approximated by:

$$n_o' \doteq g/U_{10} \quad (50)$$

for steady state conditions (Kraus, 1972).

Beta is often described in terms of dimensionless fetch, $\tilde{x}$:

$$\tilde{x} = gx/(U_*^2) \tag{51}$$

where x is the upwind fetch. Large values of β are associated with small values of fetch. Beta has also been parameterized over an applicable range of .25 to 1.0 hz by (Geernaert, et.al., 1985a):

$$\beta = 0.005 + .002n' + 1.5(C_o/U_*)^{-2} \tag{52}$$

where C_o represents the phase speed of the largest wind wave. (C_o/U_*) is defined as the wave saturation parameter, and this parameter behaves in the same manner as the wave age C/U. (C_o/U_*) is a dimensionless indicator of the degree to which the wind waves have reached steady state and is frequently related to the non-dimensional fetch as (Wu, 1985):

$$(C_o/U_*^2) = 0.05[gx/(U_*^2)]^{3/10} \tag{53}$$

Hsu (1974) related the wave saturation parameter to the roughness length, z_o, by defining the Charnock coefficient in terms of the slope of the wave of frequency n_o'. His formulation became:

$$z_o = (H/2\pi)(C_o/U_*)^{-2} \tag{54}$$

where H is the significant wave height. z_o can be seen to vary according to the local wind wave spectral peak.

Numerous wave models have incorporated these relationships in an attempt to relate variations in the surface wave energy spectrum to variations in the magnitude of the drag coefficient. Davidson (1974) formulated an empirical model in which the drag coefficient is represented by:

$$C_D = [k/[\ln(z/z_o) - \psi + b[(C_o/U_*) - 26.3]]]^2 \tag{55}$$

where b is an empirical constant found to be 0.13.

Others have employed indirect methods to calculate C_D using roughness length parameterizations. Byrne (1982) derived a roughness length in the form of an integrated slope spectrum:

$$z_o = C_B \int_o^\infty S(n')(n')^2 dn' \qquad (56)$$

where C_B is an adjustable coefficient.

Kitaigorodskii (1973) derived a roughness length model in the following form:

$$z_o = 2/30\left(\int_o^\infty S(n')e^{-2kg/n'U_* dn'}\right)^{1/2} \qquad (57)$$

One purpose of the TOWARD Experiment was to evaluate scatterometer return signals in order to examine surface roughness as a predictor of windspeed over the ocean. These signals can be correlated with windspeed since they increase with increasing surface roughness. The surface roughness is dependent on τ, which from Eqn. (2a) is a function of C_D and the ten meter height windspeed, U_{10}. The scatterometer, however, evaluates U_{10} based on signal reflection from the surface (Geernaert, 1983), while the drag coefficient has been treated as a constant or as a simple function of U_{10}. Thus, the dependence of the drag coefficient on the surface roughness is not fully understood. Because wave growth and decay affect the magnitude of C_D (Geernaert, 1985a), scatterometer predictions of windspeed based on the bulk formulae could be improved by including roughness as an additional variable.

The TOWARD Experiment was designed, in part, to look for a trend in C_D as a function of time over the course of the sea breeze. The sea breeze is characterized by growing winds and sea state along with corresponding increases in surface roughness. By observing the behavior of this coefficient with time, the interaction between wind and wave state may be better understood.

III. SYNOPTIC METEOROLOGY DURING THE TOWARD EXPERIMENT

The TOWARD experiment was conducted at the Naval Ocean Systems Center (NOSC) tower which is located two kilometers offshore of Mission Beach, San Diego. Minimal surface layer climatological data is available for the site. Blanc (1981) summarized the environmental conditions for San Nicholas Island (SNI), California, which is located roughly 150 km northwest of the NOSC tower. While wind and wave conditions are more vigorous at SNI than those at the tower, the air and sea-surface temperatures are consistent between the two sites. Blanc determined the most frequent true wind direction to be from the northwest throughout the year with mean windspeeds of 7.7 m/s in March and 6.2 m/s for both October and November. During the months of March, October and November, when the TOWARD experiment was conducted, the mean climatological daily temperatures (°C) are 15.8 for March, 20.4 for October and 18.4 for November, with average daily minimum temperatures of 12.4, 16.0 and 14.9, respectively. Mean climatological sea-surface temperatures for the same months are 14.4 for March, with values of 18.2 and 16.6 for October and November.

The mean conditions for San Nicholas Island differ somewhat from those reported onshore at Lindbergh Field in San Diego. The mean daily maximum temperatures for March, October and November are 18.9, 23.3 and 21.2, respectively, while the average daily minimum temperatures are 10.1, 14.7 and 10.8. In March and October, the prevailing winds are generally west-northwesterly but shift to a northeasterly direction in November. Mean windspeeds are also smaller with values of 3.3, 2.9 and 2.5 m/sec reported for March, October and November, respectively.

The TOWARD Experiment was designed to cover a large range of wind conditions, particularly for high winds. Measurement periods were therefore chosen to be from mid-September through mid-November 1984 (Phase I) and March 1985 (Phase II).

The almost daily presence of the local sea breeze is a factor in the environmental conditions at the NOSC tower. Sea breeze circulations develop when air over land is heated much more than the air over the ocean. Since the land usually becomes warmer than the sea during the day, density differences over the two surfaces bring cool air from the sea toward the warmer land at low levels. A return flow of warm air from the land to the ocean occurs at upper levels. At night, radiative cooling takes place over the land while the sea surface maintains a more uniform temperature due to the large heat capacity of the ocean. The result is nocturnal, low level flow from the land toward the sea (Hess, 1979).

Because the largest horizontal density gradient occurs at the coastline, the sea breeze dominates in the coastal zone, while the geostrophic wind ($\vec{V}_g$) becomes a more important factor for describing surface layer energetics farther offshore. It follows that waves generated by the sea breeze would tend to be of relatively short fetch. Fig. 3.11 from 31 October provides an example of synoptic conditions for Southern California during the TOWARD Experiment. The large scale flow ($\vec{V}_g$) can be seen to originate from the northwest. Ship observations, 300-400 km offshore, also indicate a northwesterly flow. These wind observations from offshore sites show little diurnal variation. At 1000 local time, however, reports from Lindbergh Field, San Diego, show winds from a south-southwesterly direction, indicating smaller scale, local-forcing nearer the coast. A significant diurnal shift in wind direction can also be seen in these reports.

Thus, the sea breeze appears to exert an influence less than 300 to 400 km from the shore.

Since the sea breeze is of a different scale than the synoptic, geostrophic wind, computation of $\vec{V}_g$ provides an indication of the relative magnitudes of these two types of forcing near the NOSC tower. Calculations of the geostrophic wind from synoptic charts were made for 1000 local (1800 GMT) and 1600 local (2400 GMT).

$$\vec{V}_g = (1/f\rho_a)(\partial p/\partial \vec{n}) \tag{58}$$

where $\vec{V}_g$ represents the geostrophic wind, f is the coriolis parameter, p is the atmospheric pressure and $\vec{n}$ is a unit vector normal to the isobars. These times were chosen in order to compare the differences in sea breeze magnitudes between morning and afternoon. Typically, the strongest sea breeze occurs in mid-afternoon when the land surface has heated to its daily maximum. Since final surface charts were not available for 2100 GMT (1300 local), analyses for 2400 GMT were used instead. These values were compared with windspeed observations collected at the tower and with data from ship reports in the Southern California area.

Data collected at the tower indicated a general increase in windspeed from 1000 to 1600 local (1800 GMT to 2400 GMT). The geostrophic wind velocities based on Eqn. (58) and the synoptic pressure maps were smaller and showed much less diurnal variation than those of the tower (V_t). Ship observations from 300-400 km offshore indicated consistently higher windspeeds for both time periods, usually ranging from 5-15 kt. Although the computed $\vec{V}_g$ and ship reported surface winds (V_s) showed considerable differences in magnitude, the wind directions from offshore sites during the experiment showed no statistically significant diurnal effects. Tables II and III show these results.

TABLE II

Computed $\vec{V}_g$ & Ship Reported Sfc Winds (Phase I)

(V_t, $\vec{V}_g$ and V_s in m/s)

Date	Time	V_t	Dir.	$\vec{V}_g$	Dir.	V_s	Dir.	D.(km)
10/2	18 Z	2.0	87	<1	NW	2.6	N	400
	24 Z	---	---	1.2	NW	7.7	N	400
10/3	18 Z	2.5	297	1.4	NW	---	---	---
	24 Z	5.3	309	<1	NW	7.7	N	400
10/6	18 Z	---	---	<1	NNW	2.6	W	400
	24 Z	5.9	313	1.4	NNW	7.7	N	400
10/7	18 Z	4.6	335	<1	NW	2.6	N	400
	24 Z	---	---	1.7	NW	5.2	N	400
10/11	18 Z	---	---	1.4	NW	7.7	N	400
	24 Z	---	---	1.1	NW	7.7	NW	400
10/12	18 Z	1.0	154	1.0	NE	10.2	N	400
	24 Z	8.3	317	1.4	NE	10.2	N	400
10/15	18 Z	6.0	180	1.4	NE	10.2	N	400
	24 Z	5.4	293	1.2	NE	12.8	N	400
10/16	18 Z	---	---	<1	NNW	2.6	NW	400
	24 Z	5.4	203	<1	NW	7.7	N	400
10/17	18 Z	6.7	280	1.4	N	10.2	N	400
	24 Z	6.2	181	1.7	N	7.7	NW	350
10/18	18 Z	---	---	1.0	ENE	10.2	NNW	400
	24 Z	6.8	337	<1	ENE	7.7	N	400
10/20	18 Z	5.6	255	<1	N	---	---	---
	24 Z	6.0	267	1.4	NW	10.2	N	400
10/21	18 Z	1.8	127	<1	NNE	---	---	---
	24 Z	---	---		NW	7.7	N	400
10/23	18 Z	---	---	<1	NE	5.1	N	400
	24 Z	8.7	288	<1	ENE	---	---	---
10/25	18 Z	---	---	<1	SE	2.6	N	400
	24 Z	---	---	<1	SE	2.6	NW	400
10/27	18 Z	---	---	<1	N	---	---	---
	24 Z	4.4	221	1.7	N	5.2	N	400
10/28	18 Z	---	---	<1	NE	---	---	---
	24 Z	3.9	298	<1	NW	7.7	N	400
10/29	18 Z	---	---	1.1	NE	---	---	---
	24 Z	4.4	315	<1	NE	5.2	NW	400
10/30	18 Z	1.4	231	<1	NNW	---	---	---
	24 Z	3.7	294	2.8	NW	7.7	N	400
10/31	18 Z	2.8	218	1.7	NW	---	---	---
	24 Z	5.3	296	1.7	NW	---	---	---
11/2	18 Z	2.6	298	1.7	NNW	7.7	N	400
	24 Z	6.8	325	1.4	NW	7.7	N	400
11/3	18 Z	---	---	<1	NW	2.7	SW	400
	24 Z	3.9	289	1.4	NE	10.2	N	400
11/4	18 Z	1.1	170	<1	SE	7.7	N	400
	24 Z	2.8	306	<1	SE	---	---	---
11/5	18 Z	1.4	158	<1	N	5.1	N	400
	24 Z	1.5	199	2.1	NW	7.7	N	400
11/7	18 Z	---	---	<1	NW	7.7	N	400
	24 Z	4.1	257	1.4	NW	5.1	N	400

TABLE III

Computed $\vec{V}_g$ & Ship Reported Sfc Winds (Phase II)

(V_t, $\vec{V}_g$ and V_s in m/s)

Date	Time	V_t	Dir.	$\vec{V}_g$	Dir.	V_s	Dir.	D.(km)
3/12	18 Z	---	---	1.4	NNW	5.1	N	400
	24 Z	6.0	260	<1	NW	10.8	N	400
3/13	18 Z	---	---	<1	NE	7.7	NW	250
						5.1	NW	275
	24 Z	3.0	260	1.9	N	7.7	N	400
3/15	18 Z	---	---	<1	NW	5.1	N	400
	24 Z	4.8	415	<1	NW	7.7	N	400
3/16	18 Z	4.0	003	<1	NW	2.6	NW	400
	24 Z	4.9	340	<1	NW	7.7	N	400
3/18	18 Z	---	---	1.4	NW	7.7	N	400
	24 Z	9.4	296	2.4	NW	10.3	N	400
3/19	18 Z	---	---	2.8	NW	10.3	N	400
	24 Z	4.8	275	1.7	NW	12.9	N	400
3/20	18 Z	---	---	1.3	NNW	7.7	NW	400
	24 Z	5.9	312	1.4	NW	7.7	N	400
3/21	18 Z	---	---	2.1	NW	10.3	N	400
	24 Z	3.2	315	1.8	NW	18.0	N	400
3/22	18 Z	---	---	1.4	N	12.9	N	400
	24 Z	3.6	322	1	NE	12.9	N	400
3/24	18 Z	---	---	<1	NE	5.1	NW	275
						5.1	N	400
	24 Z	---	---	<1	NNW	7.7	N	400
3/25	18 Z	---	---	1.4	NNW	7.7	N	400
	24 Z	6.1	220	1.7	NNW	10.3	N	400
3/26	18 Z	3.6	218	1.7	NW	7.7	N	400
	24 Z	3.6	265	<1	NW	10.3	N	400
3/27	18 Z	7.6	233	<1	NW	5.1	NNW	400
	24 Z	5.5	264	2.1	NW	7.7	NNW	400
3/28	18 Z	7.5	235	2.8	NW	12.9	N	400
	24 Z	---	---	2.8	NW	10.3	N	400

A. THE TOWARD SYNOPTIC AND SURFACE LAYER CONDITIONS

This section will be a presentation of the surface layer and larger scale meteorological conditions for the TOWARD experiment. The data set is divided into two sections, Phase I and Phase II. Phase I covers the period from 2 October to 8 November 1984, while Phase II covers the period of 12 to 28 March 1985. Each phase is discussed separately. Individual surface analyses for 1800 GMT will be presented

in the text for days on which data were collected. Additional figures representing wind speed and direction, as well as air and sea-surface temperatures can be found in Appendix A. The latter figures present time series of discussed quantities and provide a reference for the following discussion. Unless otherwise noted, the times are local (PDT for Phase I and PST for Phase II).

1. Phase I

During the first week of the TOWARD experiment, winds were from the northwest and windspeeds were light to moderate. A maximum value of roughly 7 m/s (Fig. A.1) was recorded on October 6th. Strong local diurnal variations due to the sea breeze also prevailed in the first week, which is particularly evident in the data from 3 and 6 October. On those dates, windspeeds increased significantly from 0900 PDT, remained steady for several hours, and then decreased markedly throughout the sampling period which ended at 2215.

Data collection resumed at 1235 PDT on October 6th. Recorded windspeeds remained fairly steady from this time to 1500, when values began decreasing. Data were only collected for one hour on 7 October. Windspeeds increased steadily from about 4 to 6 m/s over this period.

Synoptic charts for the 2-8 October period do not indicate any significant weather activity. A low pressure center was present southeast of the San Diego area early in the week, before moving farther southeast. Weather conditions were subsequently dominated by a strong offshore ridge which persisted throughout the week.

Data were collected only on the 11th and 12th of October during the second week of TOWARD. Wind directions were from the northwest on the 11th and windspeeds were low. On the 12th, winds were also out of the northwest, but had much higher velocities. A maximum of about 9 m/s was

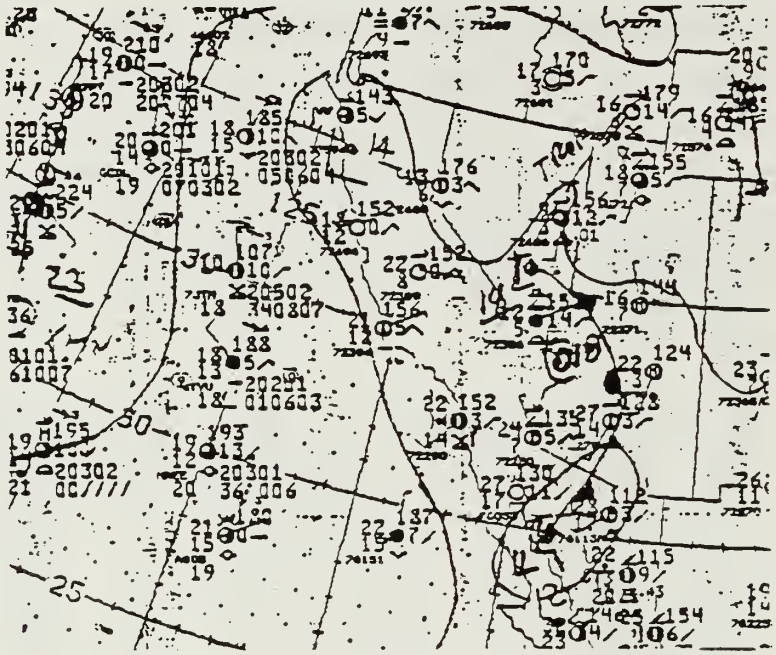

(a)

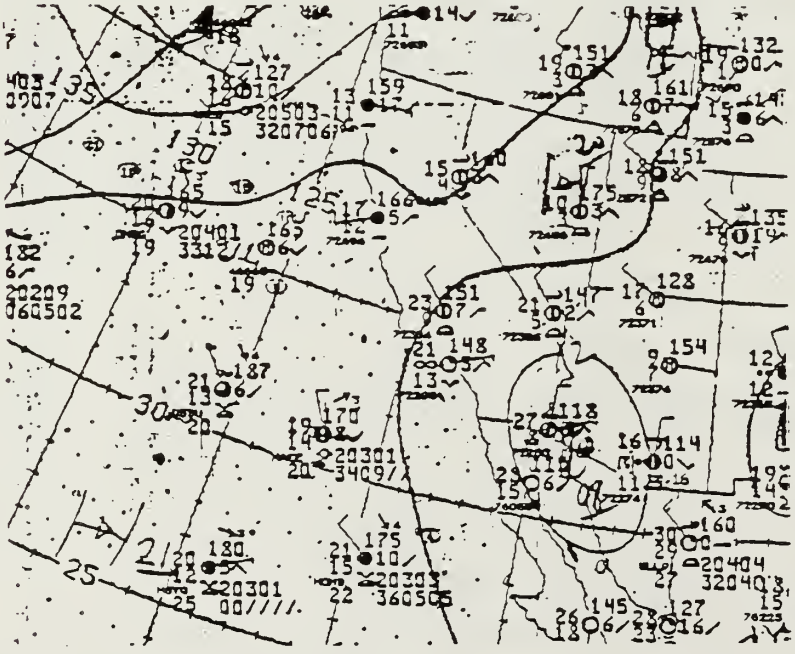

(b)

Figure 3.1 Surface analyses 1800 GMT 2 (a) and 3 (b) October 1984.

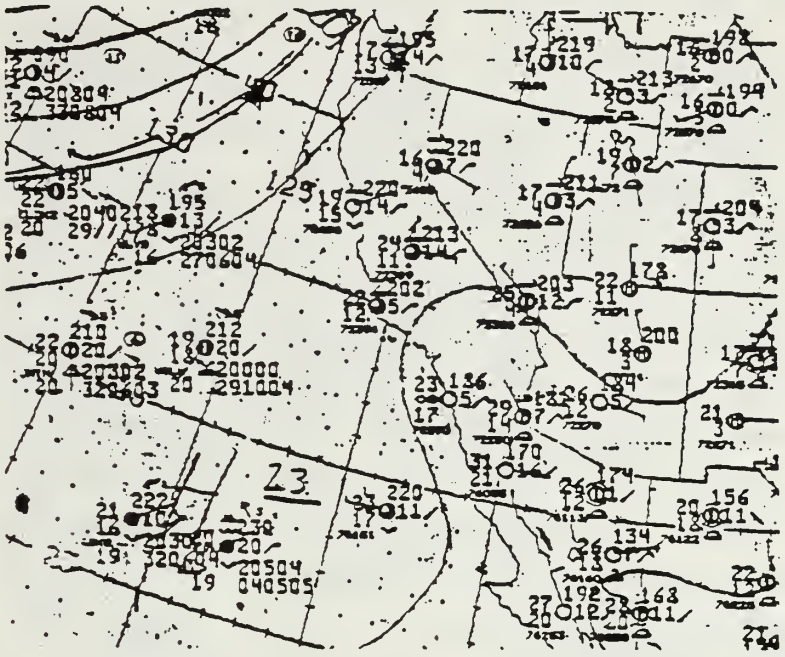

(a)

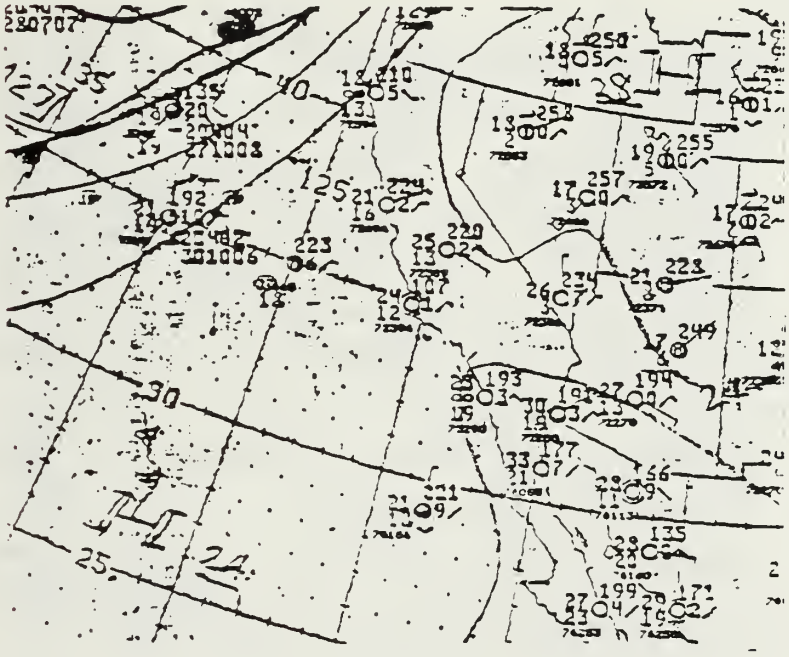

(b)

Figure 3.2 Surface analyses 1800 GMT 6 (a) and 7 (b) October 1984.

recorded on that date at 1550. Typical sea breeze patterns were also apparent in the data, particularly on the 12th. Weak easterly winds were present in the early morning. The winds shifted to the northwest near noon and increased rapidly to a maximum. These values began to drop off at approximately 1600 PDT.

The synoptic charts from this period show a frontal passage through the San Diego area on the morning of 12 October. This event cannot be correlated with the strong winds of the 12th, because the front was already several hundred kilometers to the southeast when the winds were recorded. Synoptic charts do not indicate the presence of a strong, large-scale pressure gradient associated with the trough. Thus the most likely cause of these high winds was strong diurnal heating and subsidence following the passage of the front.

Data collection for the third week of the experiment began at 0900 PDT on October 15th. A definite wind shift can be seen on the 15th accompanied by sharp fluctuations in windspeed. Synoptic charts for that date indicated the presence of a stationary front almost directly over the San Diego area at 1000 PDT. This front passed through the area at a rate of only 2 m/s. Its slow rate of movement caused it to influence weather conditions in the San Diego area through the 16th.

Wind shifts plus strong increases and decreases in windspeed were also apparent on the 16th and 17th. Synoptic charts for these dates show a front moving rapidly through the tower area at a rate of over 10 m/s. This front was well to the southeast within six hours.

October 18th provided a more typical weather pattern with northwesterly winds and a strong increase in windspeed between 1000 and 1700 local due to the diurnal heating pattern. Synoptic charts show a strong high pressure ridge

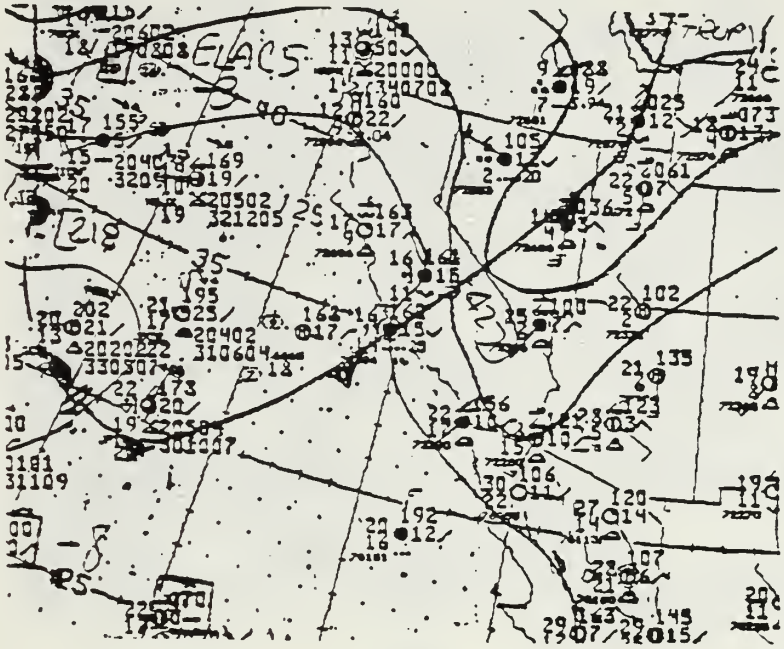

(a)

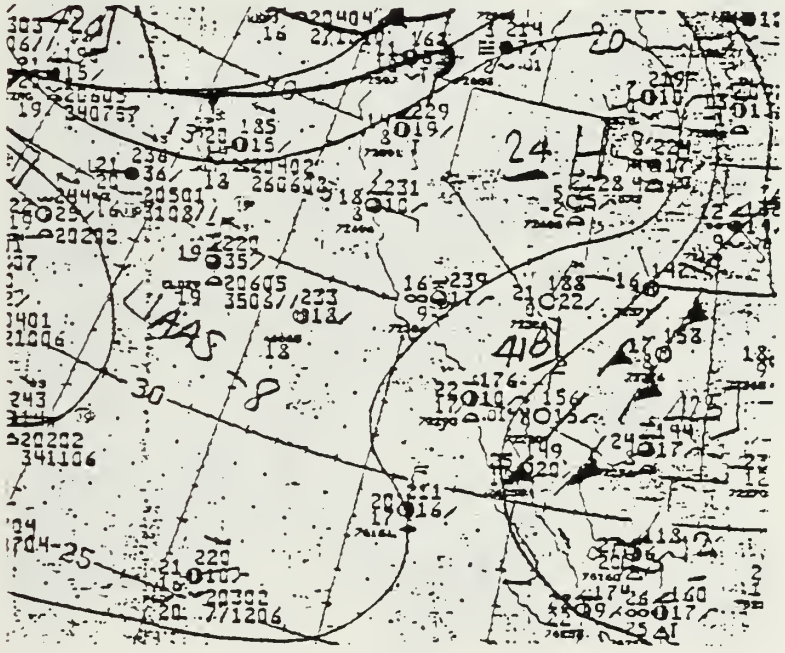

(b)

Figure 3.3 Surface analyses 1800 GMT 11 (a) and 12 (b) October 1984.

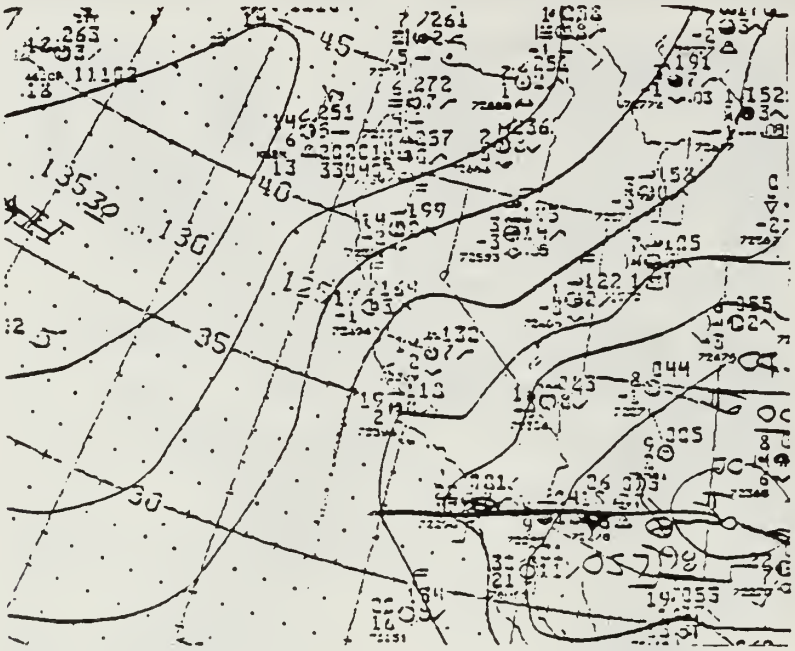

(a)

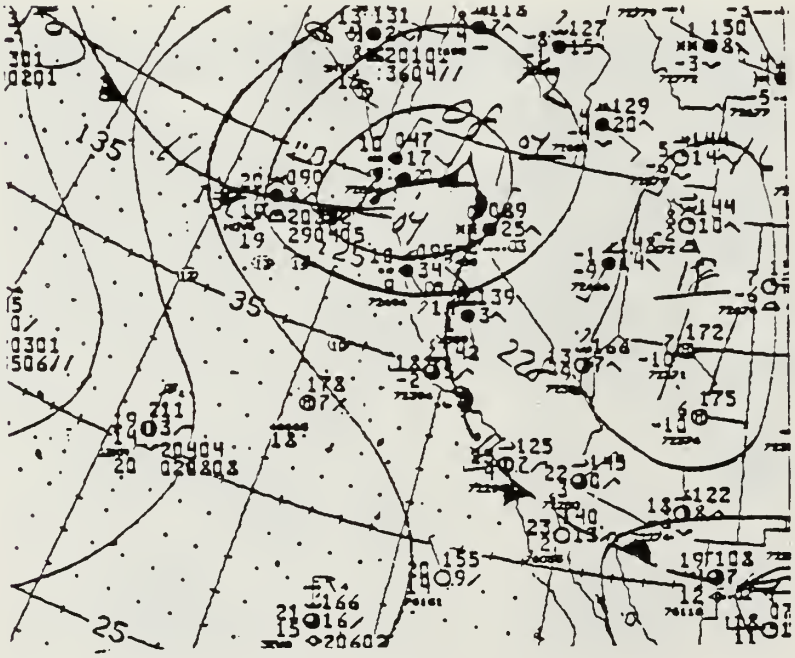

(b)

Figure 3.4 Surface analyses 1800 GMT 15 (a) and 16 (b) October 1984.

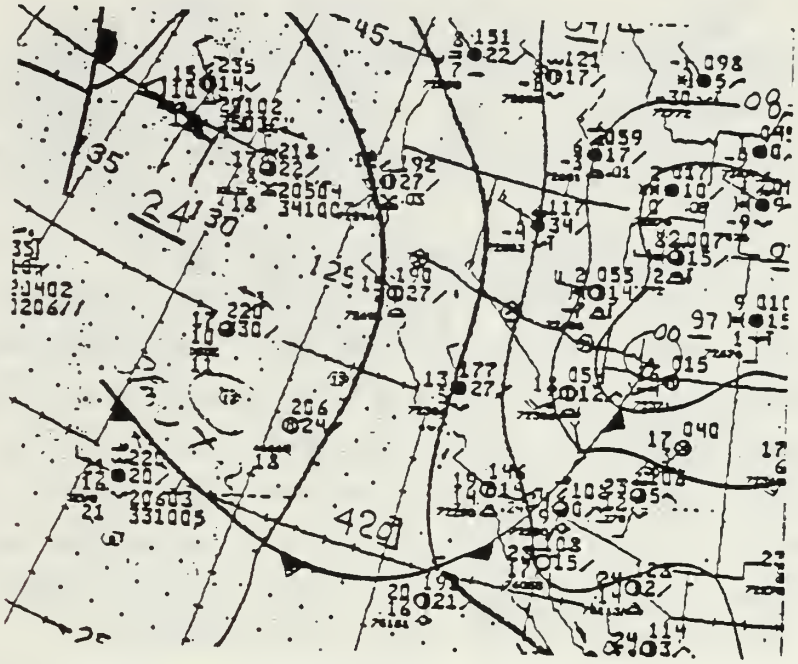

(a)

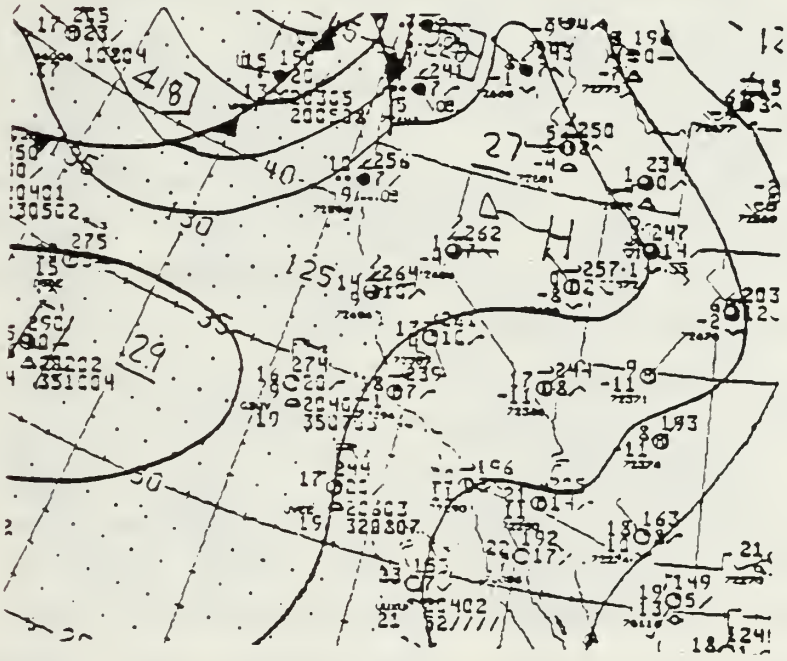

(b)

Figure 3.5 Surface analyses 1800 GMT 17 (a) and 18 (b) October 1984.

building to the southwest, with a weaker ridge to the northeast.

Winds were westerly on the morning of the 20th with a shift to an easterly flow near midnight. Velocities were moderate and fairly constant, with values decreasing in late afternoon.

The first observations for the week of 22-29 October began at 1100 on October 23rd. A strong increase in windspeed can be seen, along with a northwesterly wind direction. On the afternoon of the 25th, windspeeds again showed an increase. The wind direction was southerly in the late morning and shifted to the northwest by early afternoon. Wind speeds recorded on the 27th were moderate with little diurnal change. This pattern continued on the 28th, although the winds again originated from the northwest.

The fifth week of the TOWARD experiment was from 29 October to 5 November. Windspeeds were moderate on the 29th and 30th and were from the northwest. A wind shift and increase in windspeed began at approximately 0900 PDT on the 31st. Evaluation of synoptic charts for 31 October indicated the presence of a large-scale pressure gradient associated with an oncoming front. On November 2nd, the winds were again out of the northwest and San Diego returned to the typical sea breeze pattern.

The development of a strong high pressure center over the western United States produced the low windspeeds and shift in direction evident on 4 and 5 November. Windspeeds ranged from approximately 2 to 6 m/s.

Data collection for the final week of Phase I concluded on 7 November. Winds on the 5th were light and southwesterly. By the 7th, the typical sea breeze pattern again prevailed. Windspeeds were low and out of the west in early morning, but shifted to the northwest by early afternoon. A maximum value of about 5 m/s was recorded at 1105

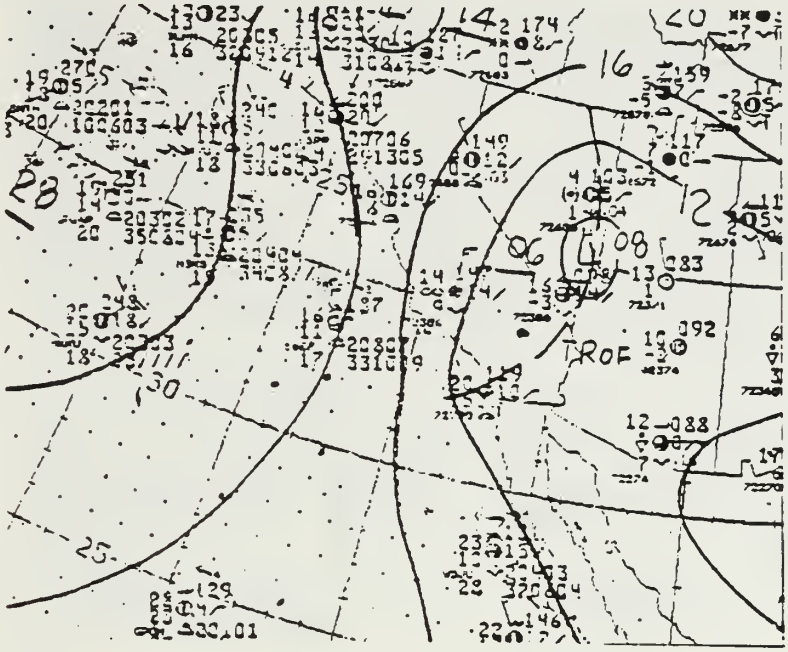

(a)

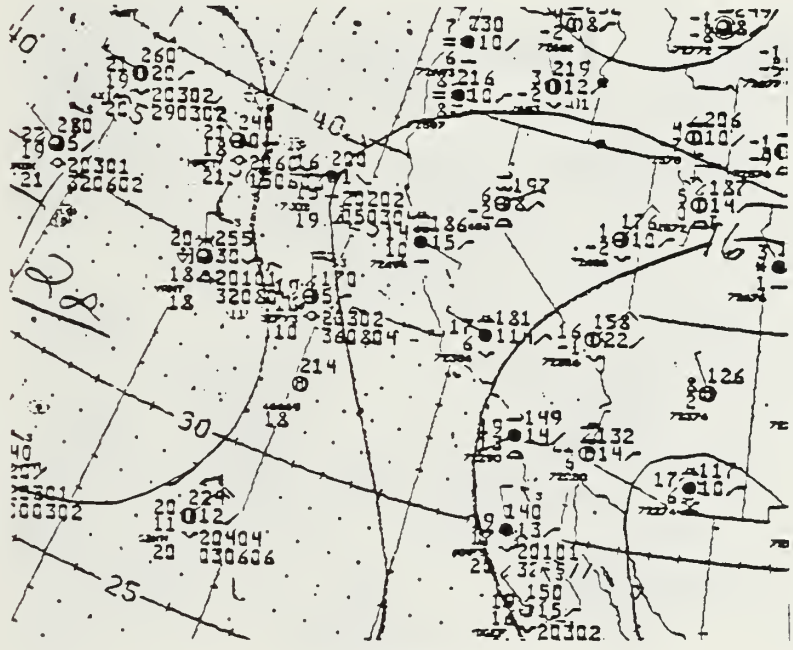

(b)

Figure 3.6 Surface analyses 1800 GMT 20 (a) and 21 (b) October 1984.

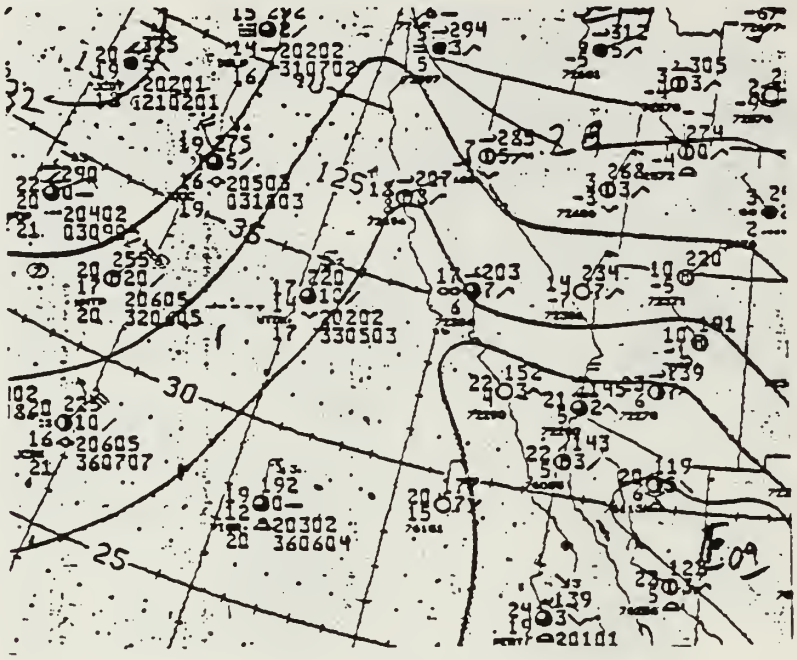

(a)

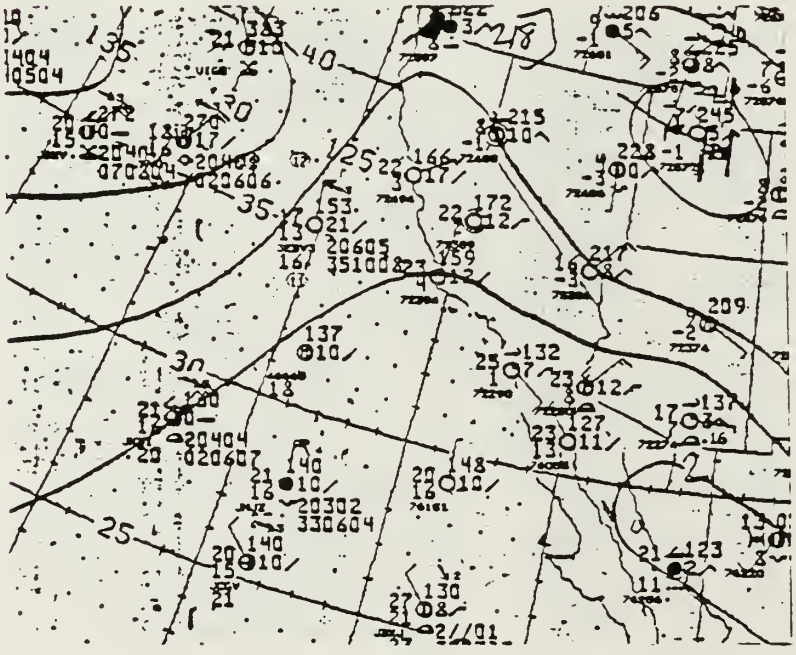

(b)

Figure 3.7 Surface analyses 1800 GMT 23 (a) and 25 (b) October 1984.

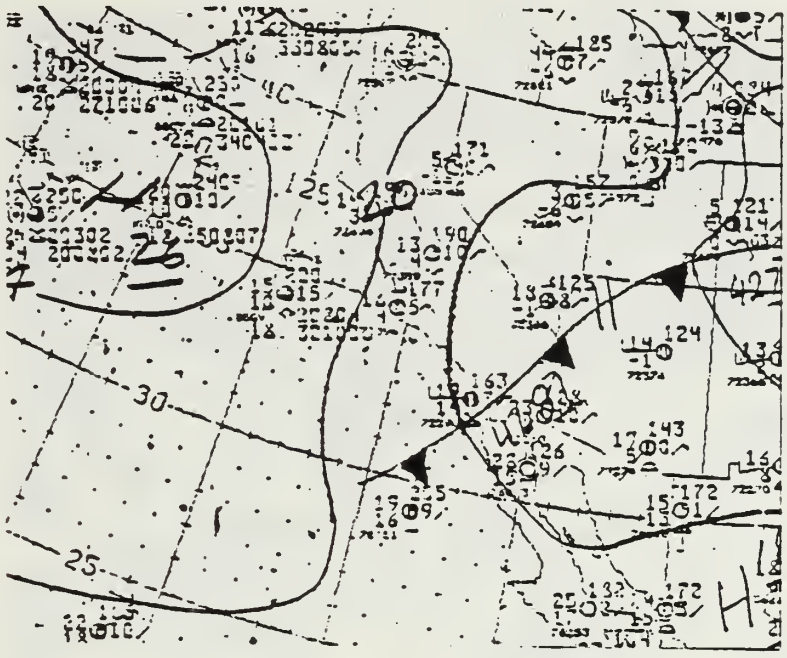

(a)

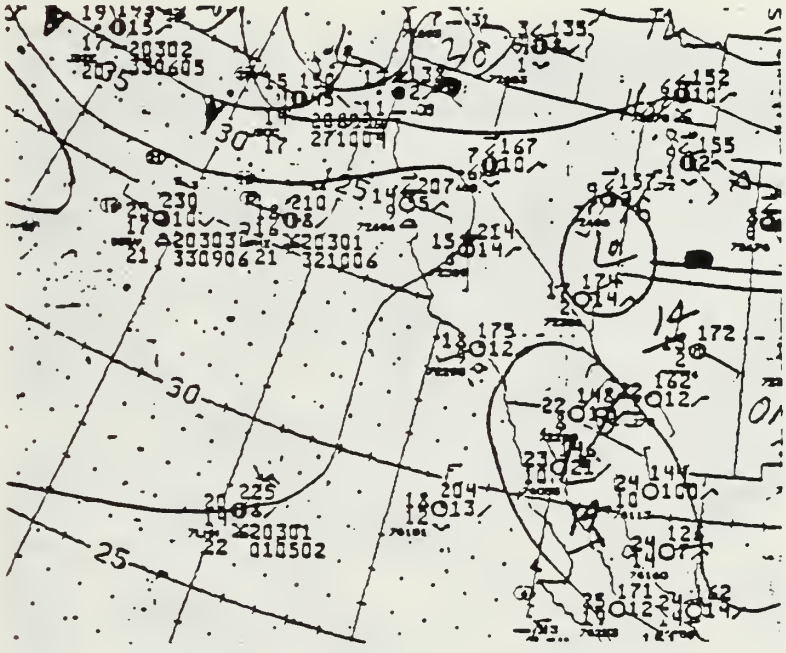

(b)

Figure 3.8 Surface analyses 1800 GMT 27 (a) and 28 (b) October 1984.

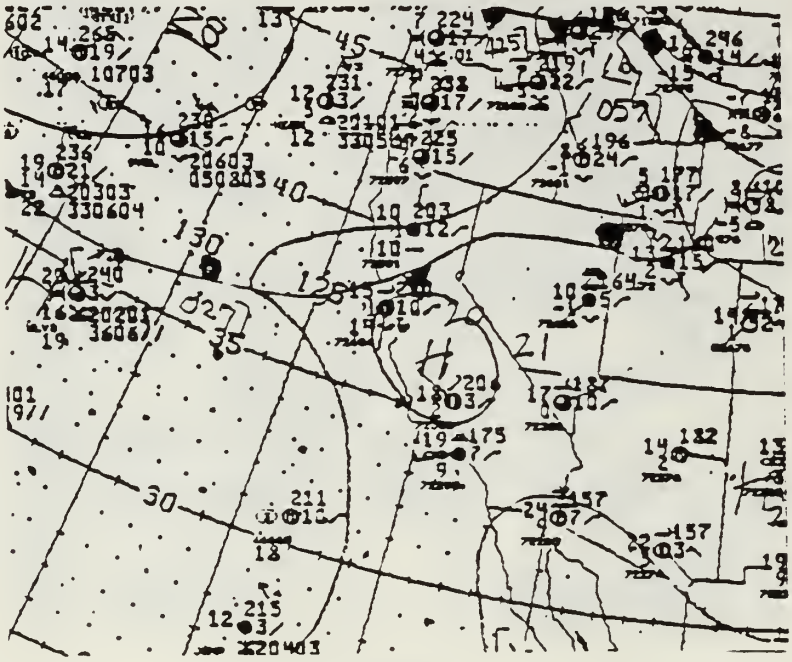

(a)

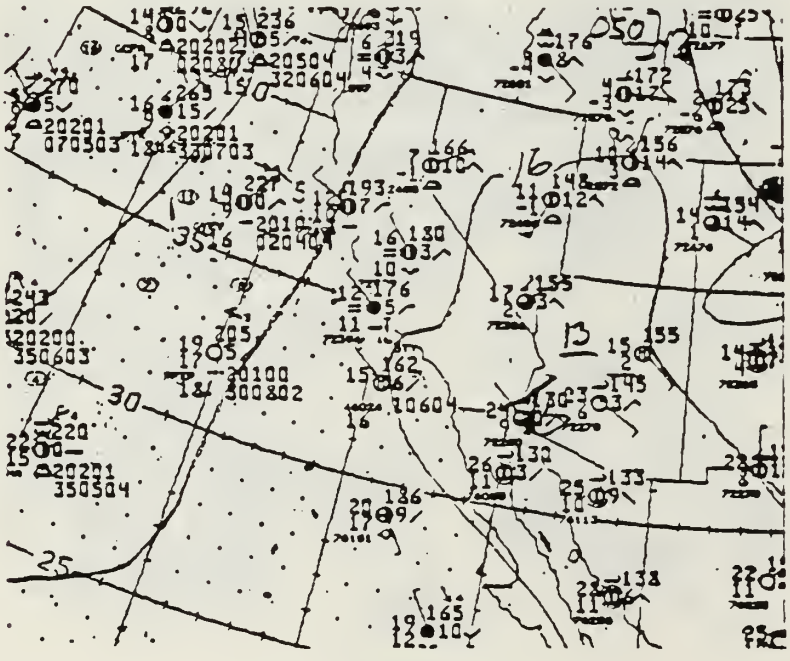

(b)

Figure 3.9 Surface analyses 1800 GMT 29 (a) and 30 (b) October 1984.

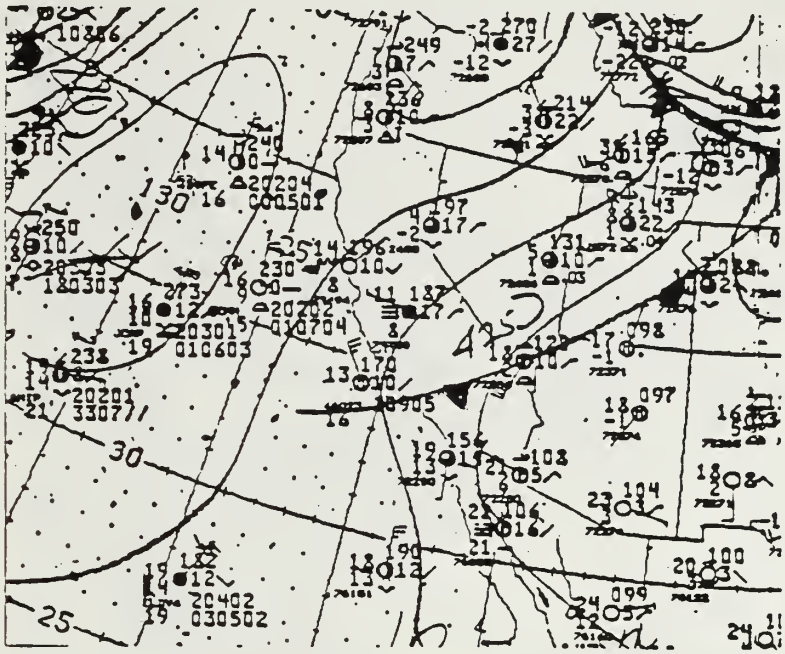

(a)

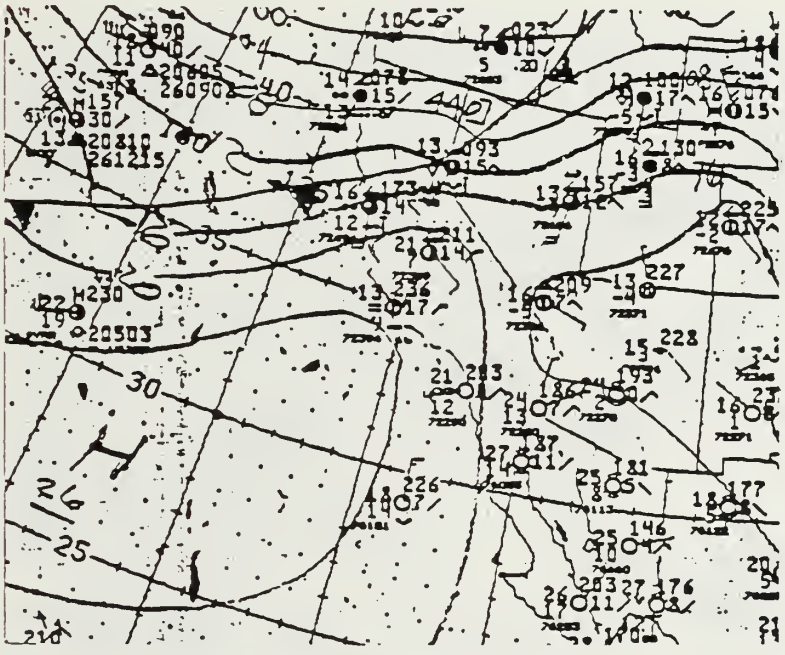

(b)

Figure 3.10 Surface analyses 1800 GMT 31 (a) and 2 (b) November 1984.

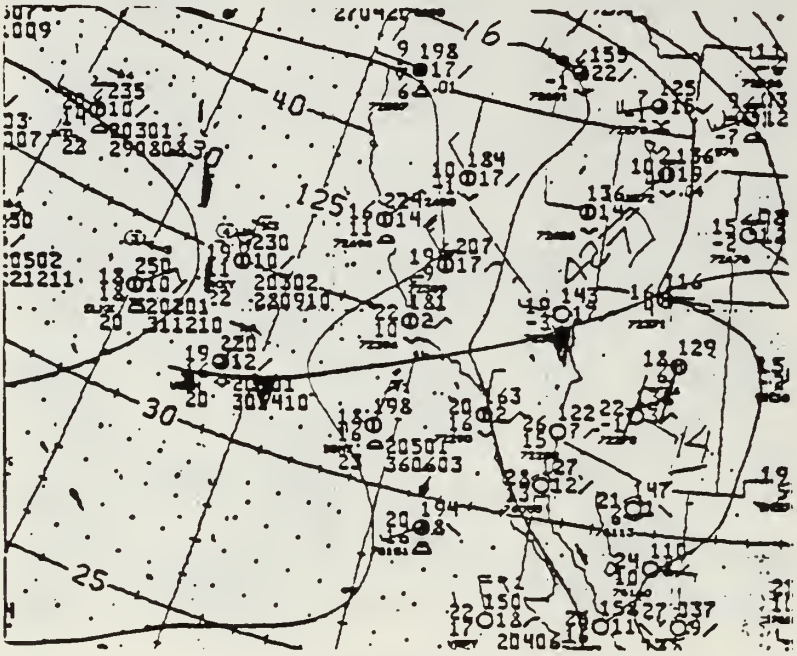

(a)

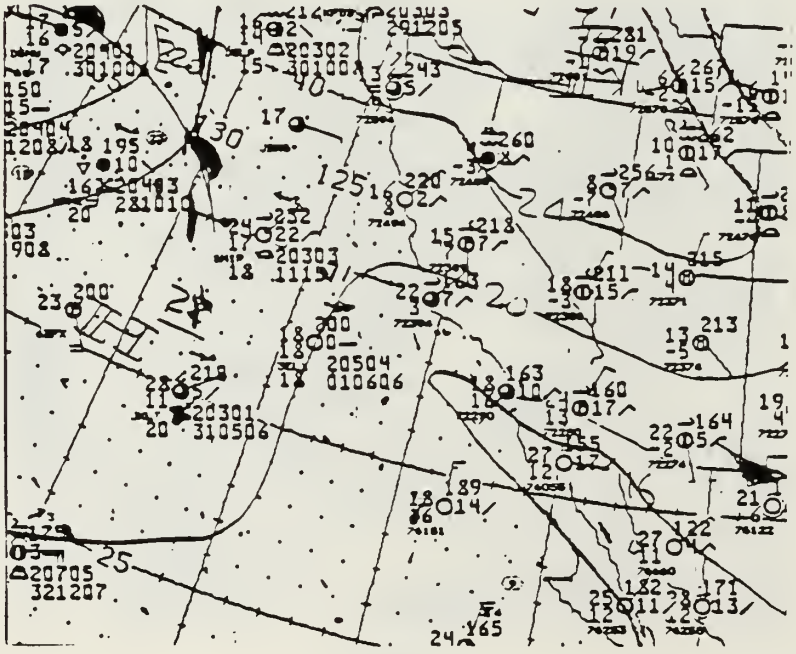

(b)

Figure 3.11 Surface analyses 1800 GMT 3 (a) and 4 (b) November 1984.

PDT followed by steadily declining values over the remainder of the sampling period.

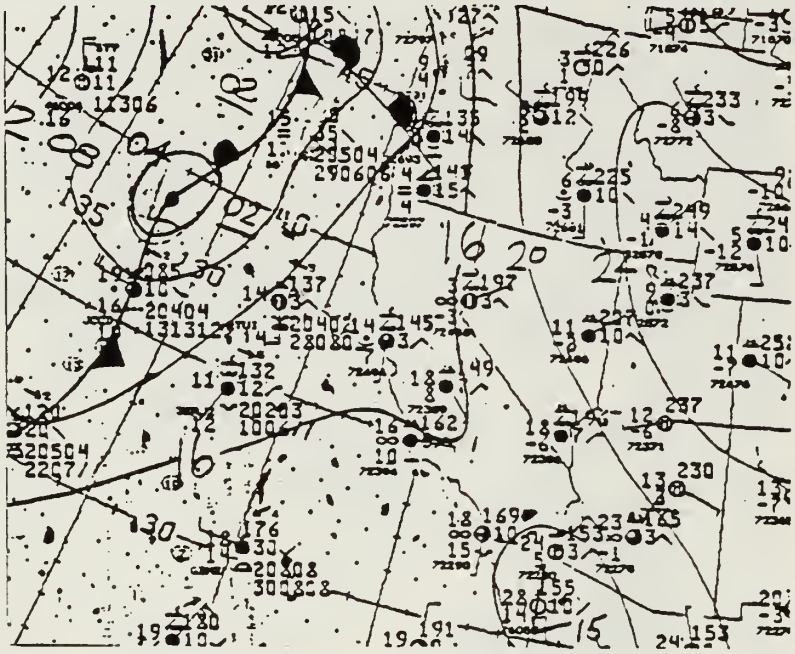

(a)

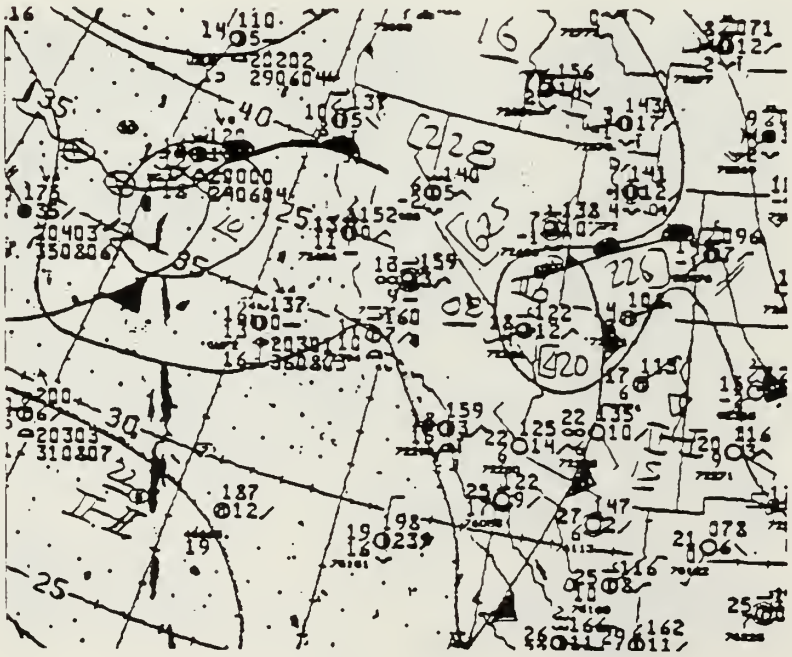

(b)

Figure 3.12 Surface analyses 1800 GMT 5 (a) and 7 (b) November 1984.

2. Phase II

Data collection for Phase II of the TOWARD experiment began on 12 March 1985. It can be seen from Fig. 3.14 that winds on the 12th and 13th were light to moderate and were primarily westerly. On March 15th and 16th winds were again moderate, but had a more typical northwesterly flow.

Synoptic charts for this period do not indicate any significant weather activity. Conditions were dominated by an offshore high pressure center throughout the week.

On March 18th, synoptic charts depict a tight pressure gradient resulting from the passage of a low pressure center through the San Diego area. The result was a sharp increase in windspeed. A maximum value of roughly 10 m/s was recorded at 1550 on that date. During the remainder of the week, the development of a strong offshore ridge reduced windspeeds and produced a northwesterly flow.

The final week of the TOWARD experiment covered 25 to 28 March. A gradual wind shift accompanied by light to moderate winds can be seen on the 25th. Synoptic charts for that date show a front passing through the San Diego area between 1000 and 1600 local time, at an approximate rate of 4-5 m/s. As it moved westward, the low deepened and the frontal band remained southeast of San Diego through 1000 on the 26th. The winds reflect this frontal movement. A shift in direction to a more typical northwesterly flow occurs in late morning and a sea breeze pattern is apparent by late afternoon. The maximum wind speed recorded was about 7 m/s at 1715.

Winds on the 27th were out of the west-southwest and had generally higher magnitudes that those recorded the previous day. These values ranged from a mimimum of about 3 m/s to a maximum of just over 8 m/s at 1015. This maximum is supported by synoptic charts for 1000 that depict a strong,

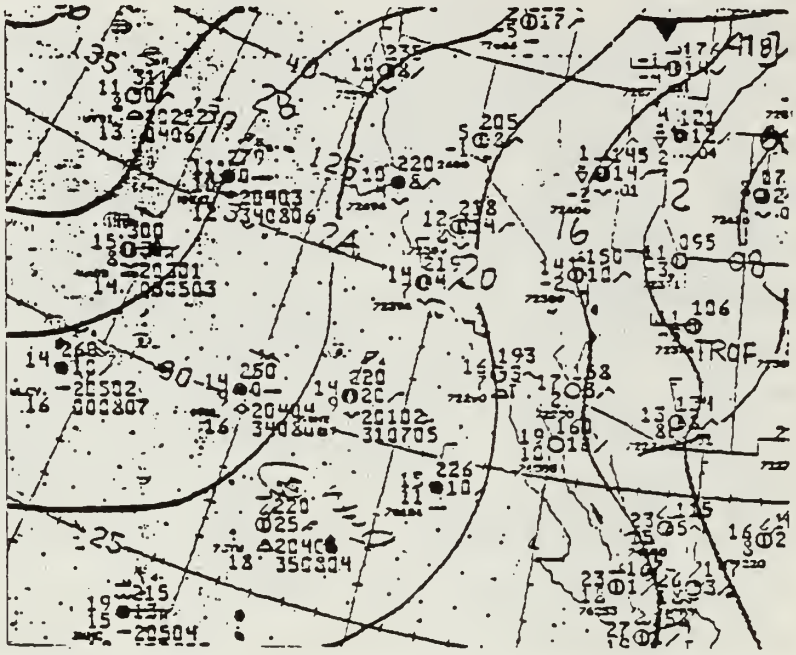

(a)

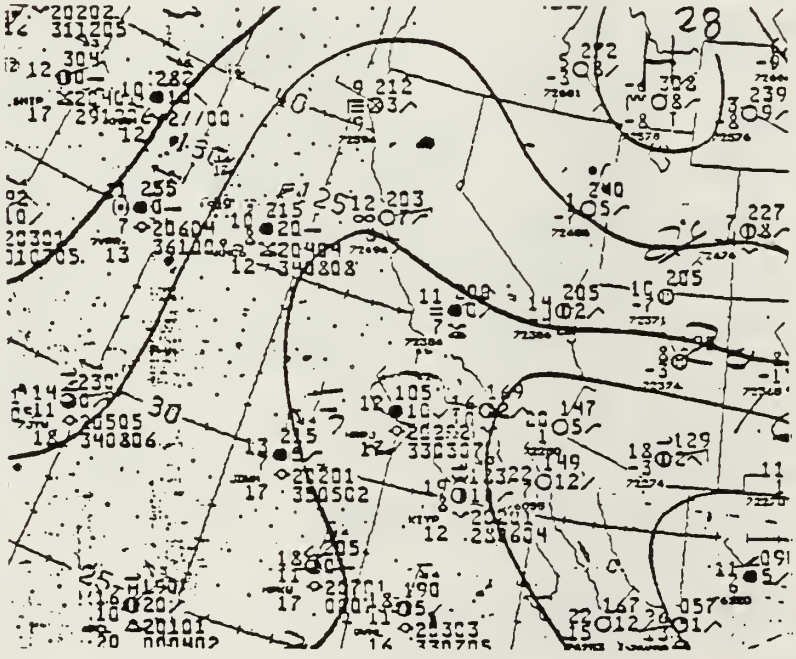

(b)

Figure 3.13 Surface analyses 1800 GMT 12 (a) and 13 (b) March 1985.

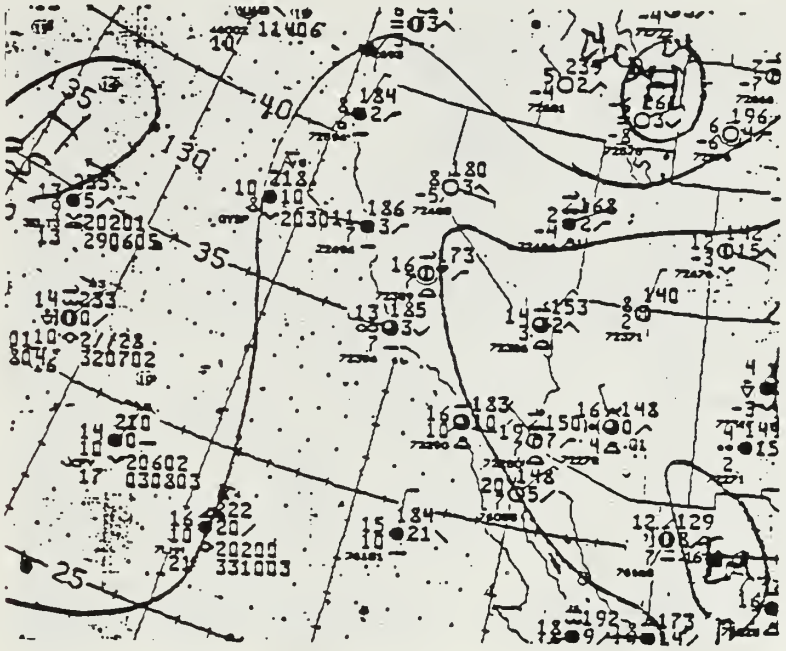

(a)

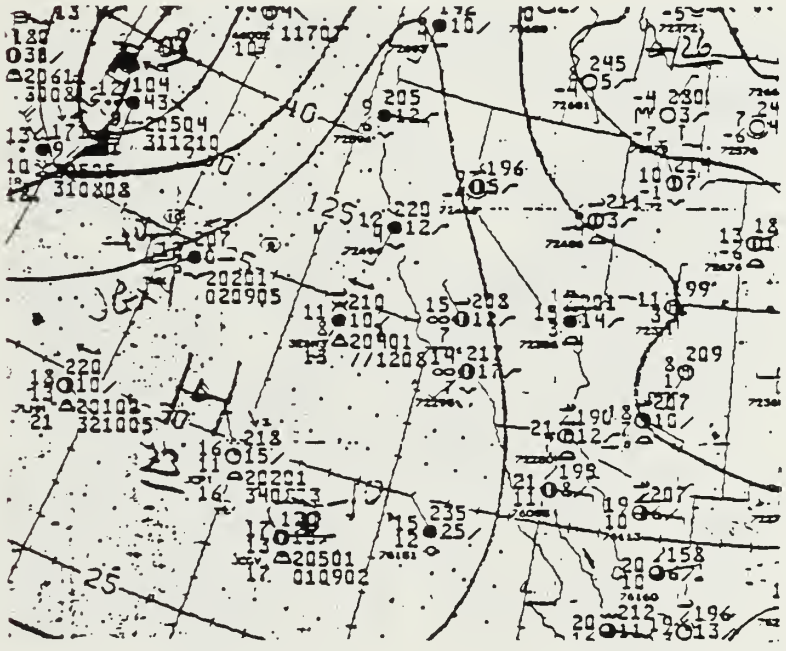

(b)

Figure 3.14 Surface analyses 1800 GMT 15 (a) and 16 (b) March 1985.

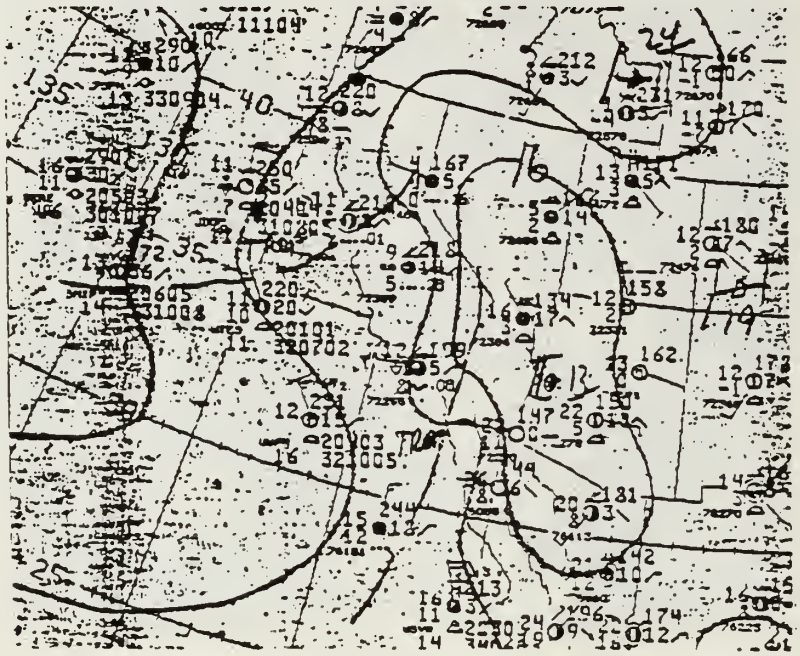

(a)

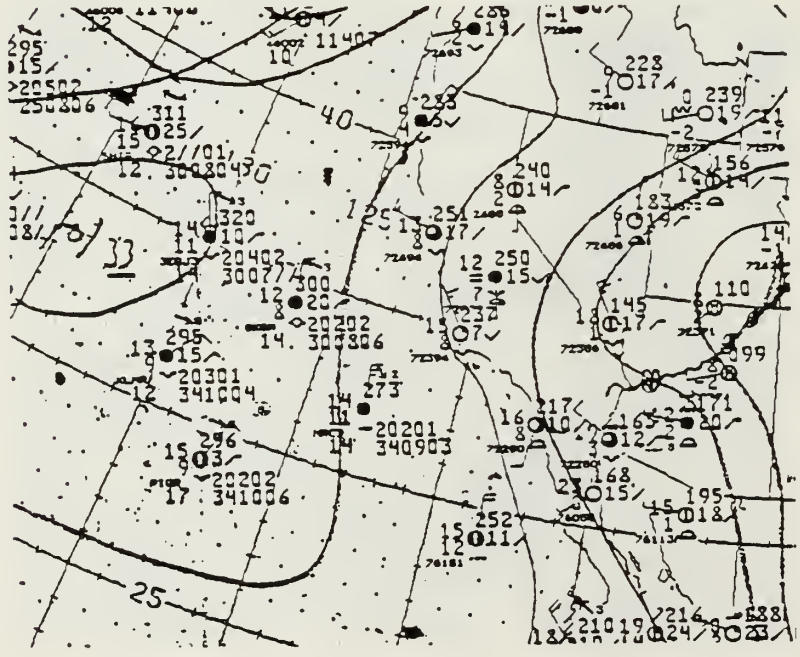

(b)

Figure 3.15 Surface analyses 1800 GMT 18 (a) and 19 (b) March 1985.

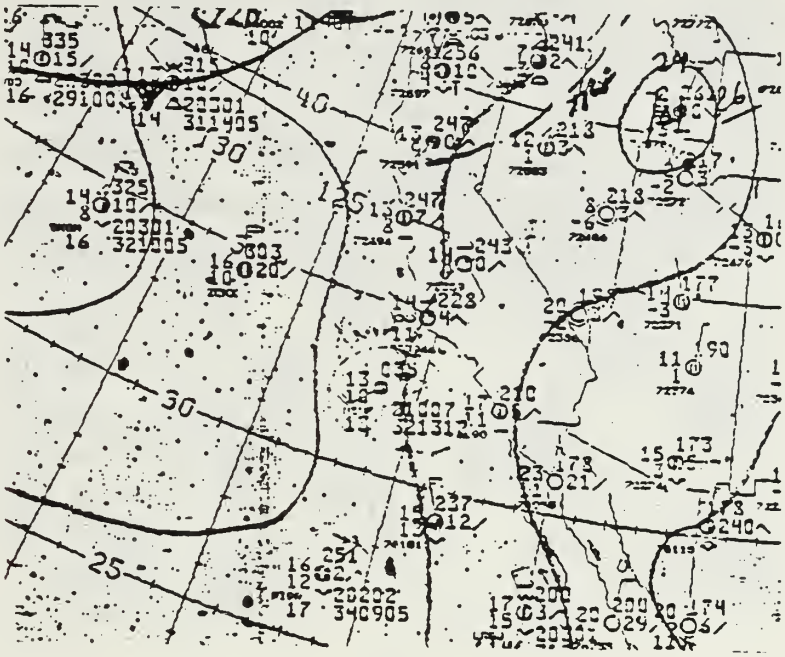

(a)

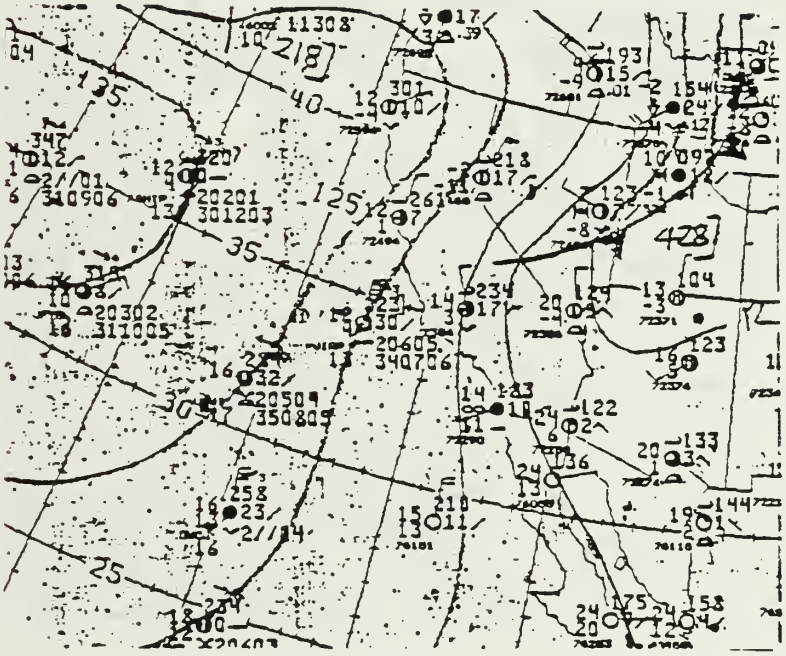

(b)

Figure 3.16 Surface analyses 1800 GMT 20 (a) and 21 (b) March 1985.

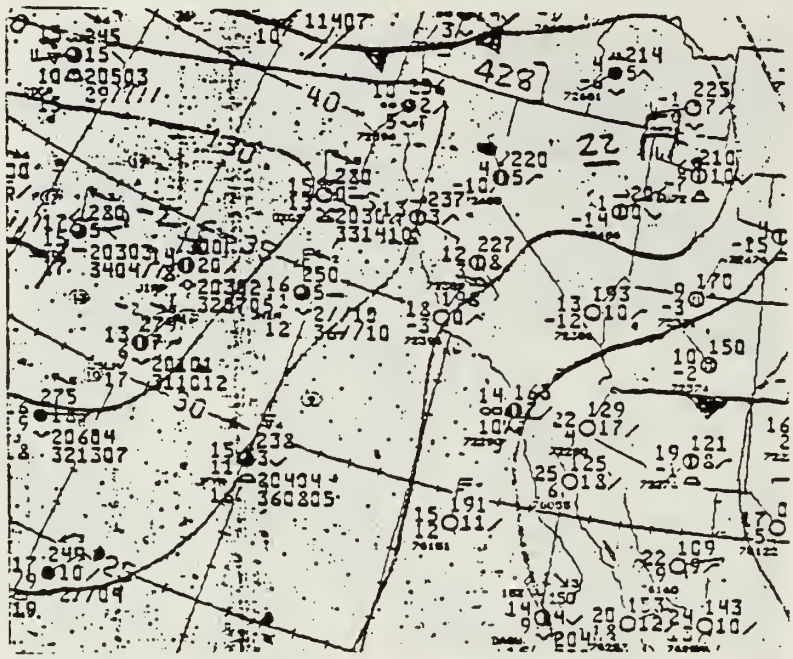

(a)

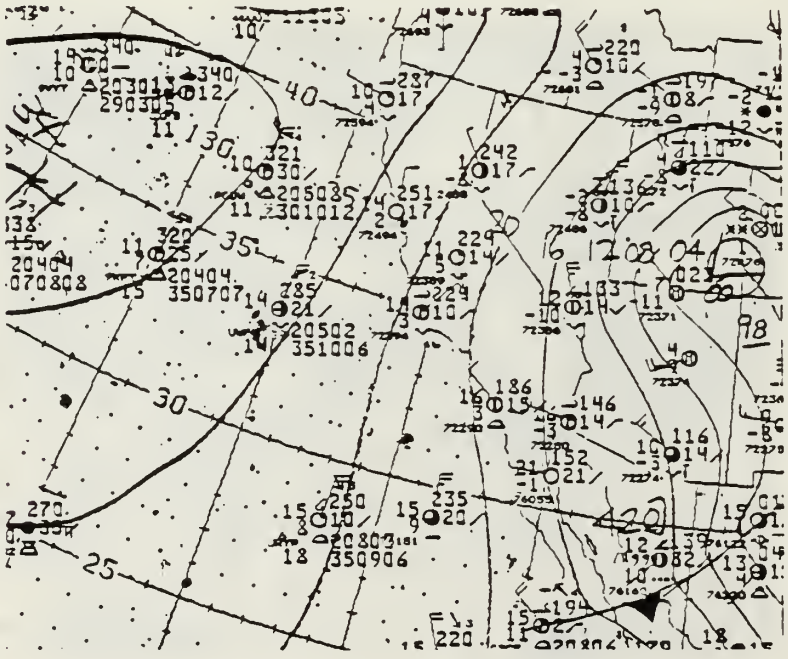

(b)

Figure 3.17 Surface analyses 1800 GMT 22 (a) and 24 (b) March 1985.

large-scale pressure gradient associated with a deep low center over Vancouver, Canada. This system quickly moved southeast, where the low center deepened over Arizona and New Mexico for the next several days. The result was a tight pressure gradient which produced the high wind values collected on 28 March. On that date, a maximum wind value of over 12 m/s was recorded at 1415.

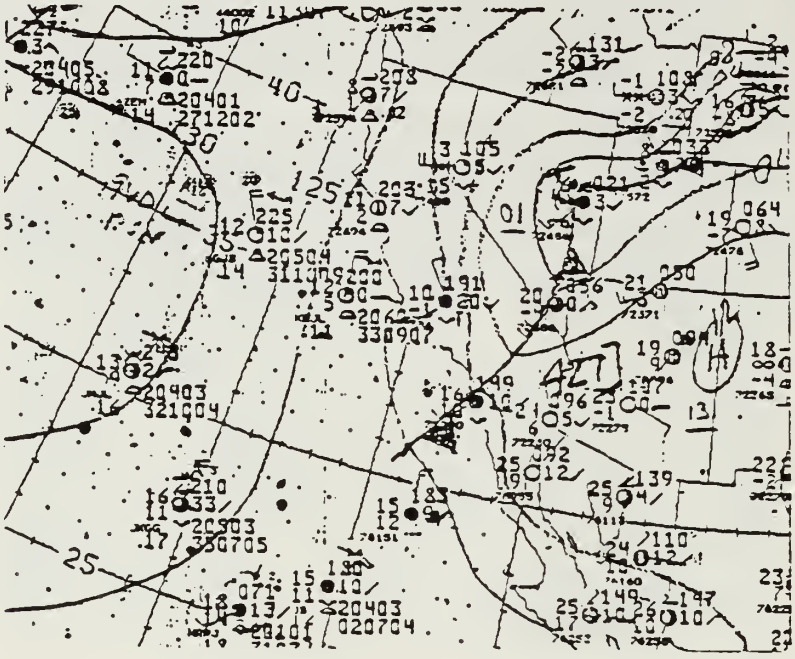

(a)

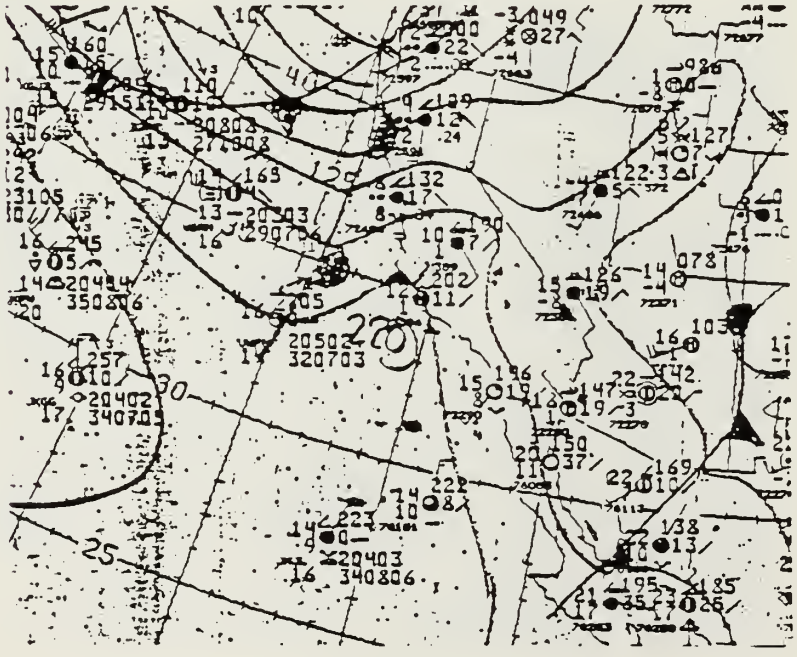

(b)

Figure 3.18 Surface analyses 1800 GMT 25 (a) and 26 (b) March 1985.

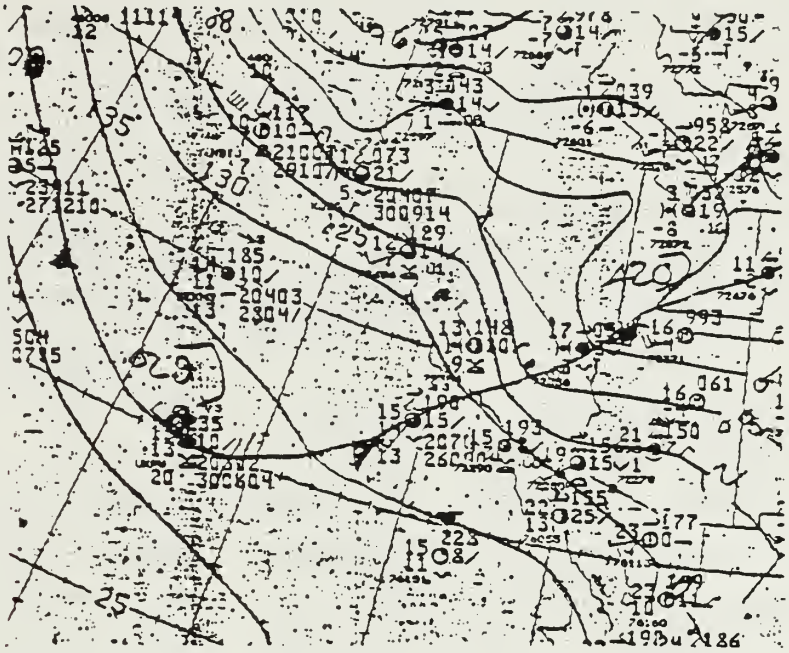

(a)

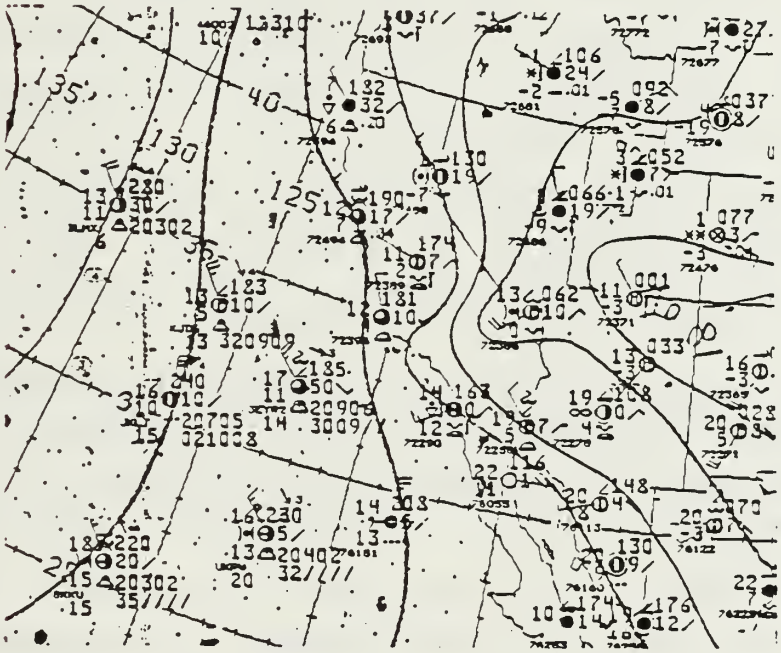

(b)

Figure 3.19 Surface analyses 1800 GMT 27 (a) and 28 (b) March 1985.

IV. DRAG COEFFICIENT RESULTS

A principal motivation of this thesis is to examine the variation of the sea-surface drag coefficient with varying wind and wave states. Since windspeed magnitudes were generally low to moderate (i.e. < 10-11 m/s) during both phases of TOWARD, the primary emphasis will be placed on C_{DN} variations as a function of wave state.

The question of whether the neutral drag coefficient is constant or increases with windspeed, wave state and fetch has received considerable study in recent years. Garratt (1977) summarized sea-surface drag coefficients from 17 experiments (based on eddy correlation and profile methods) published between 1967 and 1975. Observations of C_{DN} (representative of a height of 10 m) plotted as a function of U_{10} showed that Charnock's relation (Eqn. 26) was valid over a windspeed range of 4 to 21 m/s.

Large and Pond (1981) compared measurements of the momentum flux obtained by both Reynolds flux and dissipation methods. They reported that a comparison of both methods showed excellent agreement, on average, for windspeeds of 4-20 m/s. Large and Pond also plotted neutral drag coefficients against U_{10}. Although they found a slight increase in the average C_{DN} with windspeeds below 10 m/s, they felt that this relationship could be adequately described by a constant, where:

$$10^3 C_{DN} = 1.14 \qquad 4 < U_{10} < 10 \text{ m/s} \qquad (59)$$

Above 10 m/s, the values of C_{DN} demonstrated a more rapid, linear increase up to windspeeds of 26 m/s.

Smith (1980) used the eddy correlation method to obtain windspeed and heat flux measurements over the windspeed

range of 6-22 m/s. He noted that the Charnock relation also held for neutral sea-surface drag coefficients measured for long fetch. These C_{DN} values were clearly seen to increase with increasing windspeed. Several points were not adequately explained by the Charnock hypothesis, however. These included:

1. The dependence of the drag coefficient on windspeed was greater than predicted if the data at low windspeeds were not included.

2. If the data in Garratt's summary are viewed separately at windspeeds both above and below 10 m/s, the drag coefficient also appears to be nearly constant at windspeeds below 10 m/s. Smith's average C_{DN} value for low windspeeds was $(1.11)10^3$. At higher windspeeds, this coeffcient tends to increase rapidly as a function of windspeed.

Thus, all three studies indicate a relatively constant C_{DN} value at windspeeds below 10 m/s. It follows then that variations in the neutral drag coefficient at low to moderate windspeeds must be due to changes in the sea state.

Garratt did not explore the behavior of C_{DN} with respect to fetch or sea state. He felt that current quantitative information was insufficient to adequately determine the dependence of the drag coefficient on factors other than windspeed.

Large and Pond found the C_{DN} to be largely independent of fetch. For both long and short fetches, the mean drag coefficient remained at 1.14×10^3 for windspeeds less than 10 m/s.

Smith's comparison of C_{DN} with fetch showed higher drag coefficients at short fetches than those at longer fetches. This is to be expected since at short fetches actively growing waves absorb momentum from the wind while waves at longer fetches tend to be more in equilibrium with the wind field.

Smith also considered the variation of the neutral drag coefficient with sea state. A linear regression of C_{D10} vs. rms-wave height showed an increase in C_{DN} with an increase in wave height, although the correlation coefficient was rather low (.58).

More recent studies have included a drag coefficient model discussed by Geernaert (1985a). Geernaert found the model exhibited considerable sensitivity to fetch. The influence of fetch on the model calculations was due to the wave spectral variations incurred by the dependence of the Phillips coefficient on the wave saturation parameter, Co/U_*, where Co represents the phase speed. Geernaert observed that high drag coefficients often resulted from fetch limited conditions.

Wu (1985) also looked at fetch as influenced by the Phillips spectral coefficient. He found larger spectral coefficients at shorter fetches than those at longer fetches.

Measurements of the neutral drag coefficient over the sea by all methods often yield considerable scatter and the data must be carefully edited. Several types of data have been removed from this analysis based on dissipation methods. They include:

1. Data collected during rain or fog conditions. Water droplets striking the hot film result in latent heat release. This sudden cooling induces a large jump in voltage, producing spikes in the data. In the inertial subrange particularly, noise from droplet contact contaminates the high frequencies and results in very large drag coefficient estimates.

2. Periods of light winds also produce erratic C_{DN} values as a result of convection off the tower mast.

3. Flow distortion is a problem with light or moderate winds, particularly from the south. The best direction for data collection is from west to north.

4. Radio transmissions, particularly in the autumn, also posed problems. The hot films serve as antennae for transmitted energy, occasionally producing unreliable C_{DN} values.

Analysis was based on plotting C_{DN} as a function of U_{10}, as in the earlier studies by Garratt, Large and Pond, and Smith (Fig. 4.1). The data were then separated into two sets in order to compare short and long fetch conditions. Short fetch waves occurred when winds originated from north to east (Fig. 4.2), while long fetch conditions were approximated during west to northwesterly winds (Fig. 4.3).

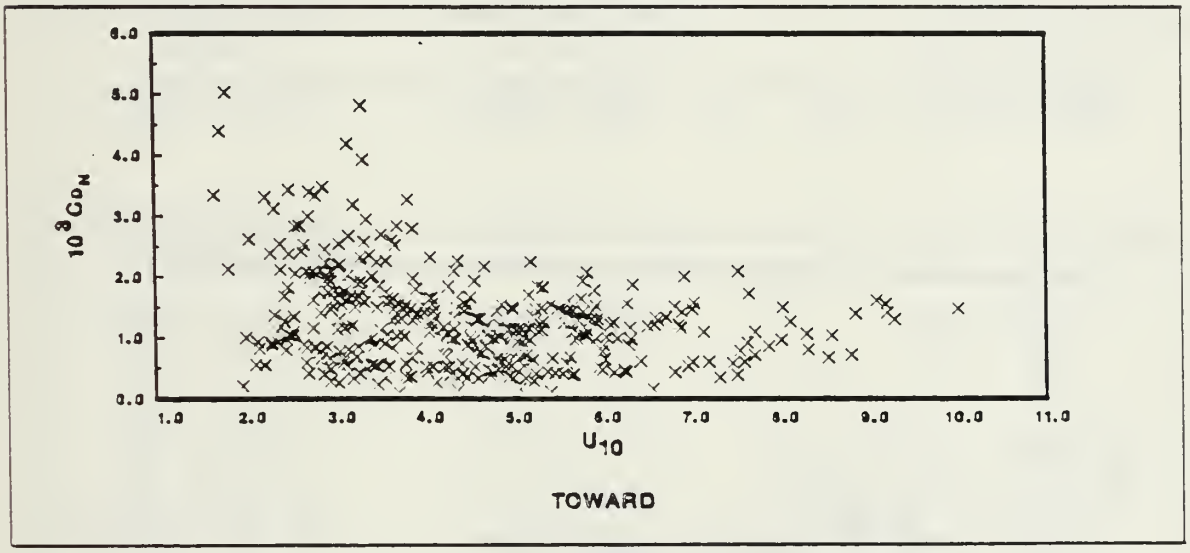

Figure 4.1 C_{DN} vs U_{10} for long and short fetches.

C_{DN} was again plotted against U_{10} for each fetch condition. The mean and standard deviation for each 1 m/s velocity band was calculated and can be found in Table III.

Table III indicates that higher drag coefficient values did result from short fetch conditions. Mean C_{DN} values for both the 2-3 and 3-4 m/s bands under short fetch conditions significantly exceeded those for long fetch.

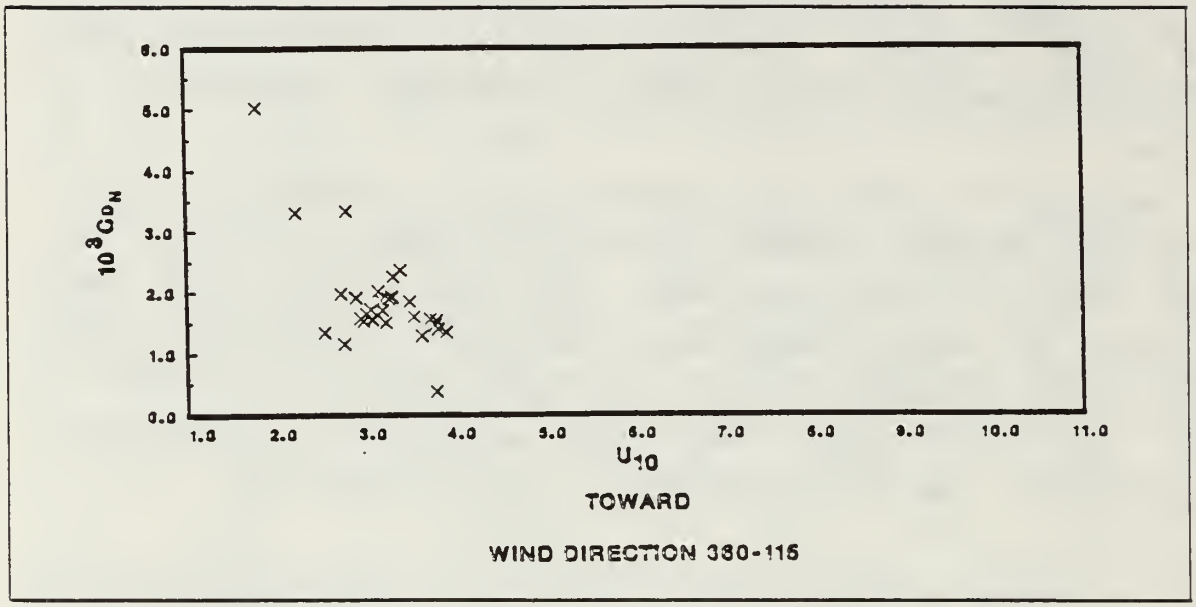

Figure 4.2 C_{DN} vs U_{10} for short fetch conditions.

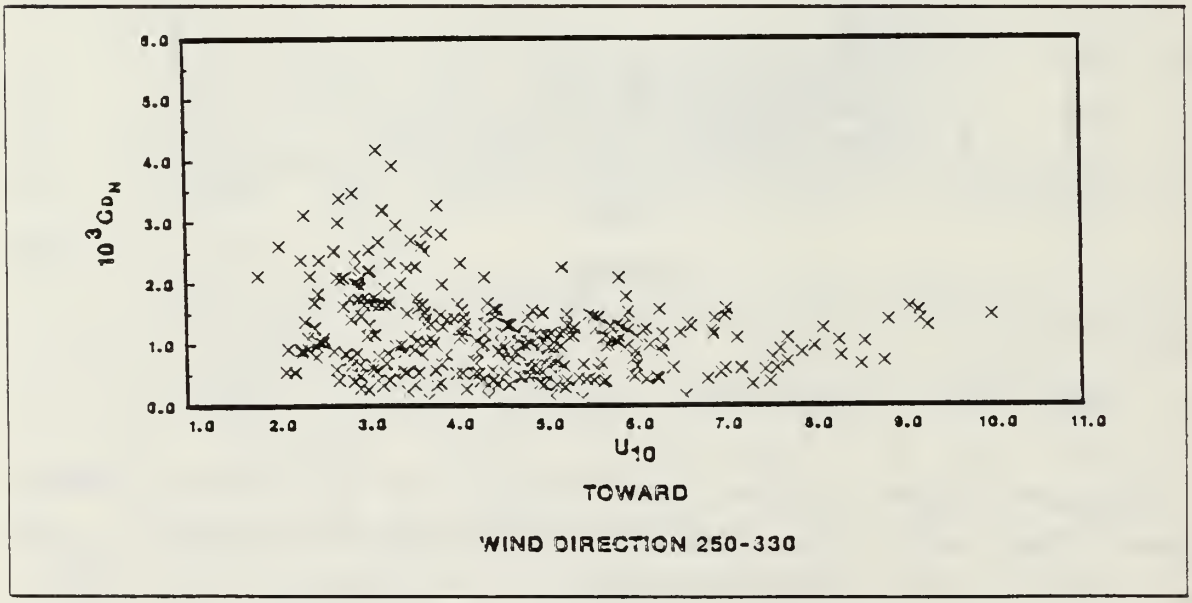

Figure 4.3 C_{DN} vs U_{10} for long fetch conditions.

C_{DN} values for long fetch conditions also varied and were not constant as earlier predicted. Magnitudes were

TABLE IV

C_{DN} vs. U_{10} for Long and Short Fetches

SHORT FETCH CONDITIONS: 360-115 DEGREES

1.0-2.0 m/s	2.0-3.0 m/s	3.0-4.0 m/s
(1 point)	(8 points)	(21 points)
value=5.027 s.d.=---	mean=2.017 s.d.=.851	mean=1.656 s.d.=.407

LONG FETCH CONDITIONS: 250-330 DEGREES

1.0-2.0 m/s	2.0-3.0 m/s	3.0-4.0 m/s
(1 point)	(53 points)	(81 points)
value=2.119 s.d.=---	mean=1.485 s.d.=.828	mean=1.432 s.d.=.850

4.0-5.0 m/s	5.0-6.0 m/s	6.0-7.0 m/s
(79 points)	(63 points)	(26 points)
mean=.955 s.d.=.442	mean=.980 s.d.=.444	mean=.896 s.d.=.377

7.0-8.0 m/s	8.0-9.0 m/s	9.0-10.0 m/s
(14 points)	(8 points)	(4 points)
mean=.856 s.d.=.463	mean=.939 s.d.=.254	mean=1.413 s.d.=.104

	10.0-11.0 m/s	
	(1 point)	
	value=1.479 s.d.=---	

fairly high for the 1-4 m/s bands, dropped off between 4-8 m/s, and subsequently increased between 8-11 m/s.

Overall, the dependence of the drag coefficient on windspeed was found to be insignificant above 4 m/s, based on scatter in the data as well as the large standard deviation at each windspeed interval. Below 4 m/s, each there was an apparent increase in the C_{DN} with a decrease in windspeed. These values are somewhat suspect, however, due to the uncertainty in the quality of the data at very low velocities.

Daily time series of wind stress were also examined, with both C_{DN} and U_* plotted against time. Lack of data, low winds or strong stability prevented a close examination of the wind stress in some instances. Several case studies are described below, however. Appendix A contains figures relevant to the discussion.

1. Frontal Cases: 15, 16-18 October and 26-29 March

Fig. A.6 shows the results when a front was passing the tower on 15 October. C_{DN} values ranged from .584 to 2.058. Magnitudes can be seen to rise with rising winds until 0900, fall with decreasing winds between 0900 to 1030, and remain fairly steady with the winds near constant values. A sharp drop in windspeed at 1200 did not produce a corresponding drop in C_{DN} values. C_{DN} increased during this period of low winds to a maximum at 1500, and then dropped off sharply. Synoptically, Fig. A.6 shows a wind shift between 1400-1500 for southerly to westerly winds with a corresponding increase in windspeed. C_{DN} values began rising shortly afterward and continued to increase up to the end of the sampling period depite a drop in windspeed beginning at approximately 1700.

A similar frontal case is presented in Fig. A.7 for 16-18 October. Both U_* and C_{DN} can be clearly seen to increase with rising winds to a maximum at 0600 on the 18th. A wind shift from southerly to northwesterly winds occurred

shortly after 6 am and several sharp drops in windspeed took place before the wind leveled off at approximately 6 m/s. The drag coefficient shows a similar trend but does not reflect the rapid decreases evident in the windspeed between 0500 to 0800.

On 26-29 March, passage of a front as well as southerly winds produce high C_{DN} values with considerable scatter (Fig. A.31).

In each of these frontal cases, C_{DN} increased just before passage of the front. This trend is consistent with an earlier study by Denman and Miyake (1973) in which drag coefficients were seen to increase on the leading edge of a storm, and then decrease slightly or remain constant. They attributed this behavior to the nature of the wave field. Geernaert (1985b) also observed higher drag coefficients preceding an approaching front. He postulated that wave fields far ahead of and behind cold fronts are semi-independent of one another and are generally in equilibrim with local winds. Waves generated behind the front, often in a direction perpendicular to the baroclinic zone, can under certain circumstances travel through the front and interact with the wave field just ahead of it. Since the waves in the warm sector often run parallel to the local winds, the convergence of the two fields produces a much more energetic sea state just ahead of the front. The result would be higher C_{DN} estimates.

2. Sea Breeze Cases: 18, 27, 29 October and 13, 15, 18 March

The sea breeze effect is apparent in much of the data from the TOWARD experiment. On each of the above dates (Figs. A.8, A.12, A.14, A.22, A.23 and A.25), the C_{DN} rises sharply and then decreases slowly to near equilibrium. Described in terms of surface roughness, drag coefficient

values are known to increase with growing wave state. As the wave field becomes increasingly saturated with momentum, absorption of energy slows, resulting in drag coefficients that approach a smaller and more constant value.

3. Shift from Long to Short Fetch Conditions: 3-5 November

Data from 3-5 November depict a shift from long to short fetch conditions. Long fetch conditions are present until approximately 2300 on 3 November, as indicated by northwesterly winds. The drag coefficient estimates (Fig. A.18) are correspondingly low. With the shift to northerly winds at 2300, a sharp increase can be seen in C_{DN}. Although these values decline over the next three hours, they again increase due to the variable wind direction produced by a series of wind shifts on the 4th.

4. Variable Winds: 7 November

High C_{DN} values as result of variable wind directions can be seen between 0900 to 1200 on 7 November (Fig. A.20). Magnitudes become more constant as winds shift to a steadier direction.

5. Long Fetch and a C_{DN} Decrease with Time: 16,19, 22 March

These examples indicate long fetch conditions due to the northwesterly winds, as well as a general decrease in C_{DN} with time (Figs. A.24, A.26 and A.29). Since long fetch waves are known to be more steady state, they tend to absorb less momentum than would short fetch waves. Consequently, the drag coefficient estimates have lower magnitudes and tend to approach a constant value more rapidly than those seen in earlier examples.

In summary, case studies suggest a C_{DN} dependence on sea state as illustrated by both surface roughness and the degree of equilibrium between U_{10} and the waves (i.e. the amount of momentum entering the wave field for growth). Basic to this hypothesis on wind-wave coupling is that C_{DN} is generally independent of U_{10} for windspeeds between 4-9 m/s, and that the large amount of scatter is associated with systematic trends in sea state, such as frontal and sea breeze conditions. This scatter should be reduced once wave state is incorporated as an additional parameter in C_{DN} formulations.

V. SUMMARY AND CONCLUSIONS

Surface layer measurements covering a wide range of windpeeds have been analyzed for both phases of the TOWARD experiment. These measurements have been correlated with relevant mesoscale and synoptic features. The results were then interpreted relative to the C_{DN}.

Neutral drag coefficient values for both phases of TOWARD showed no significant windspeed dependence in the range between 4 and 9 m/s. The mean value was determined to be $(.94 \pm 0.4)10^3$, which is somewhat smaller than results obtained by Smith (1980) and Large and Pond (1981). These differences appear to be insignificant, however, due to the scatter present in all three data sets. C_{DN} values are higher for windspeeds less than 4 m/sec, but these values are suspect as low windspeeds often produce unreliable drag coefficient estimates.

Definite trends were observed in C_{DN} with fetch and sea state. Short fetch conditions produced generally higher C_{DN} values than those for long fetch. Trends in sea state such as frontal and sea breeze conditions were reflected in drag coefficient estimates as well. As with Large and Pond, C_{DN} estimates were seen to increase sharply just prior to the passage of a front. During sea breeze conditions, the C_{DN} values increased with time. As windspeeds and the wave field reached equilibrium, however, the drag coefficients decreased toward a more constant value.

APPENDIX A
TOWARD DAILY TIME SERIES

This appendix contains daily time series for wind speed and direction, air and sea surface temperatures, the neutral drag coefficient and U_*, for both phases of the TOWARD experiment. These figures provide a reference for the discussion provided in chapters three and four.

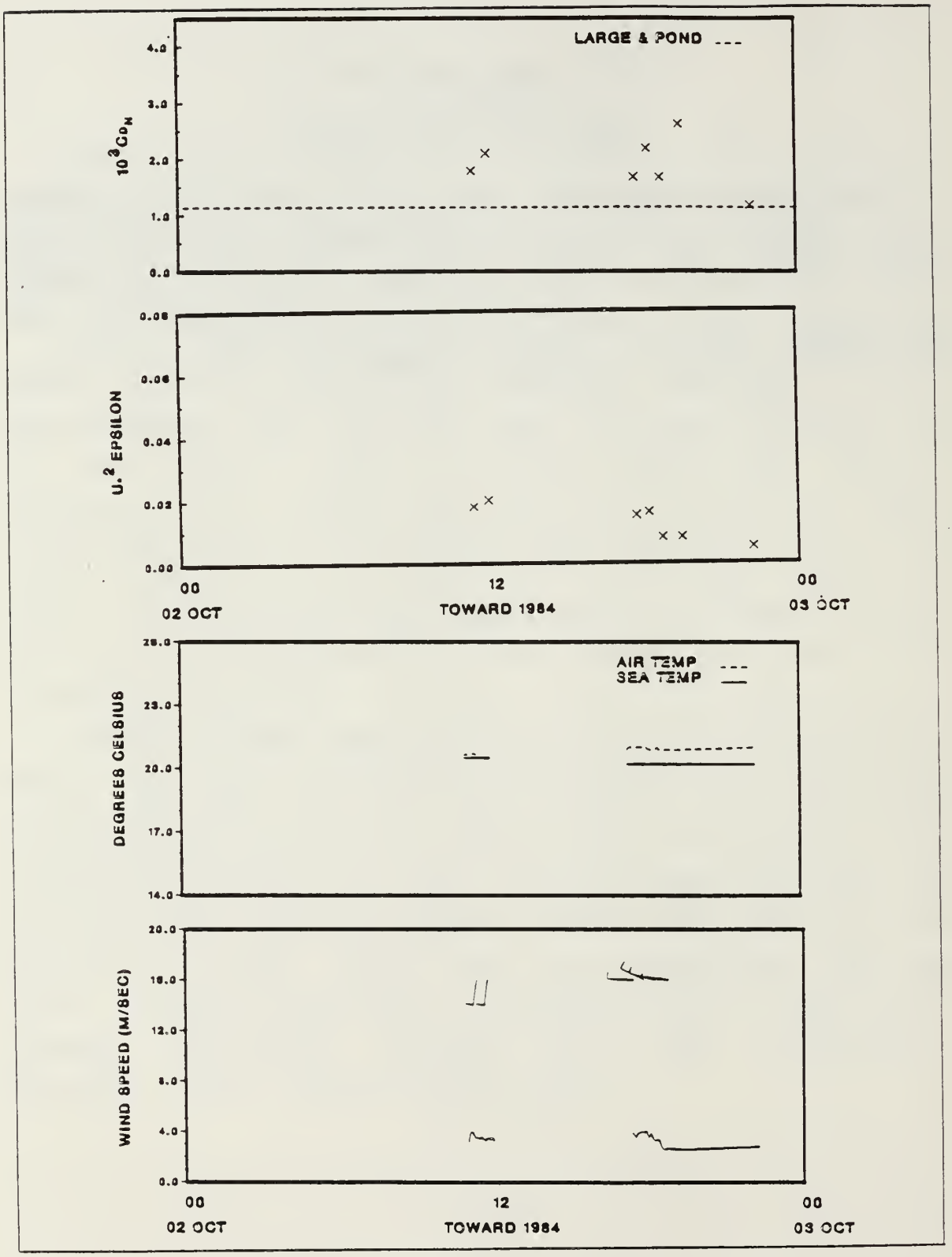

Figure A.1 2 October 1984.

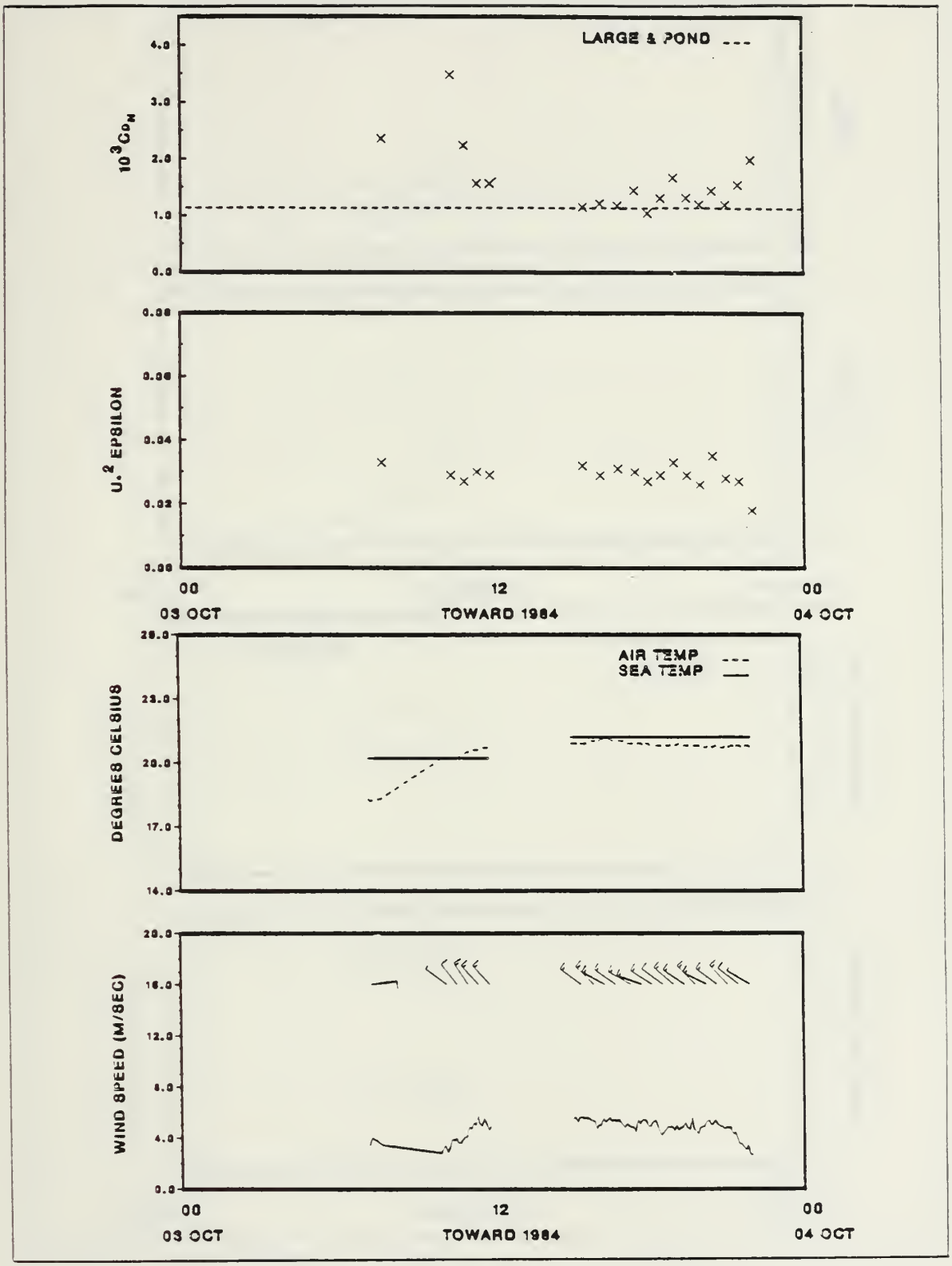

Figure A.2 3 October 1984.

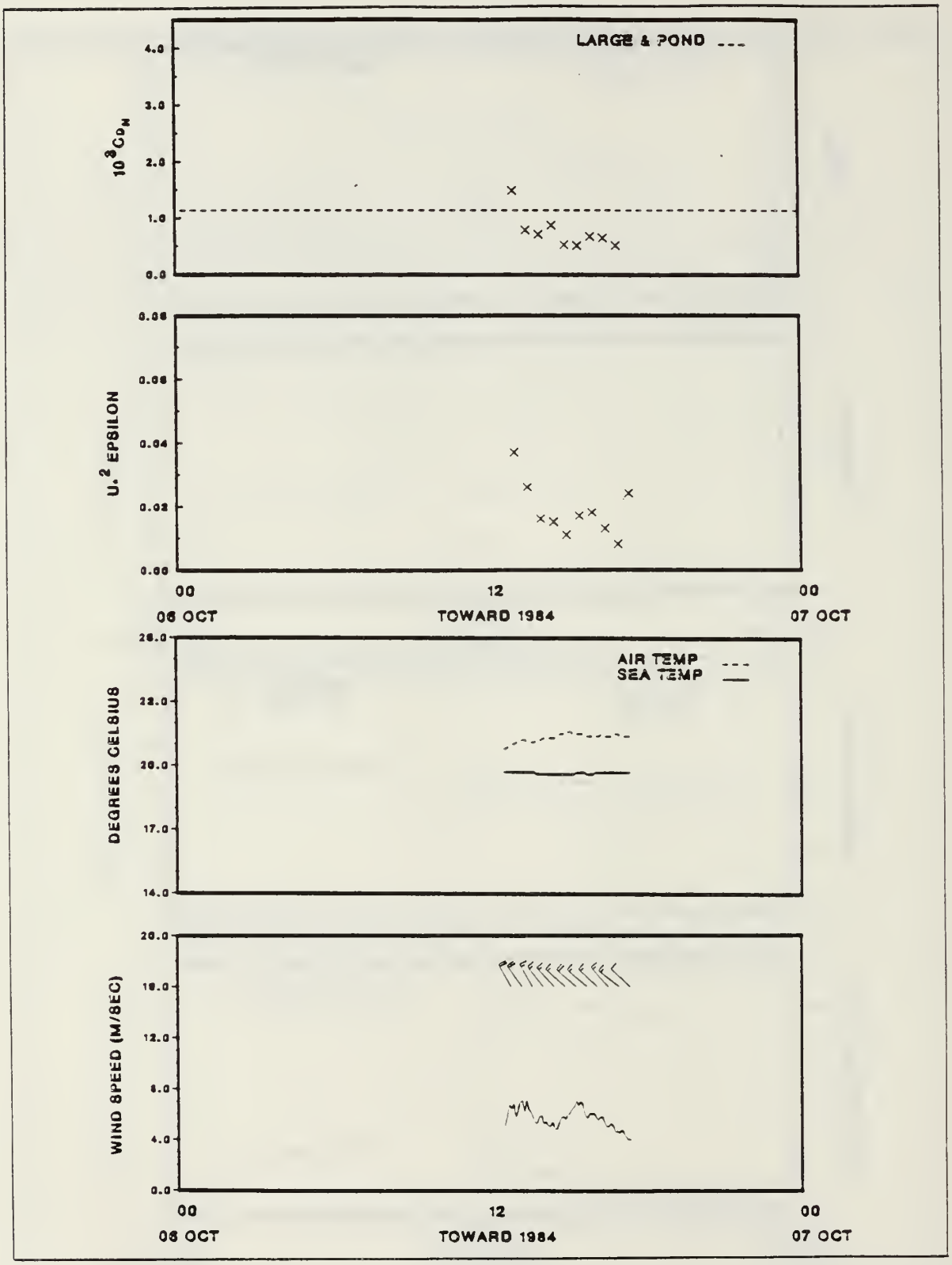

Figure A.3 6 October 1984.

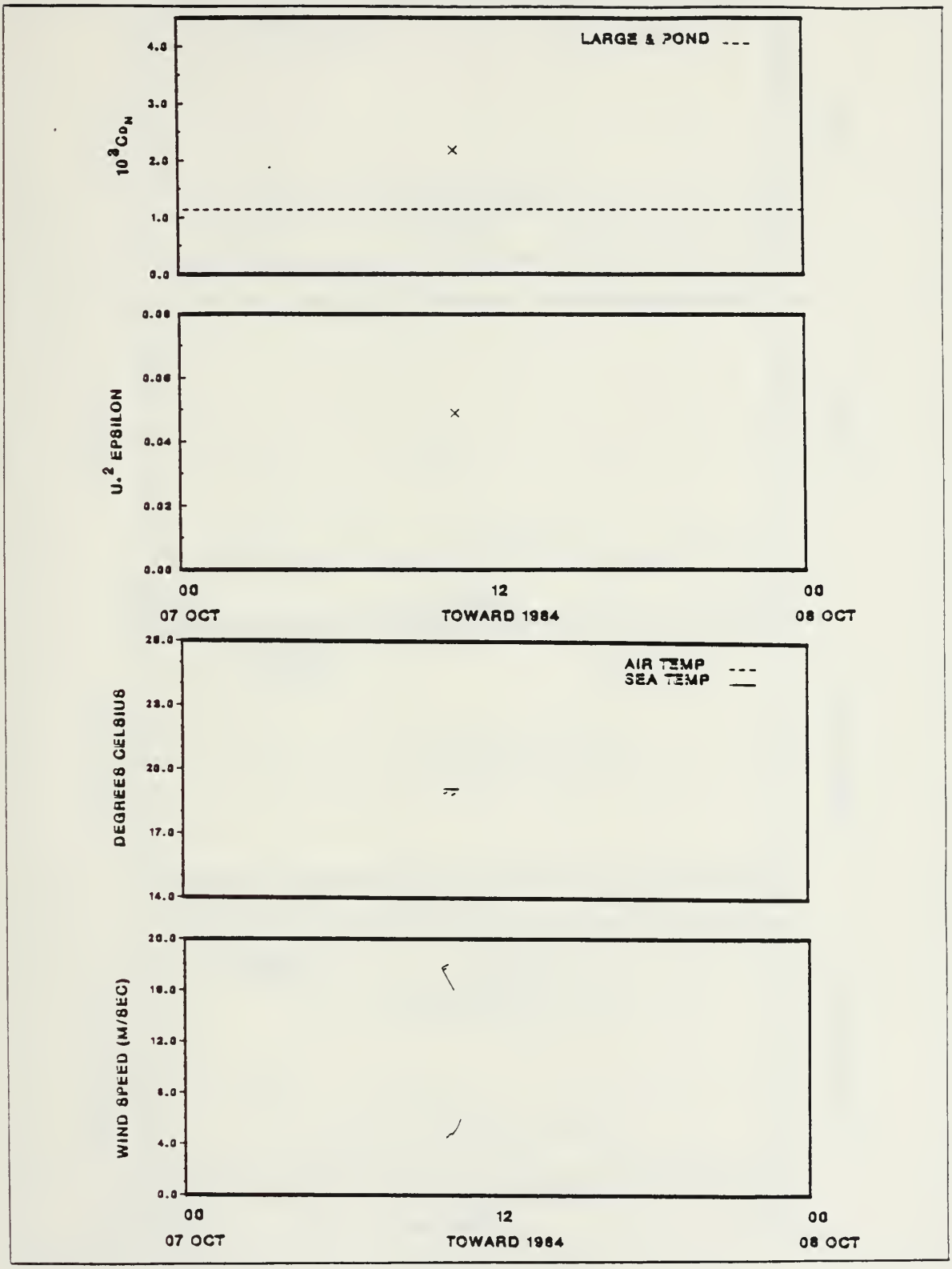

Figure A.4 7 October 1984.

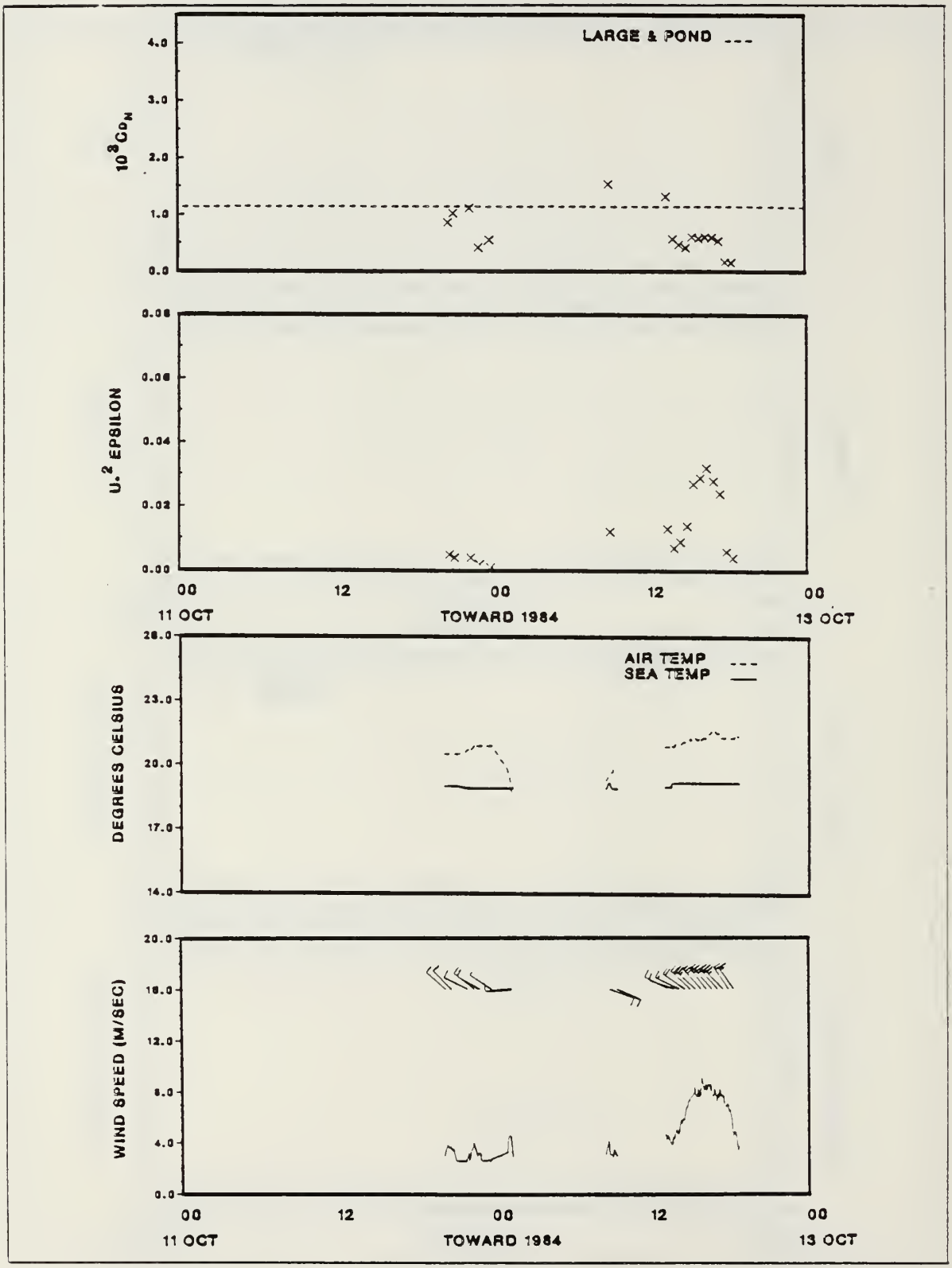

Figure A.5 11 to 13 October 1984.

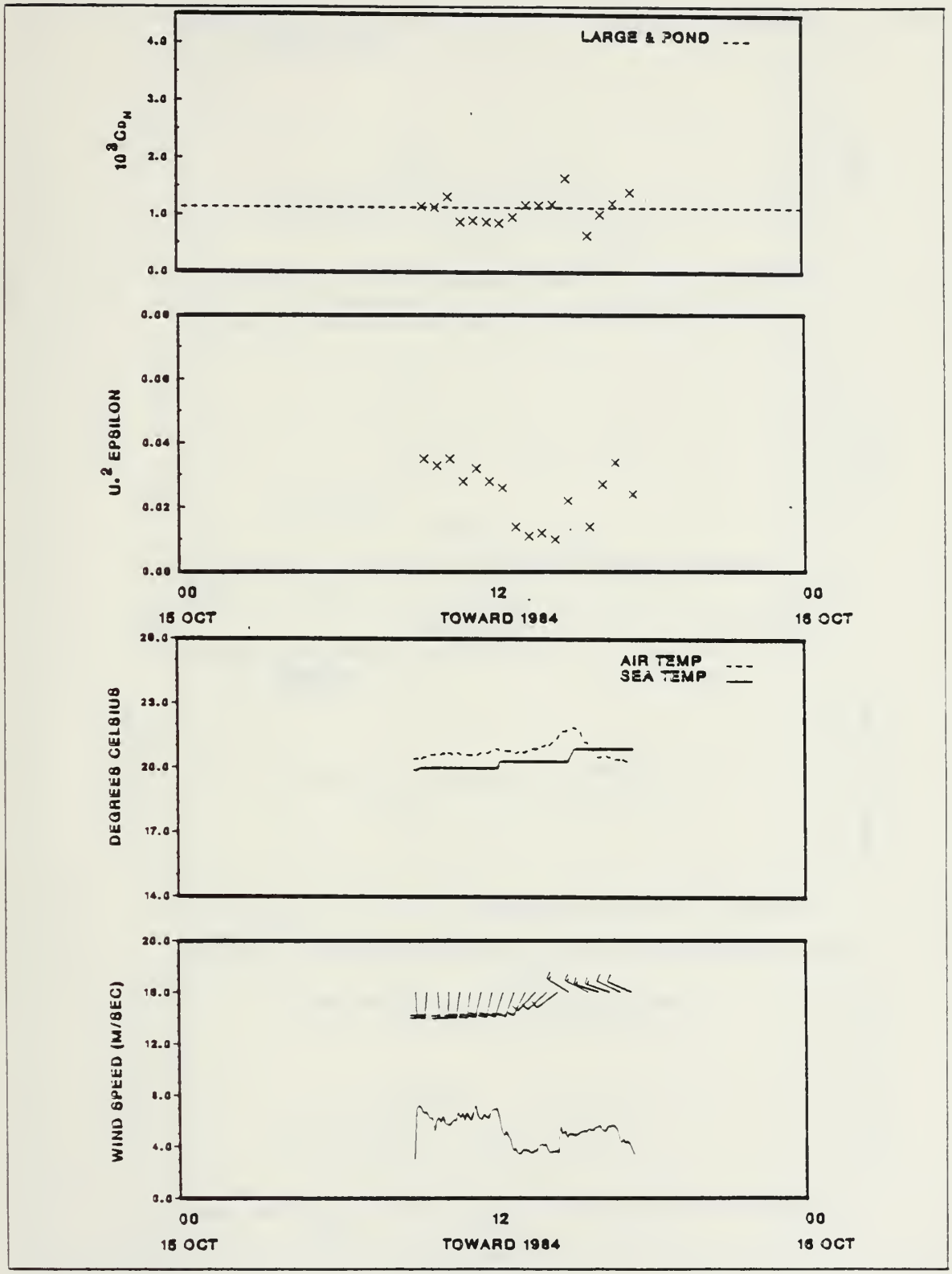

Figure A.6 15 October 1984.

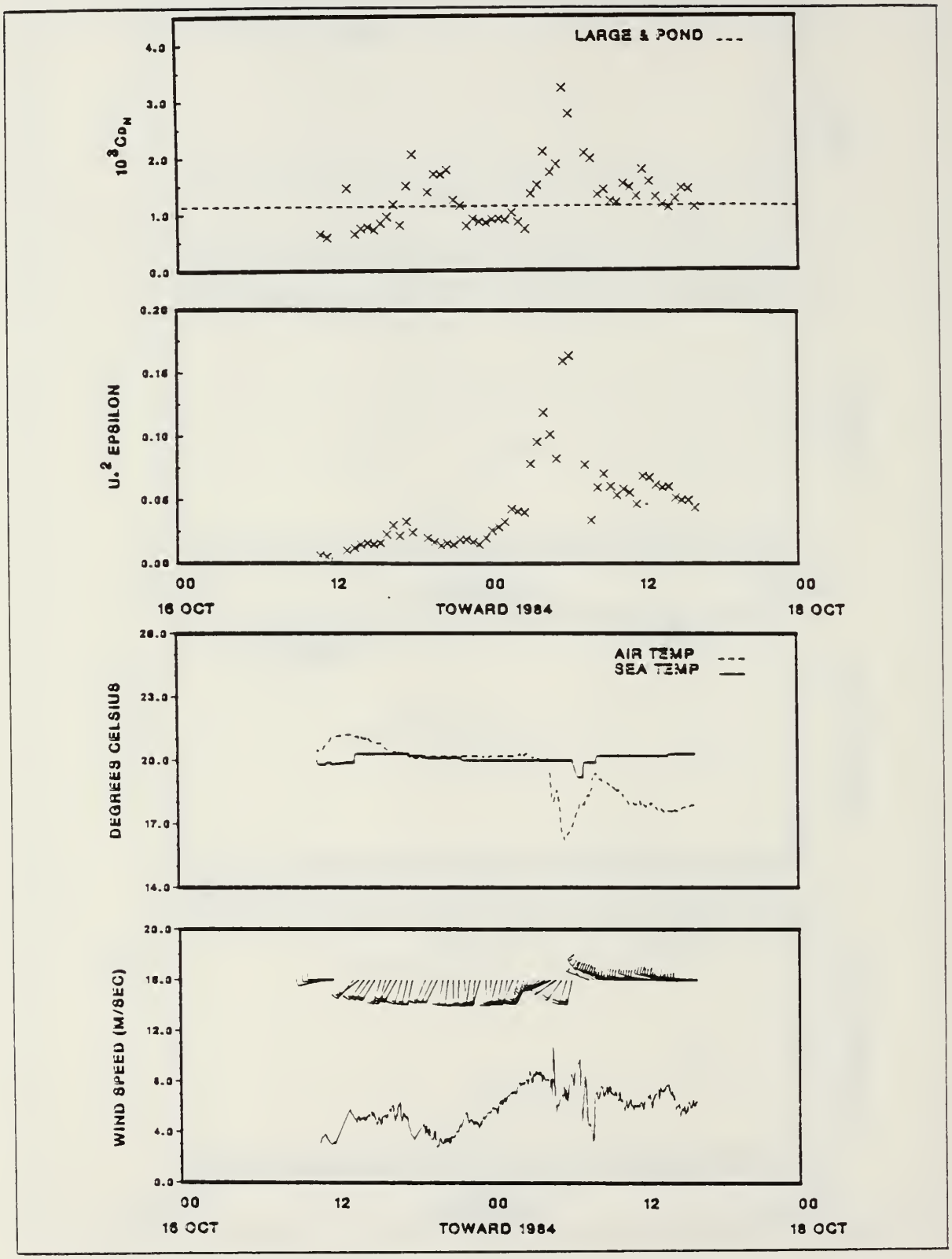

Figure A.7 16 to 18 October 1984.

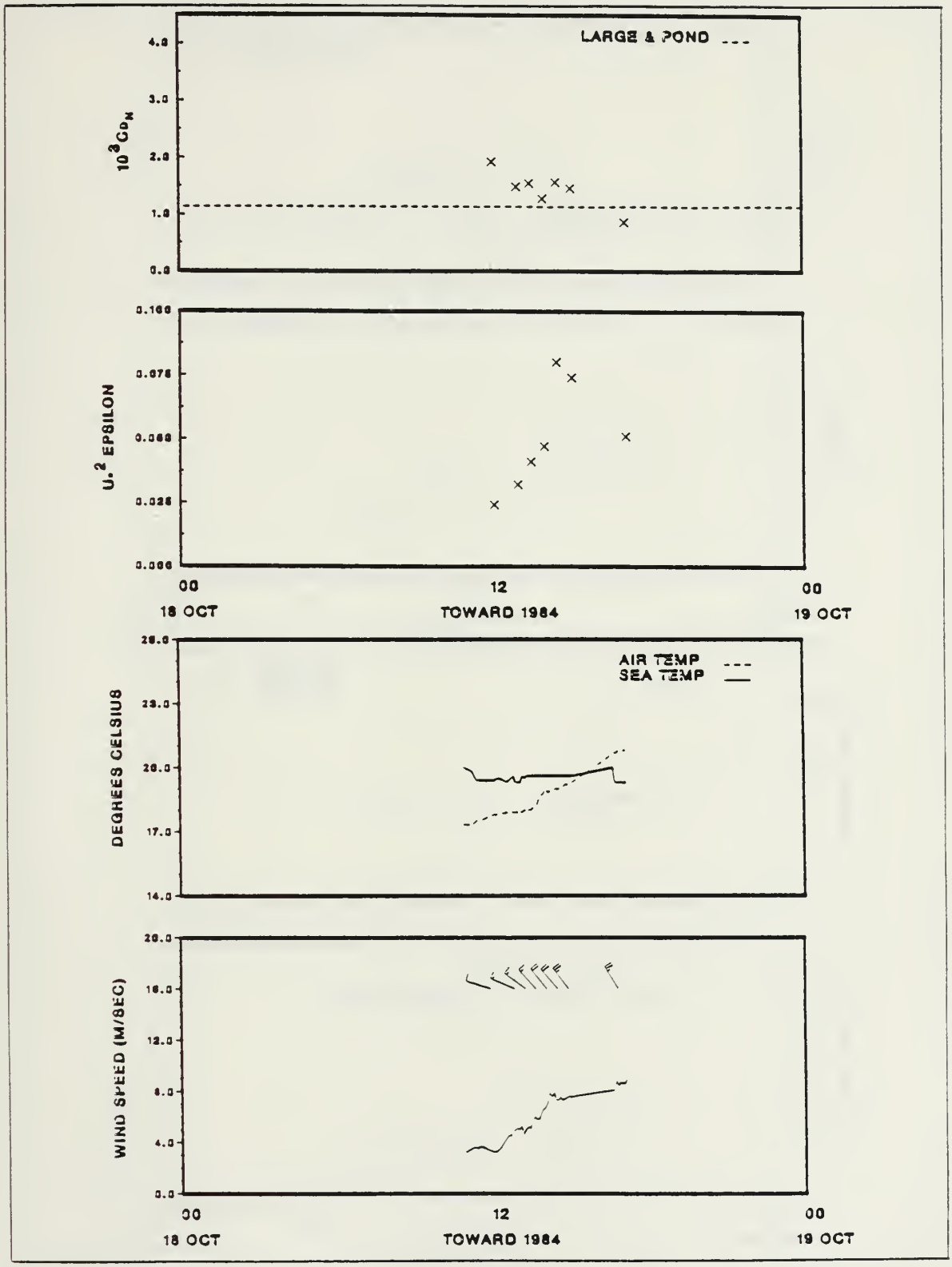

Figure A.8 18 October 1984.

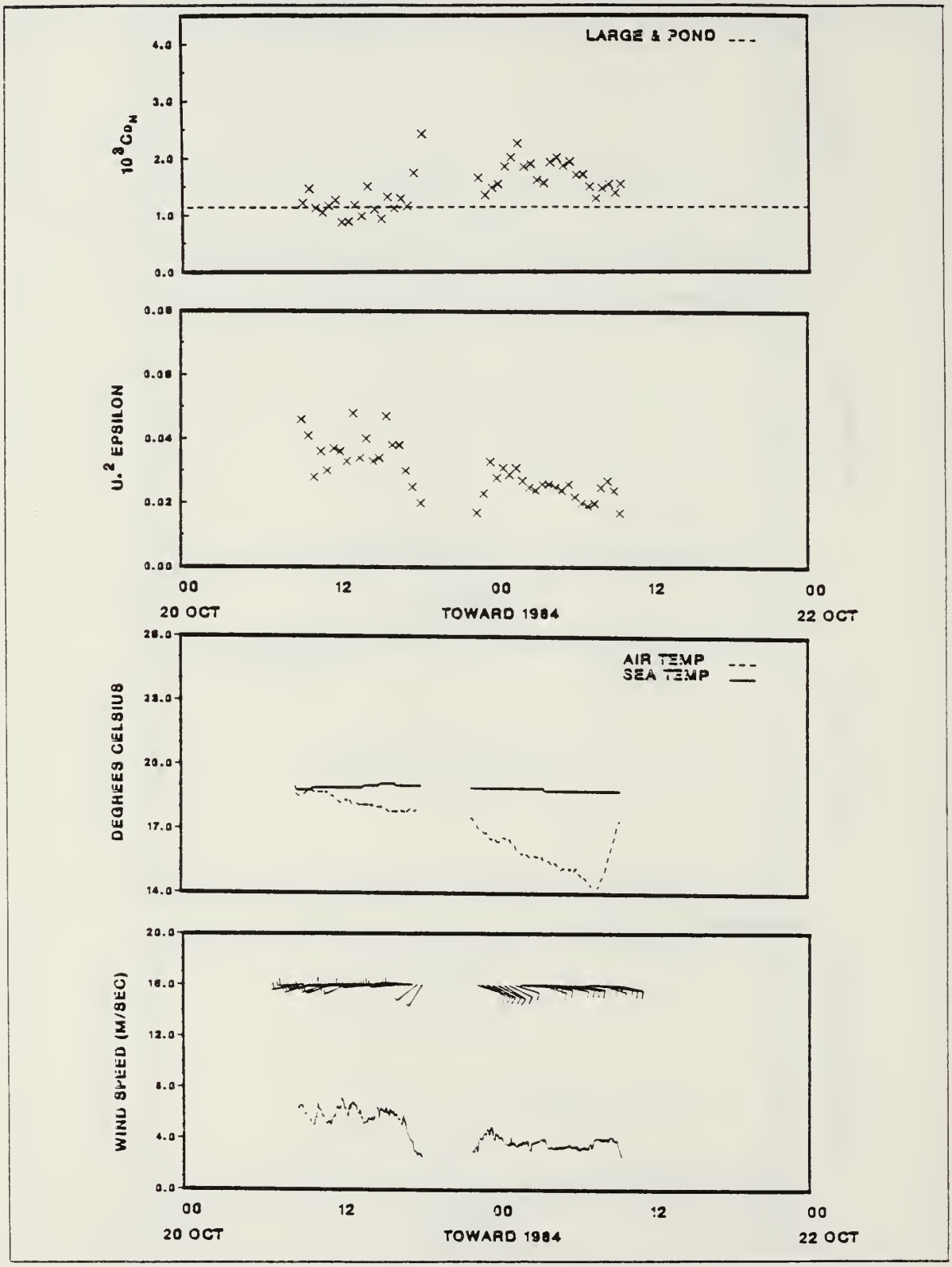

Figure A.9 20 to 22 October 1984.

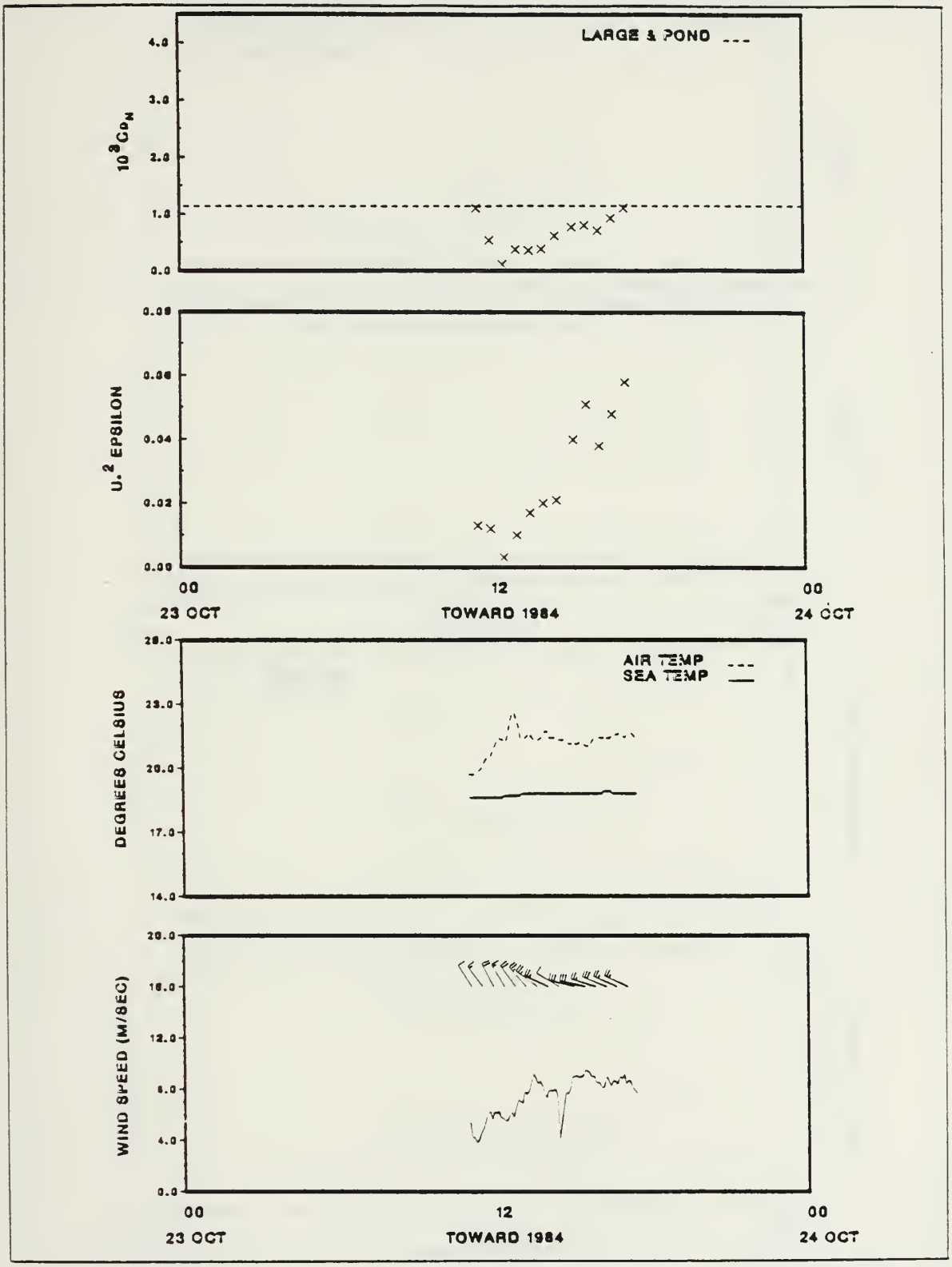

Figure A.10 23 October 1984.

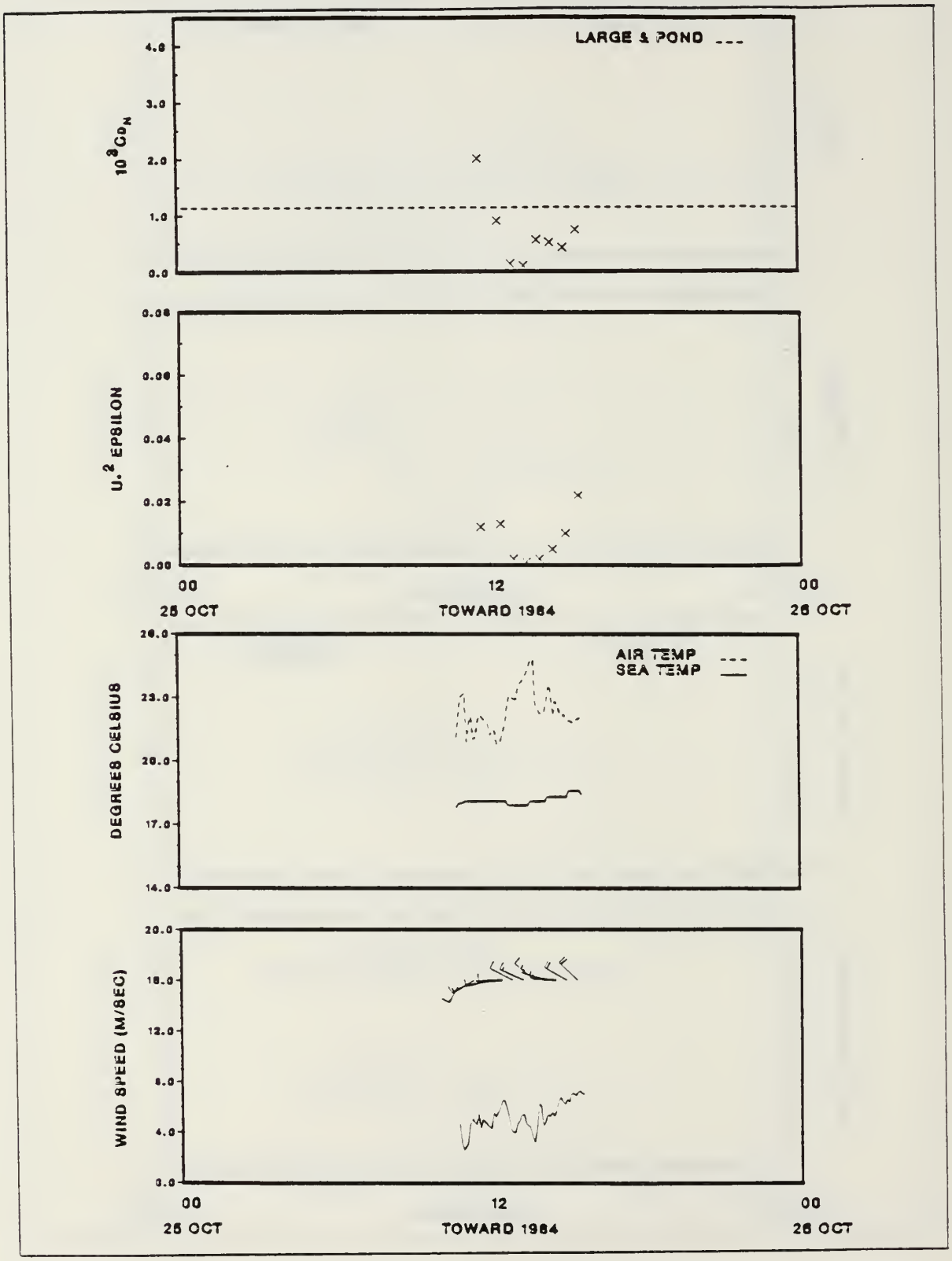

Figure A.11 25 October 1984.

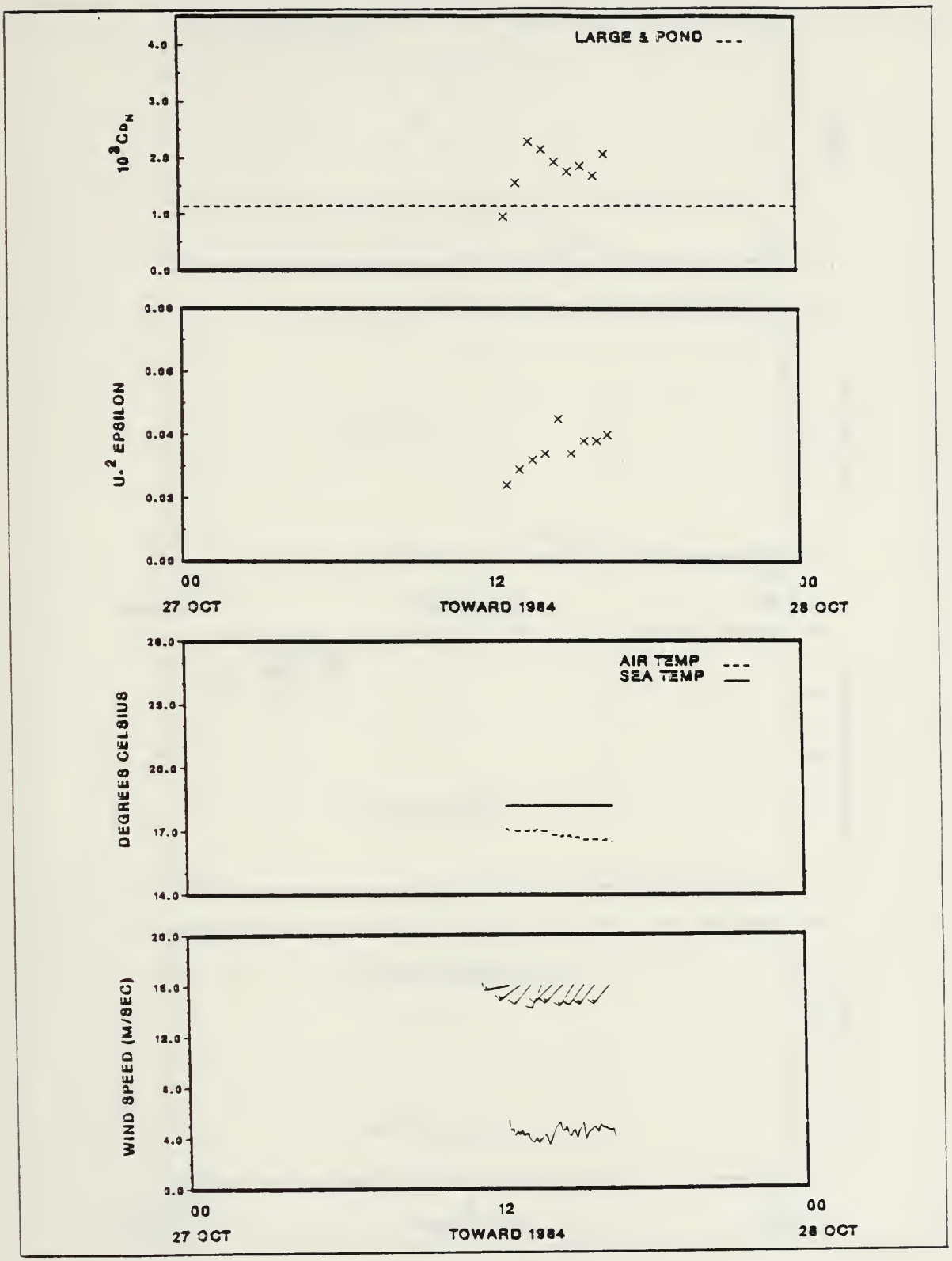

Figure A.12 27 October 1984.

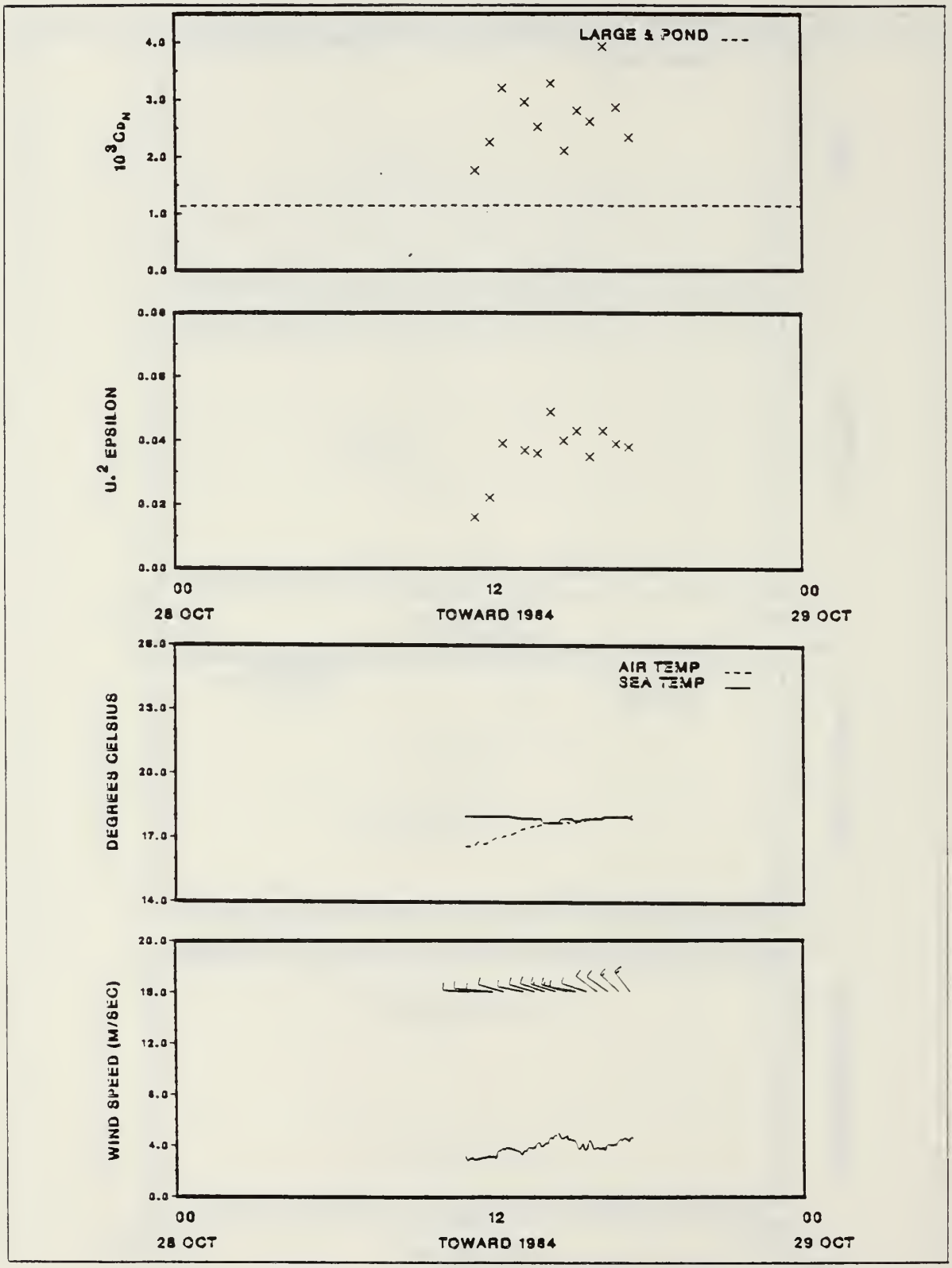

Figure A.13 28 October 1984.

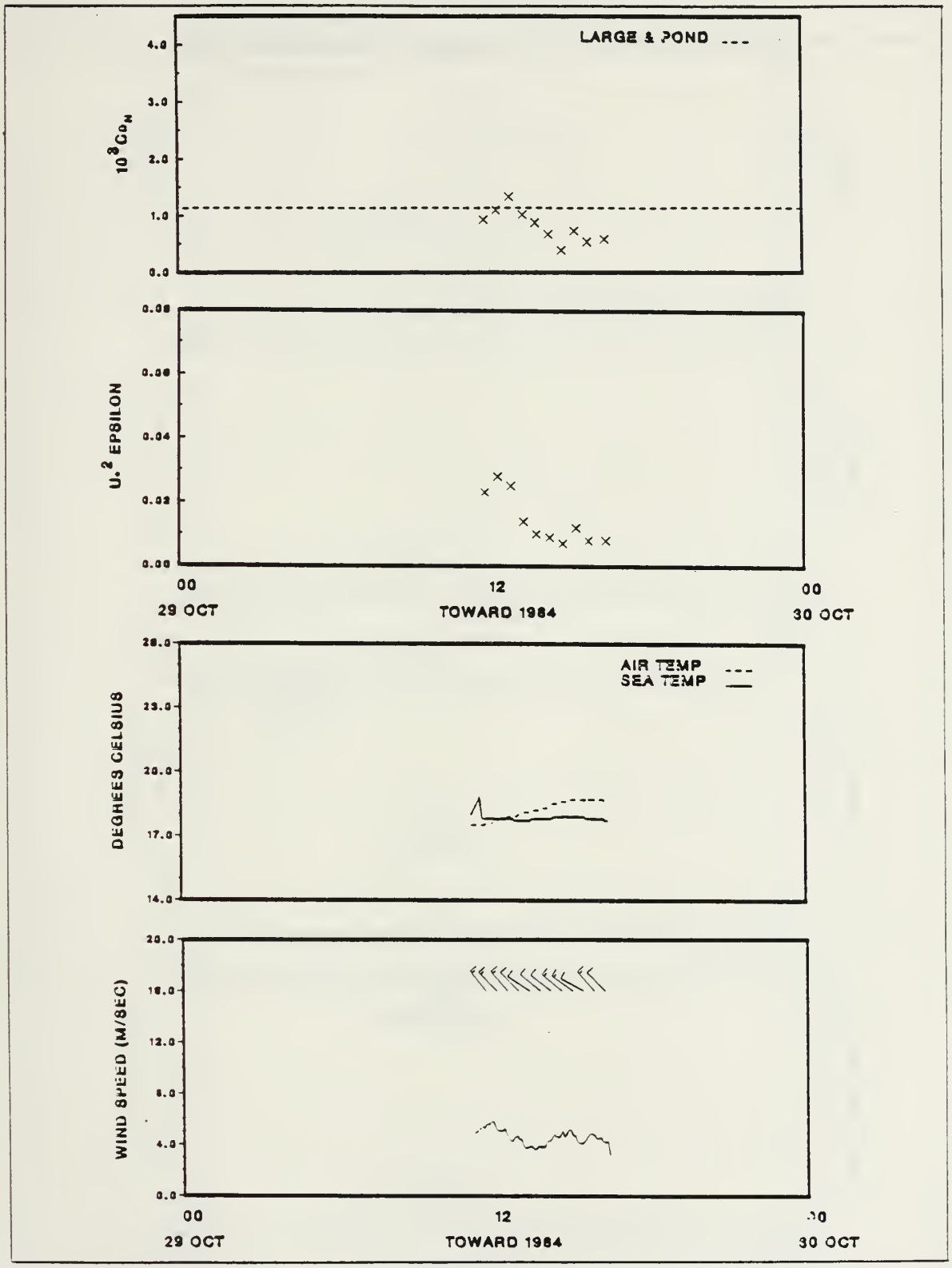

Figure A.14 29 October 1984.

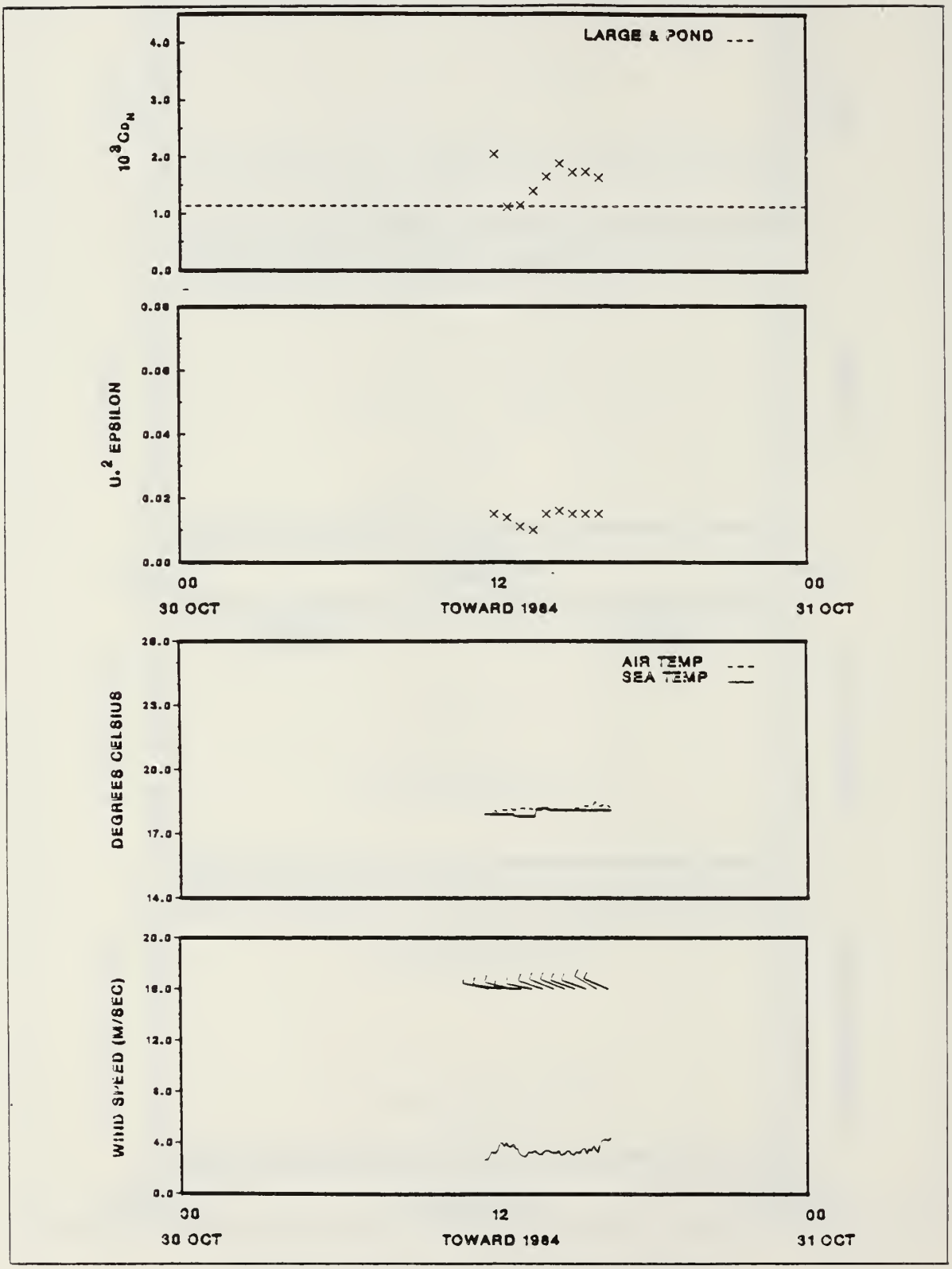

Figure A.15 30 October 1984.

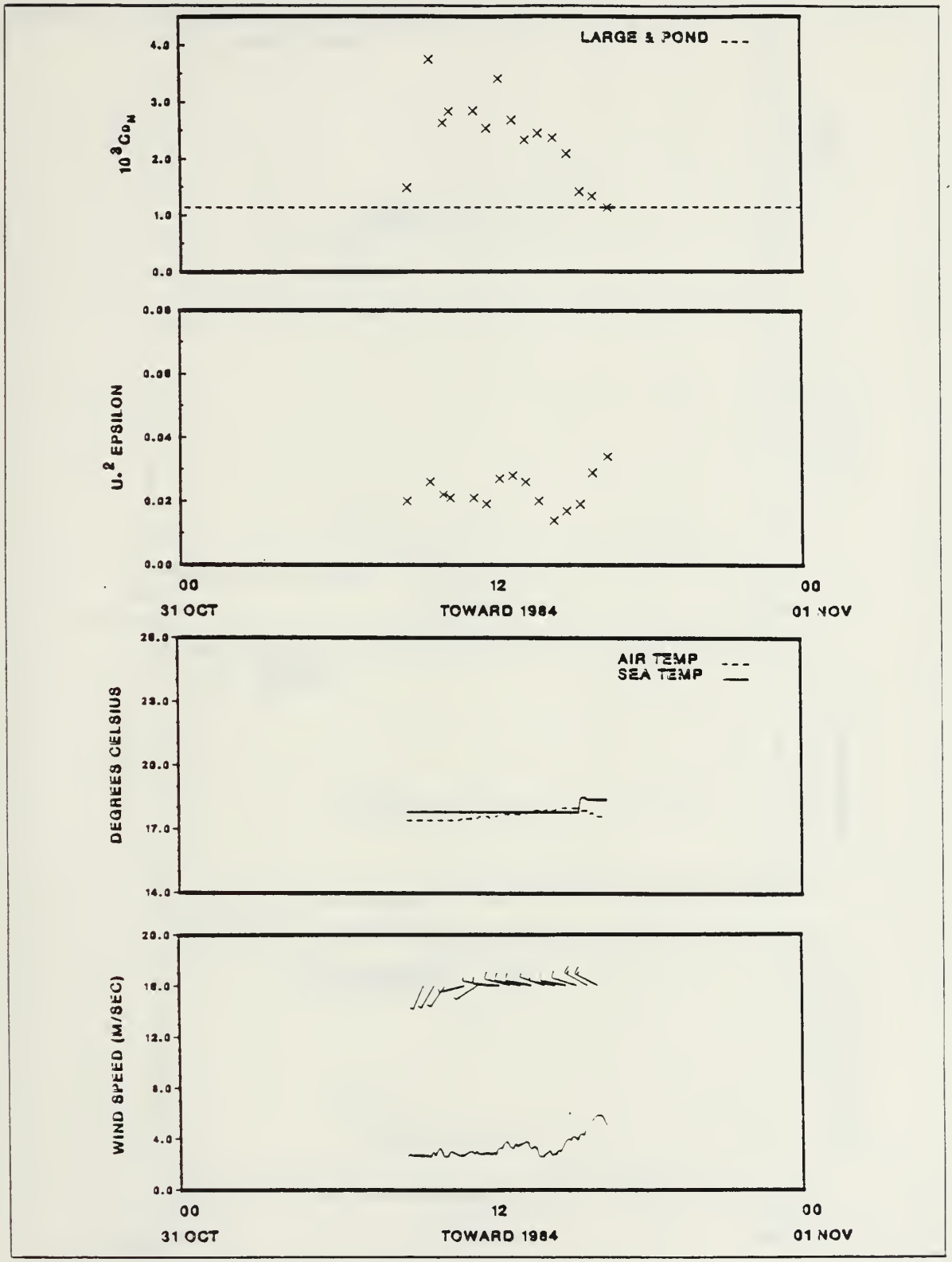

Figure A.16 31 October 1984.

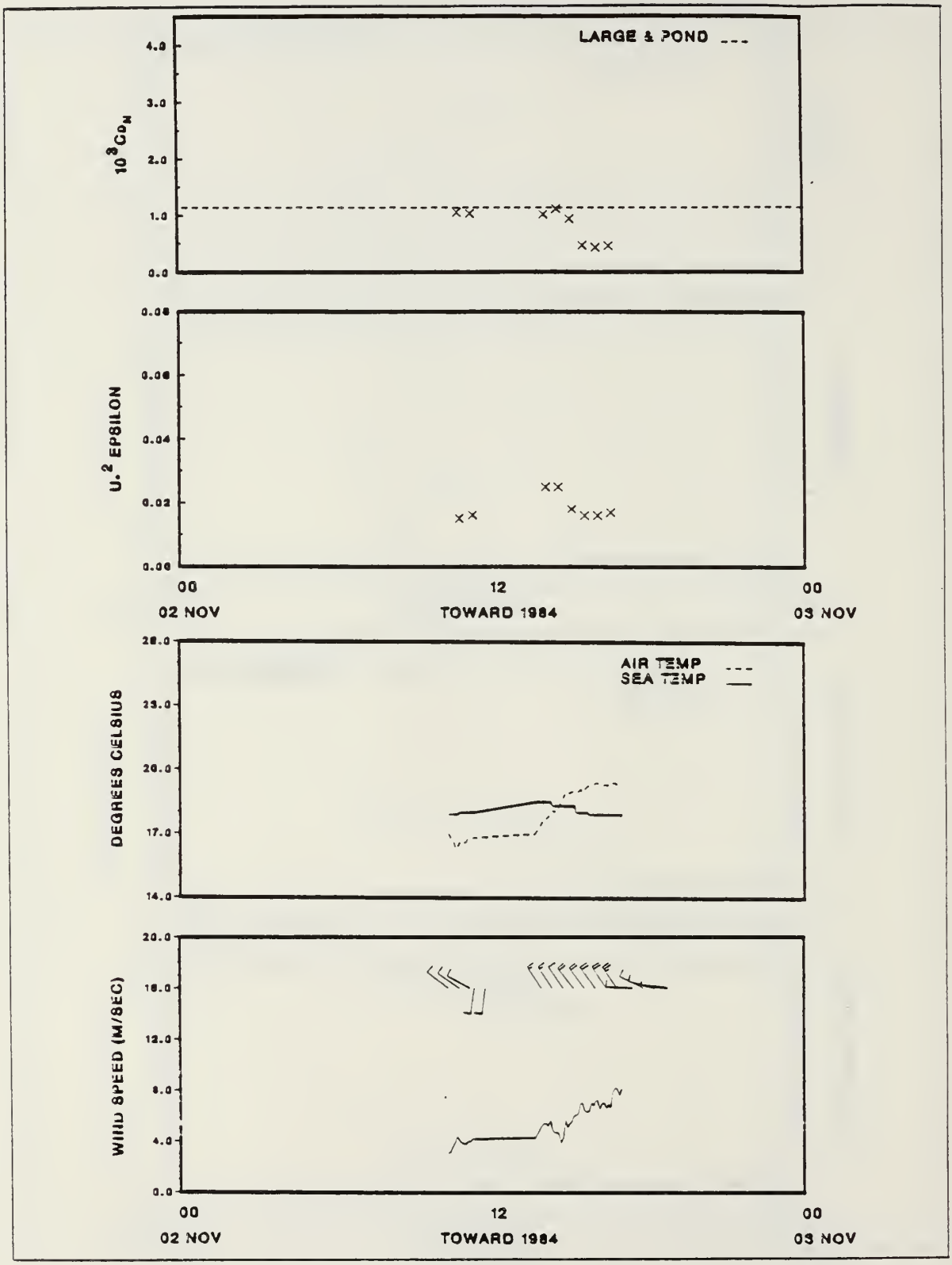

Figure A.17 2 November 1984.

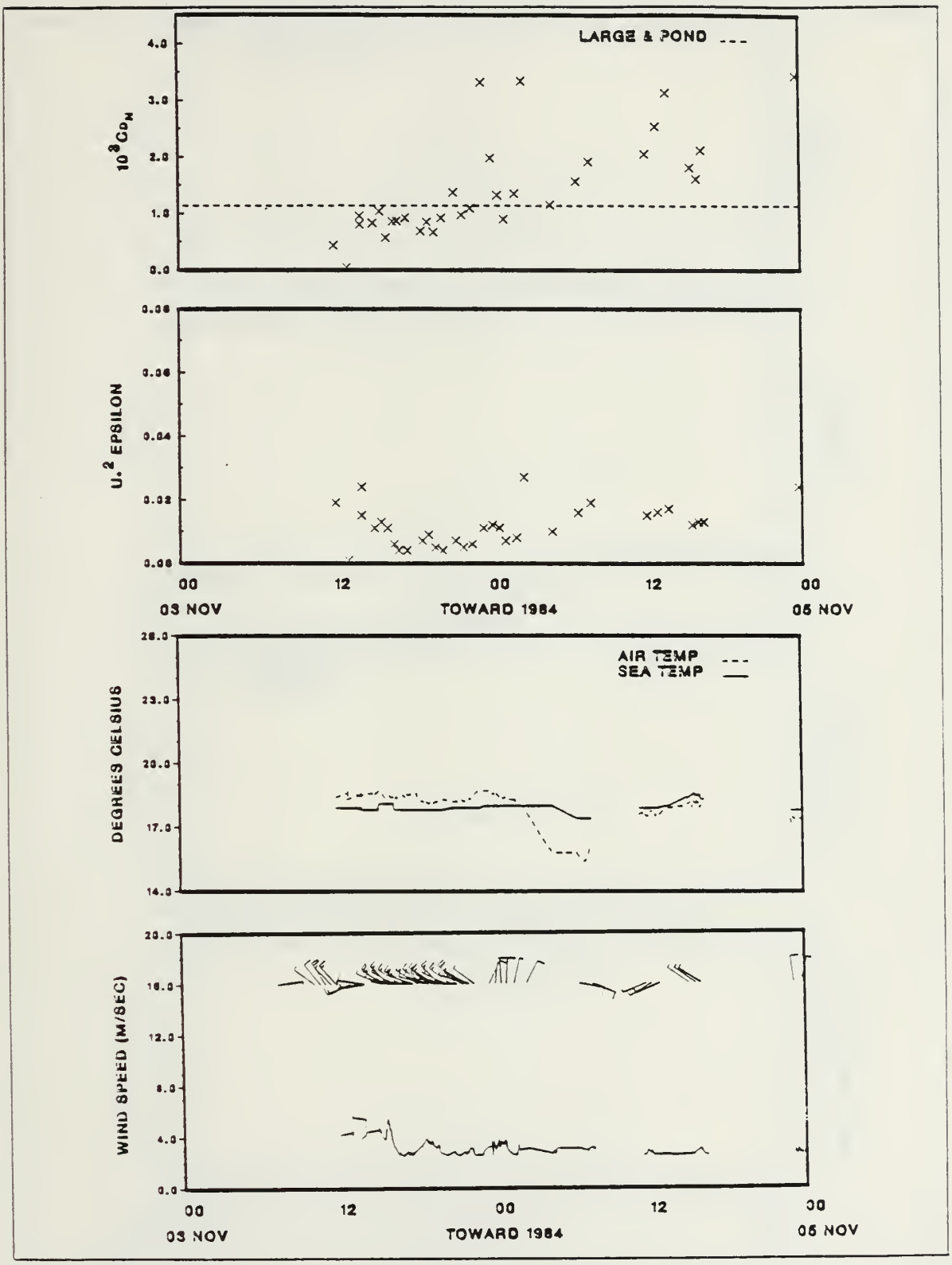

Figure A.18 3 to 5 November 1984.

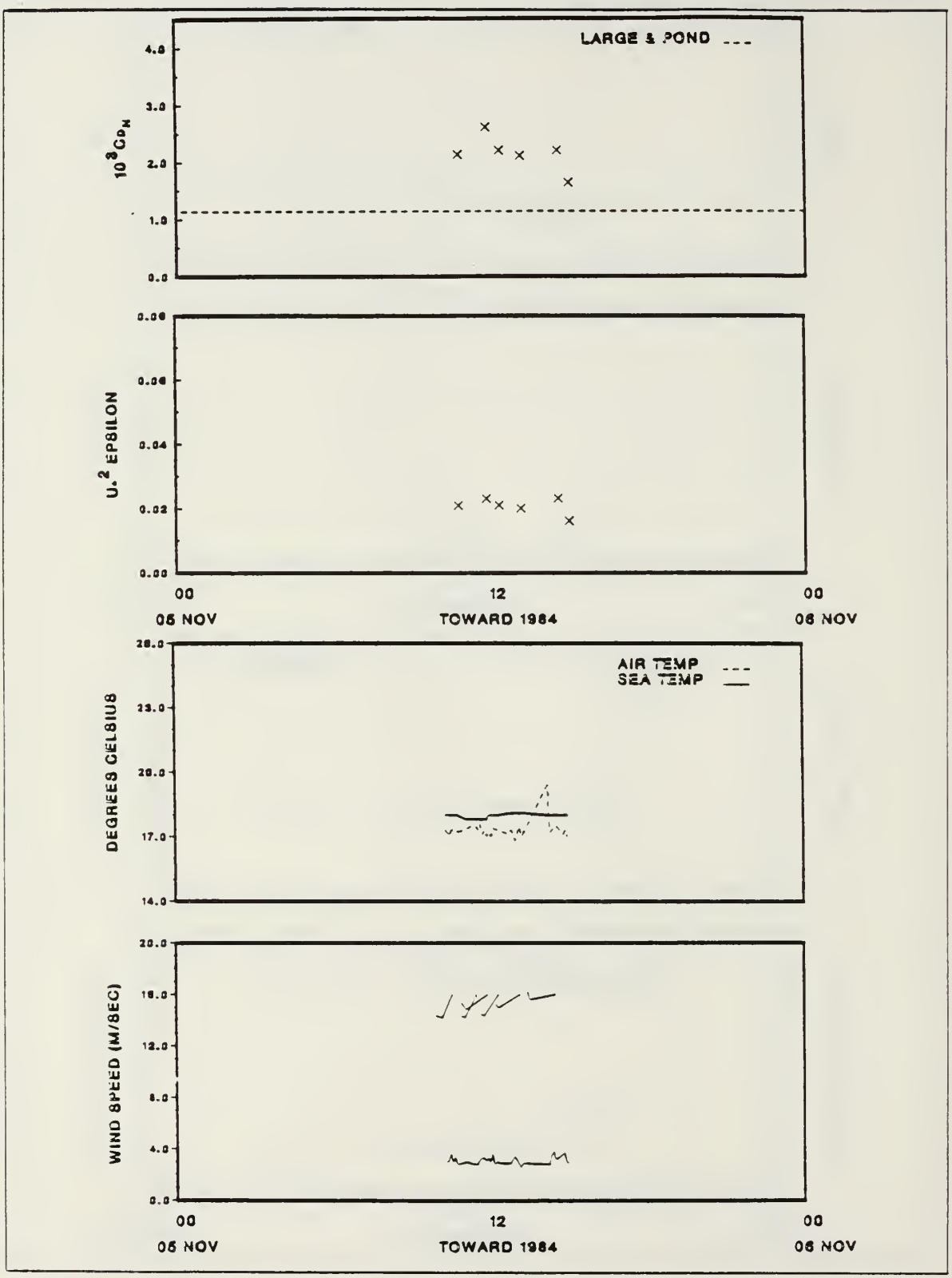

Figure A.19 5 November 1984.

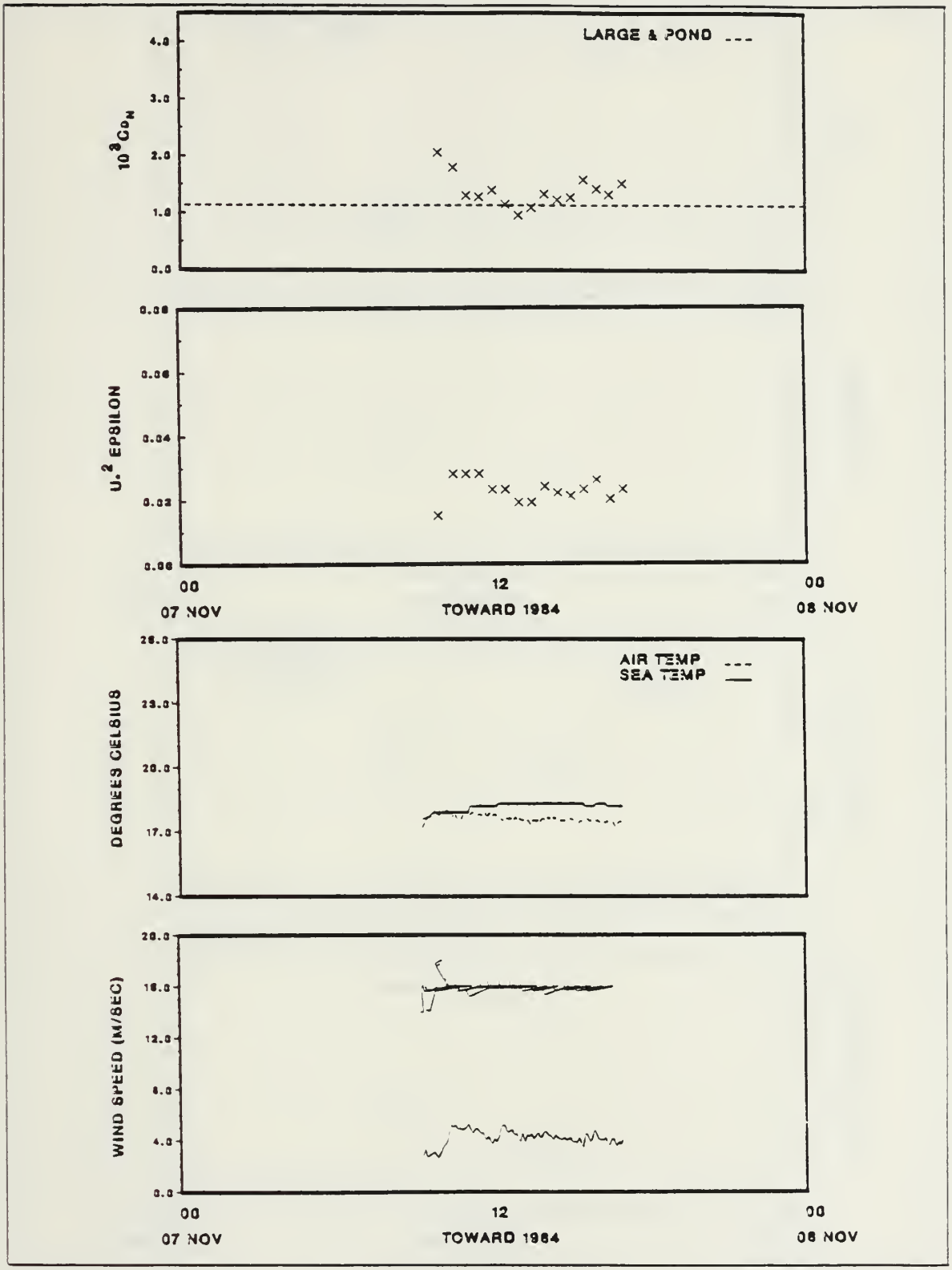

Figure A.20 7 November 1984.

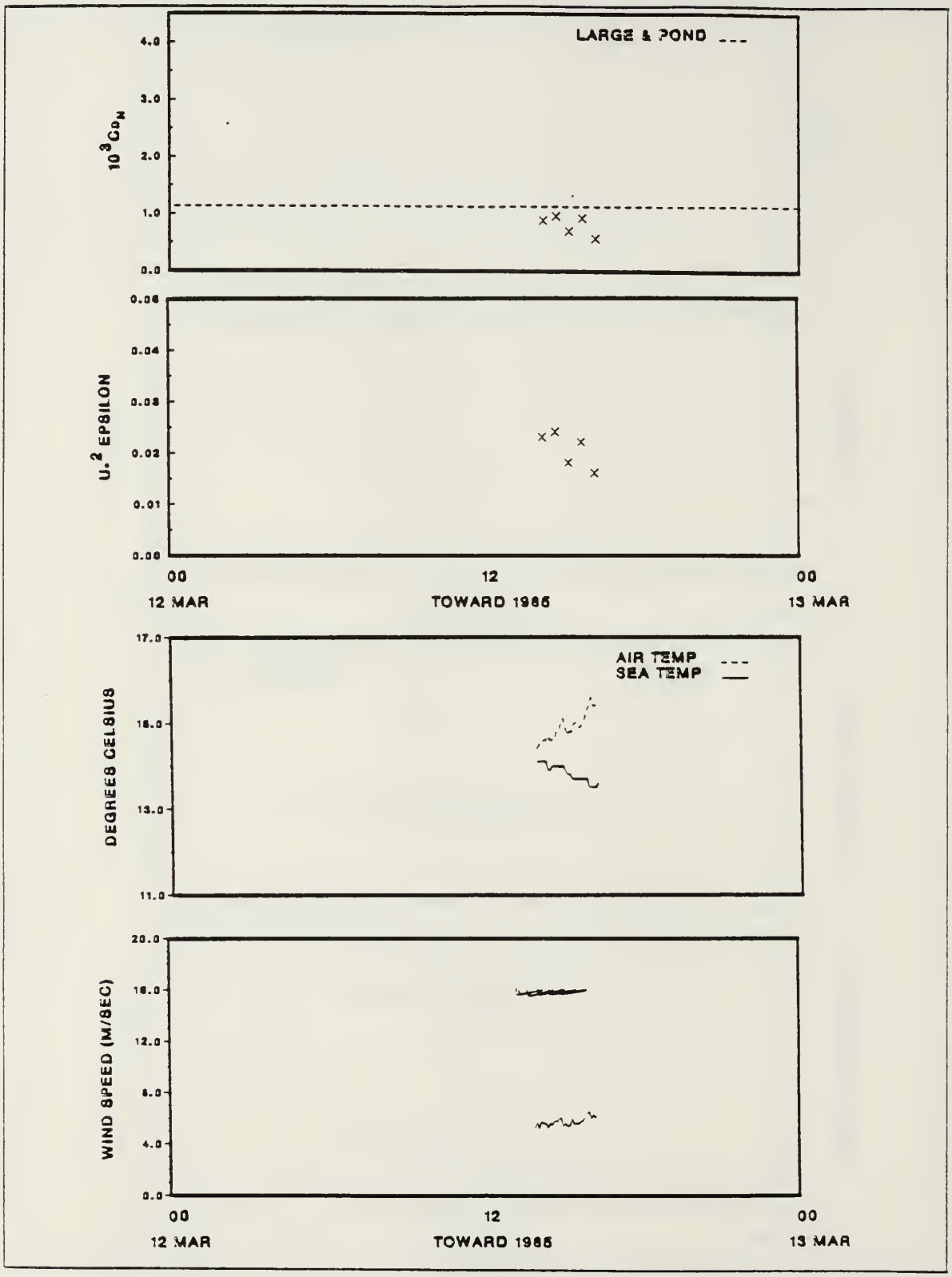

Figure A.21 12 March 1985.

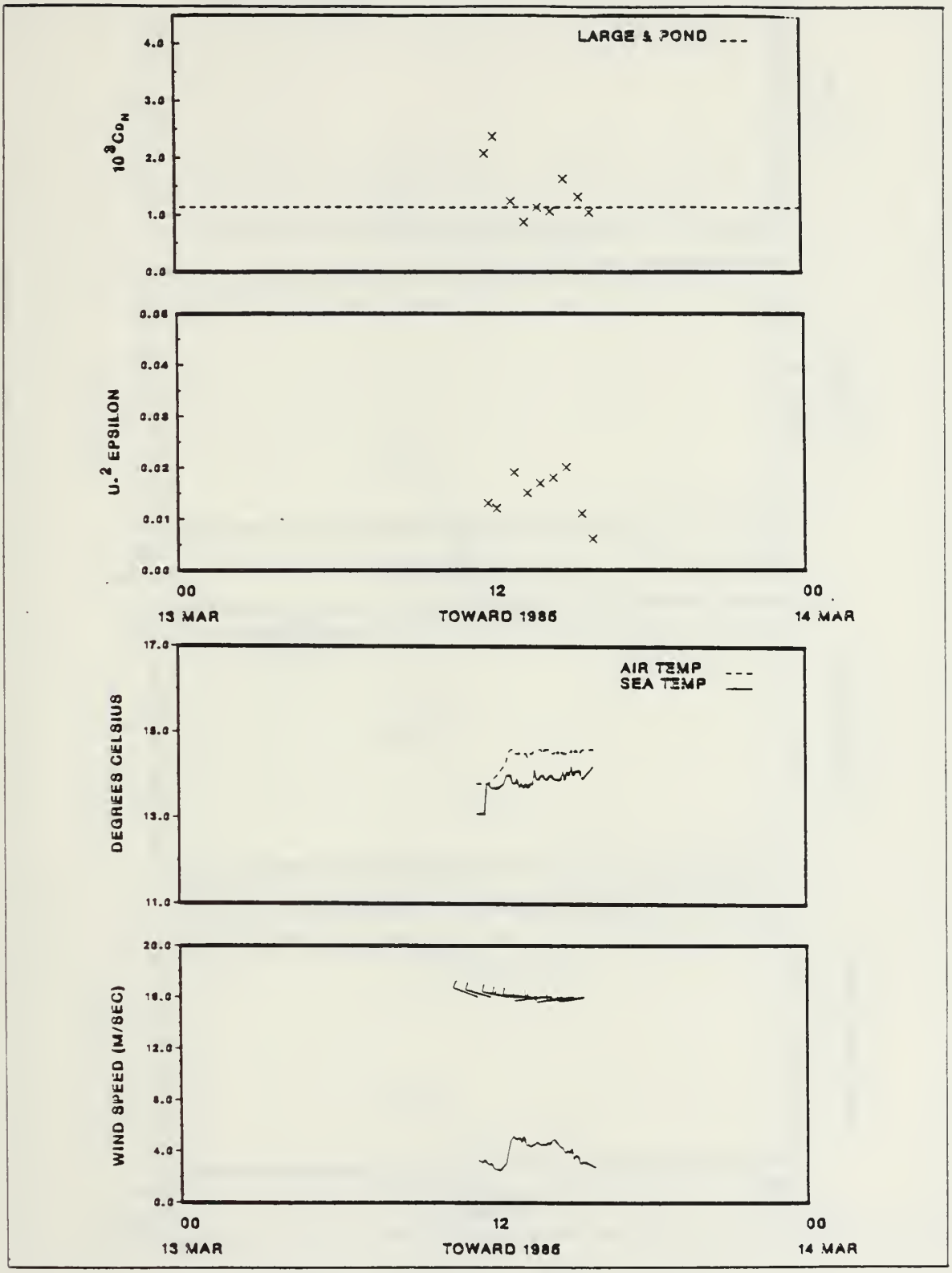

Figure A.22 13 March 1985.

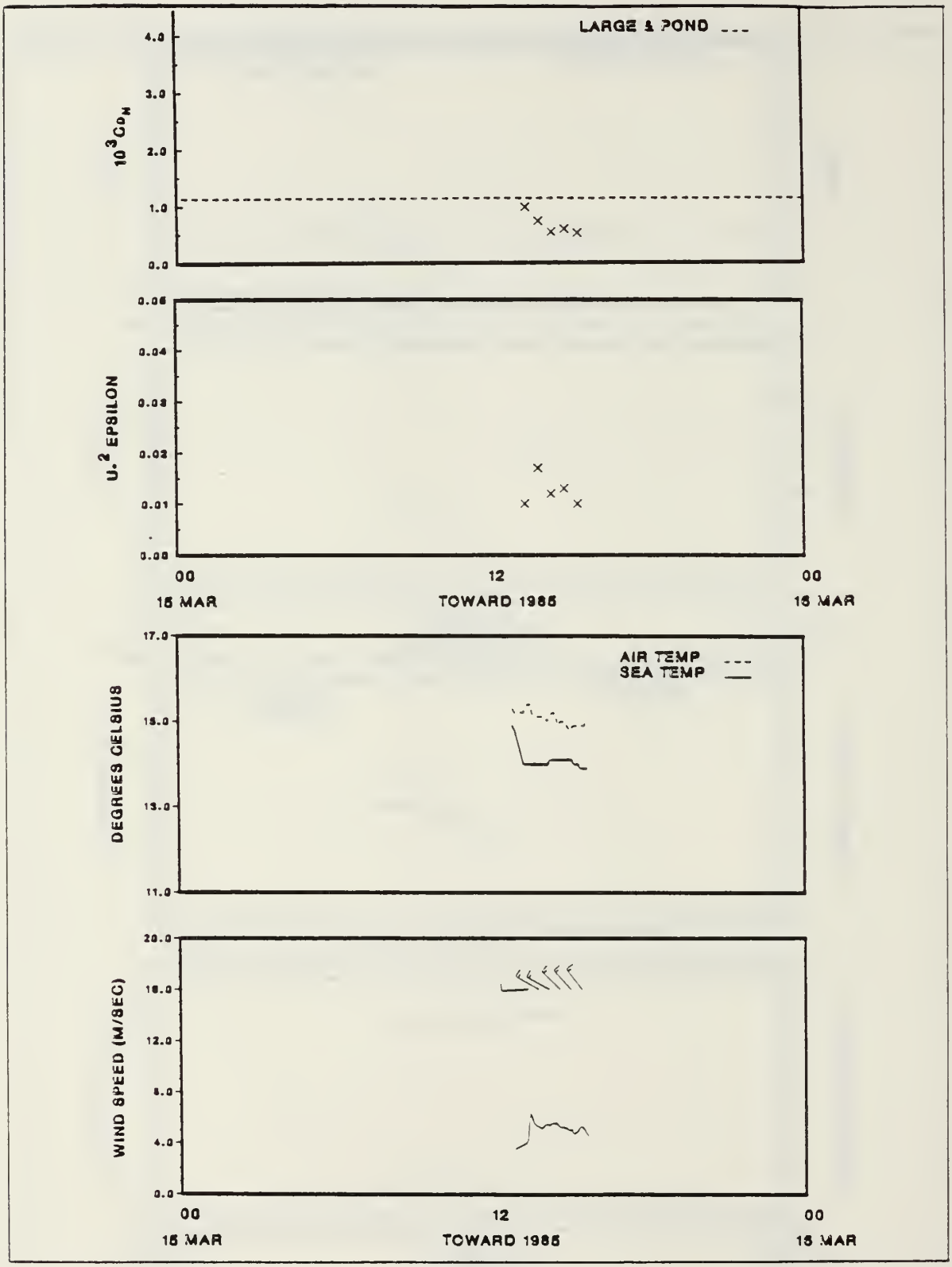

Figure A.23 15 March 1985.

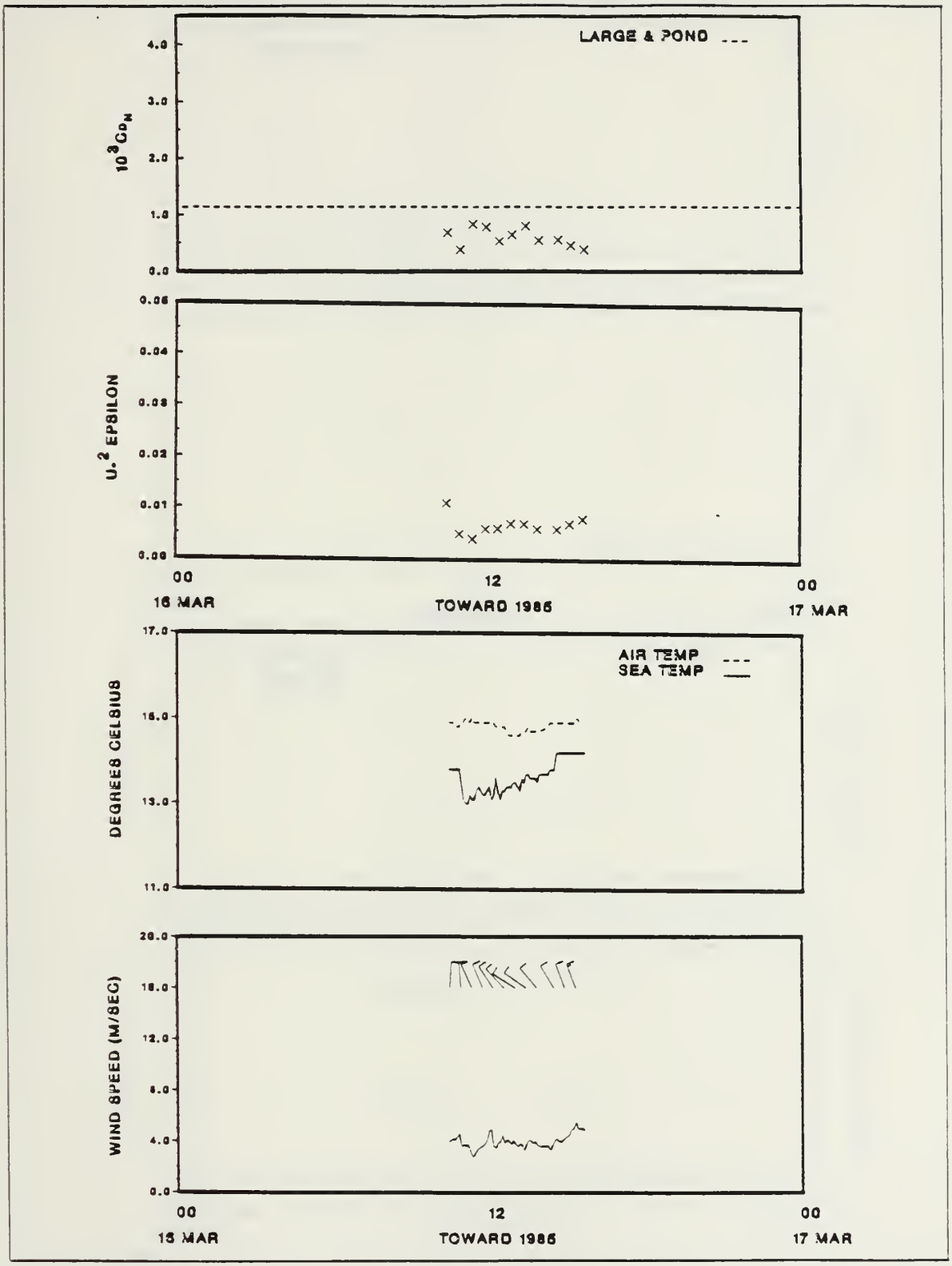

Figure A.24 16 March 1985.

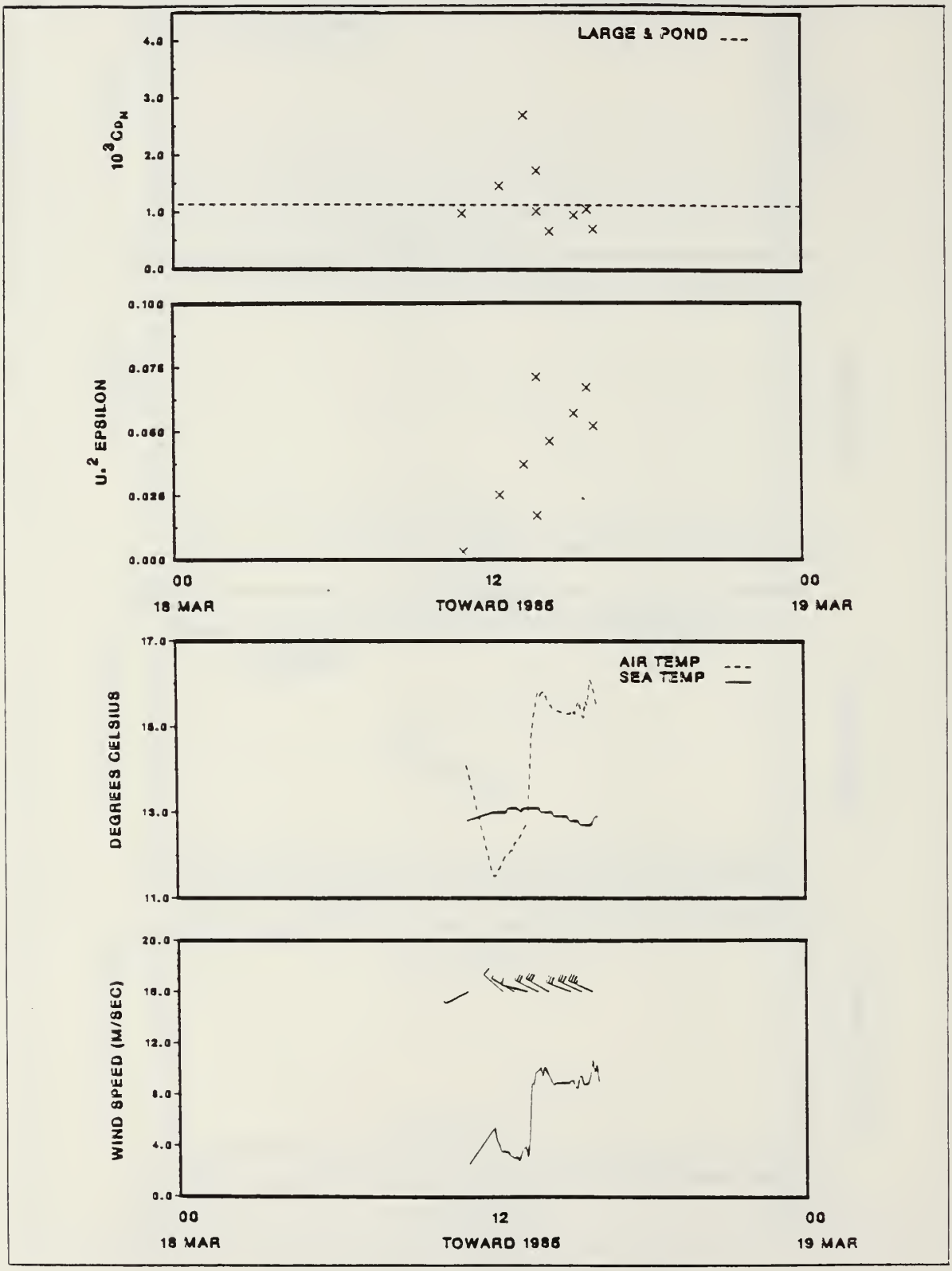

Figure A.25 18 March 1985.

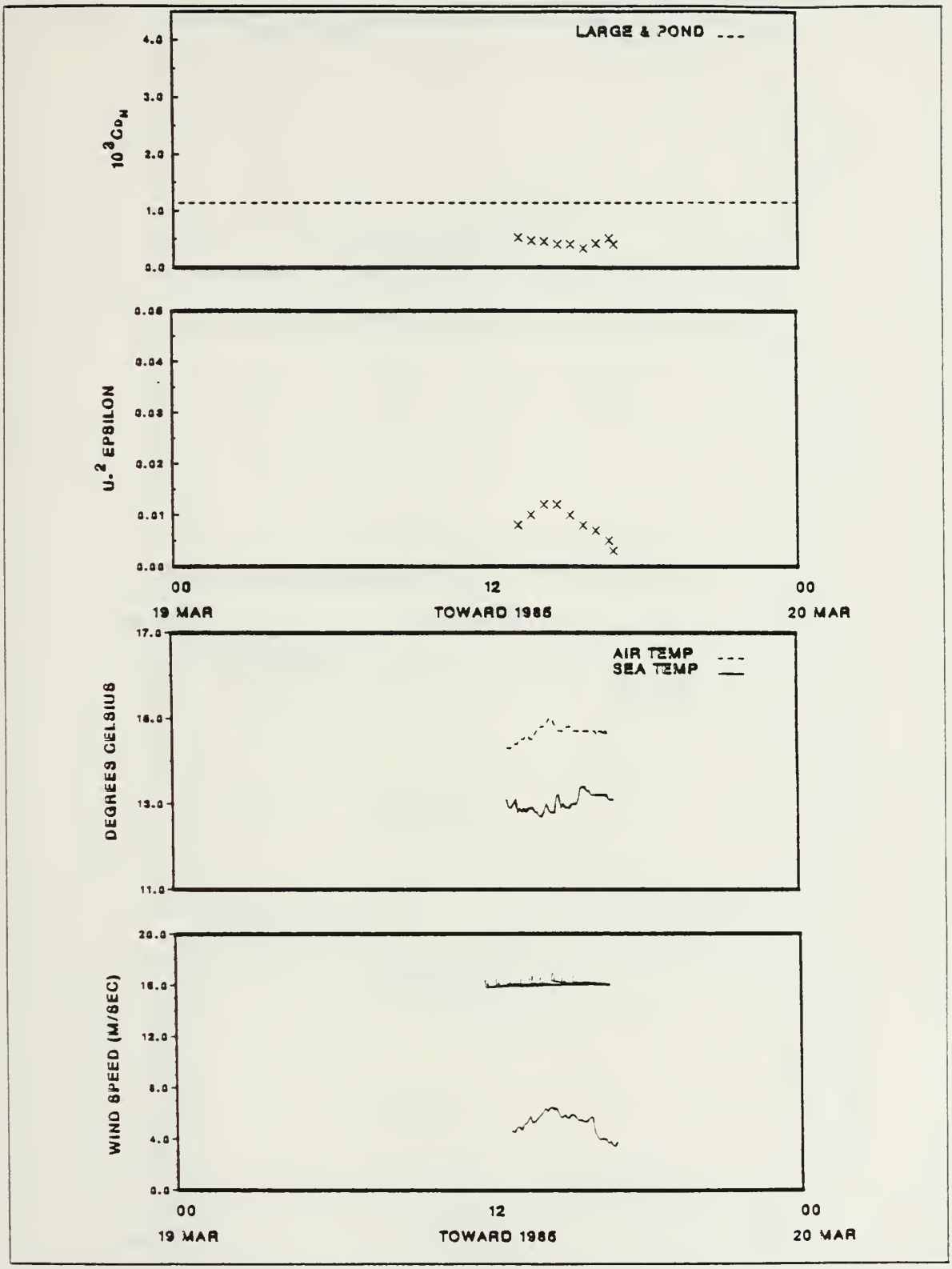

Figure A.26 19 March 1985.

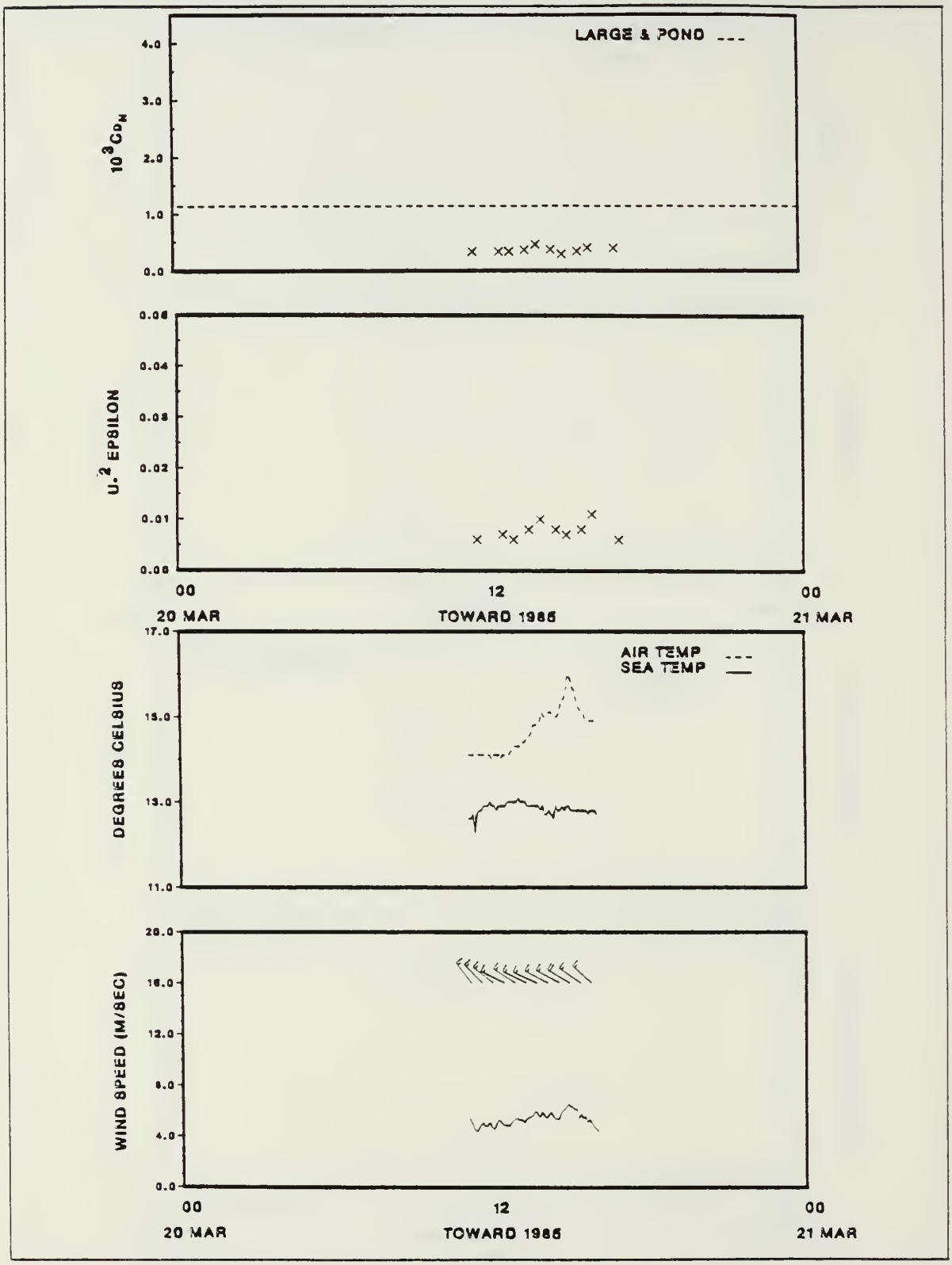

Figure A.27 20 March 1985.

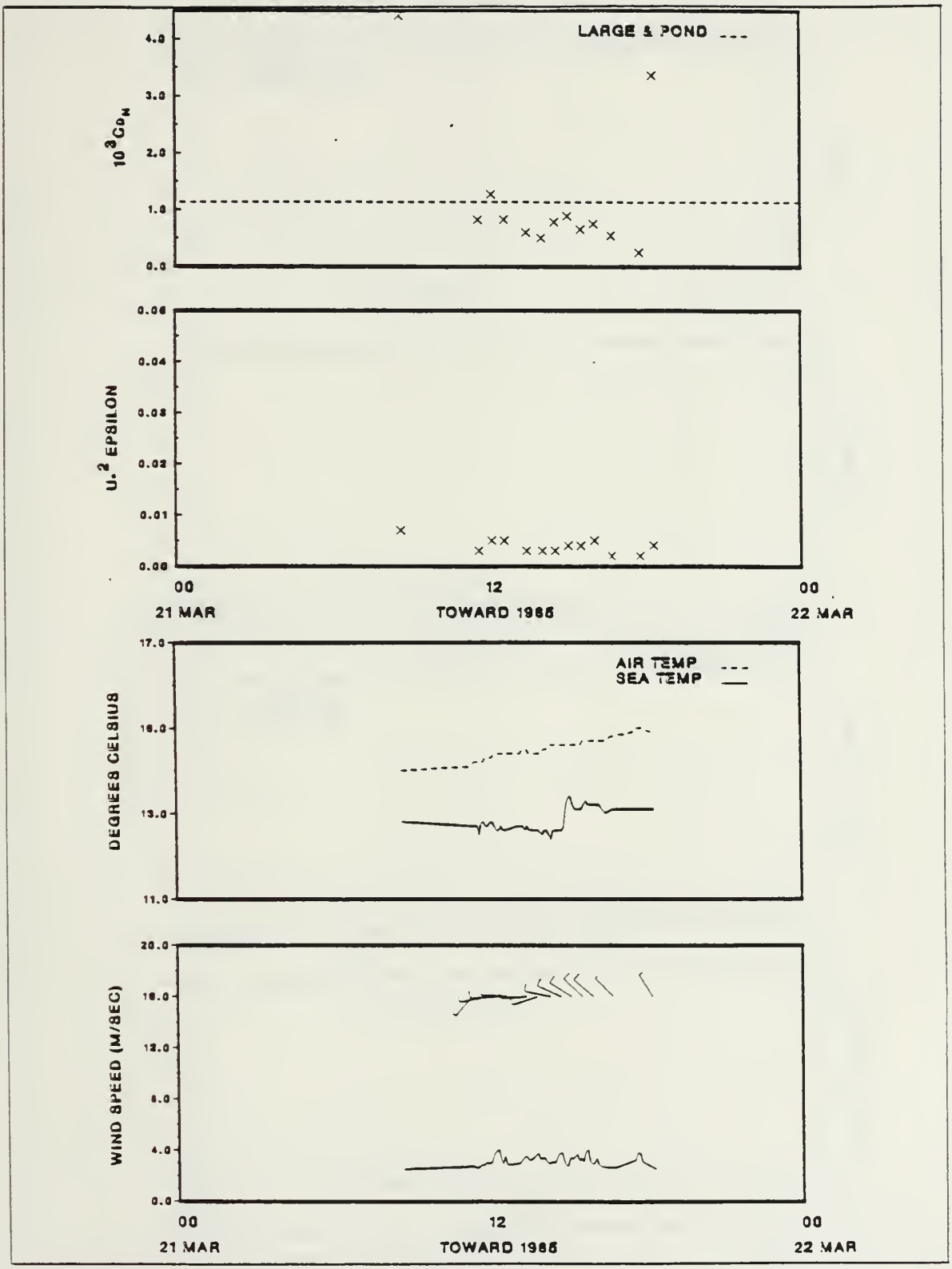

Figure A.28 21 March 1985.

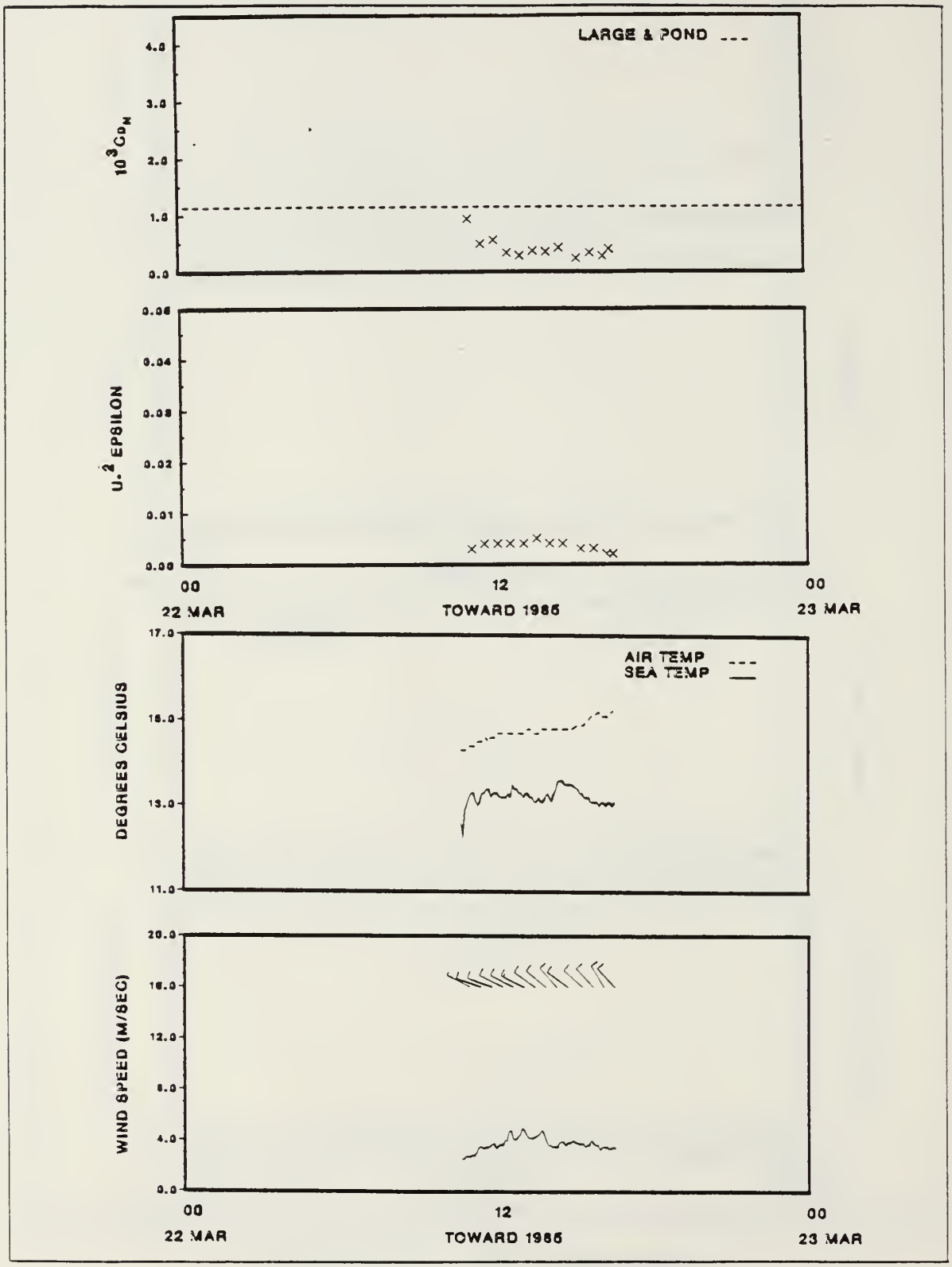

Figure A.29 22 March 1985.

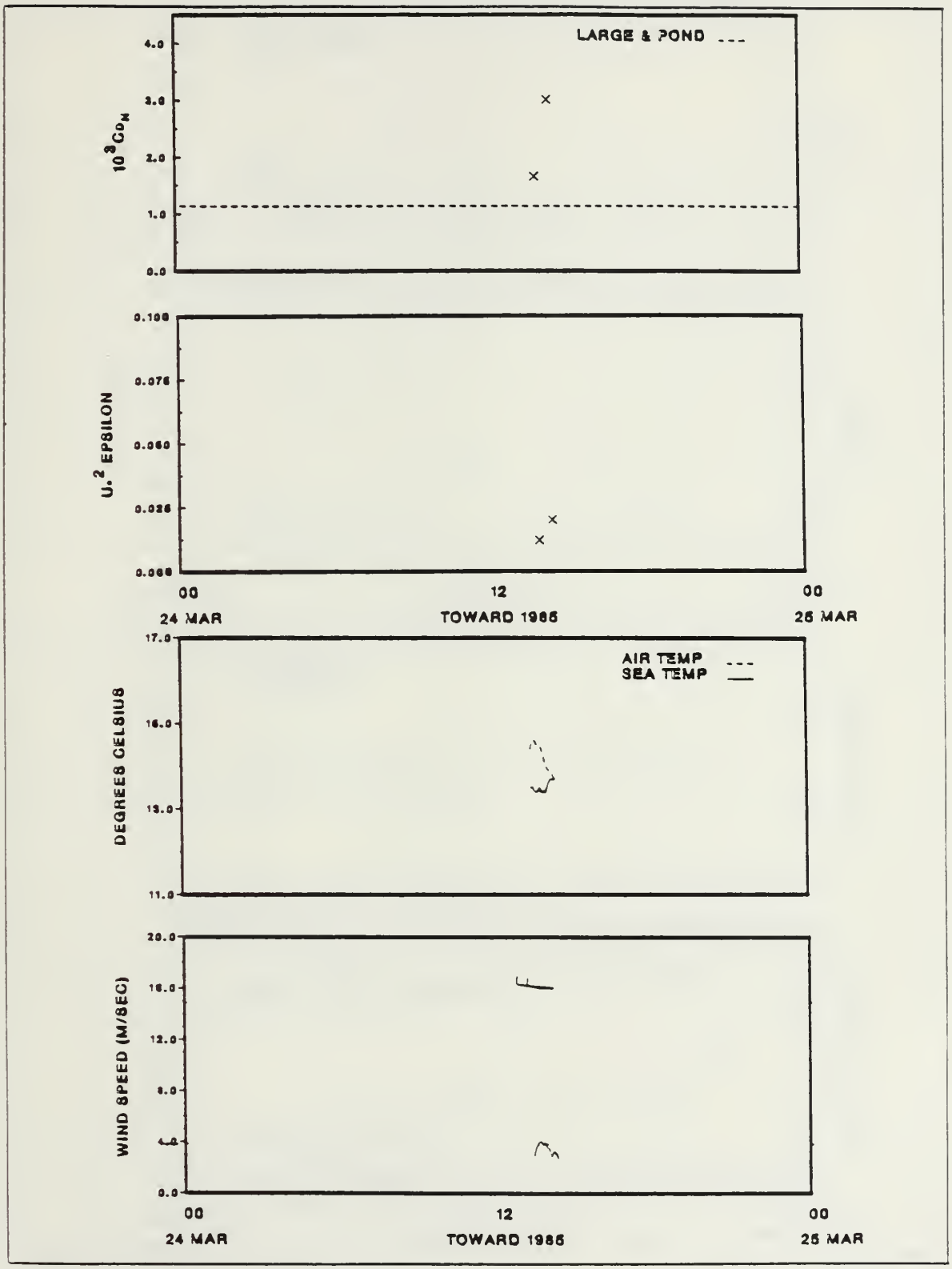

Figure A.30 24 March 1985.

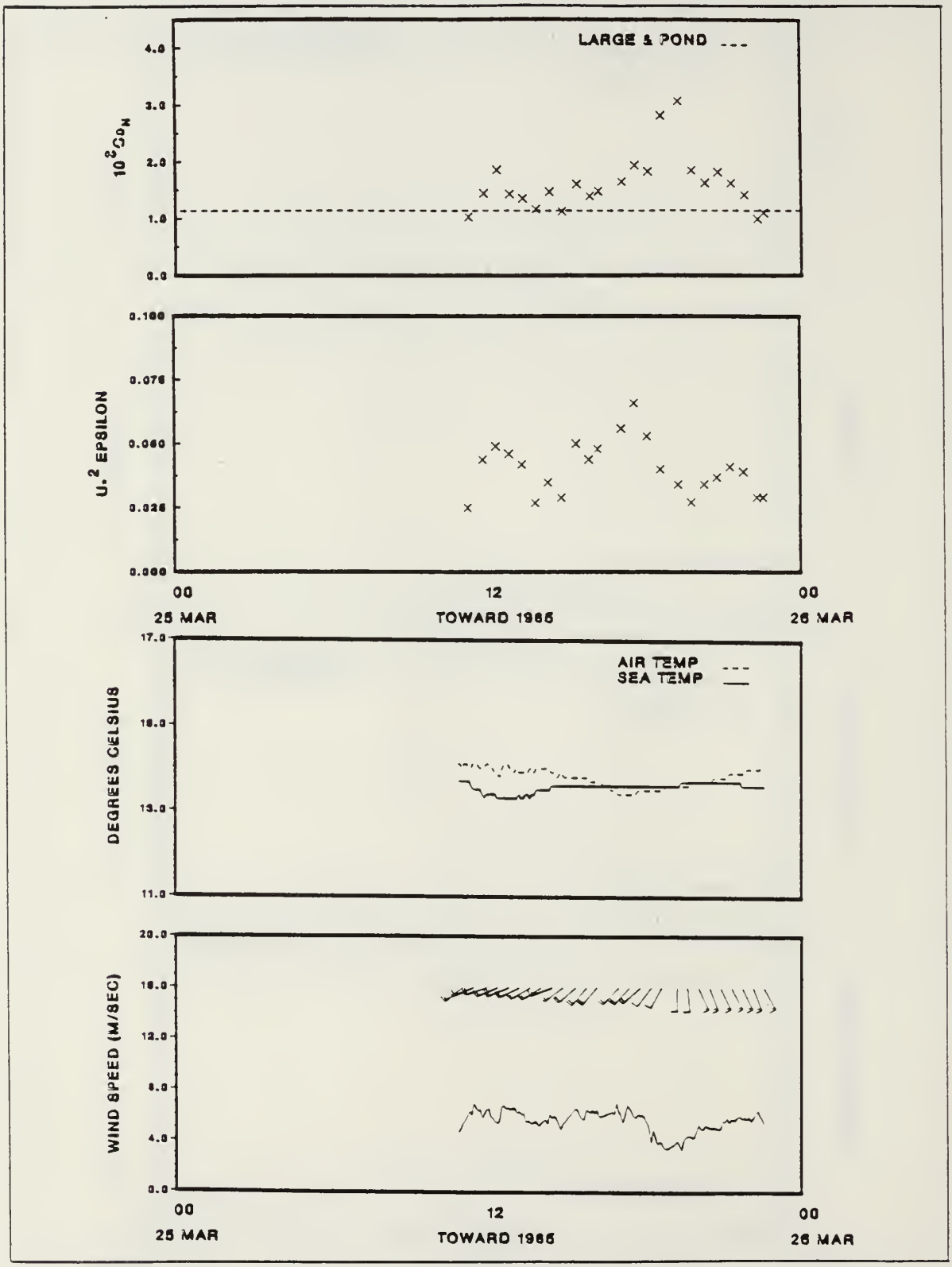

Figure A.31 25 March 1985.

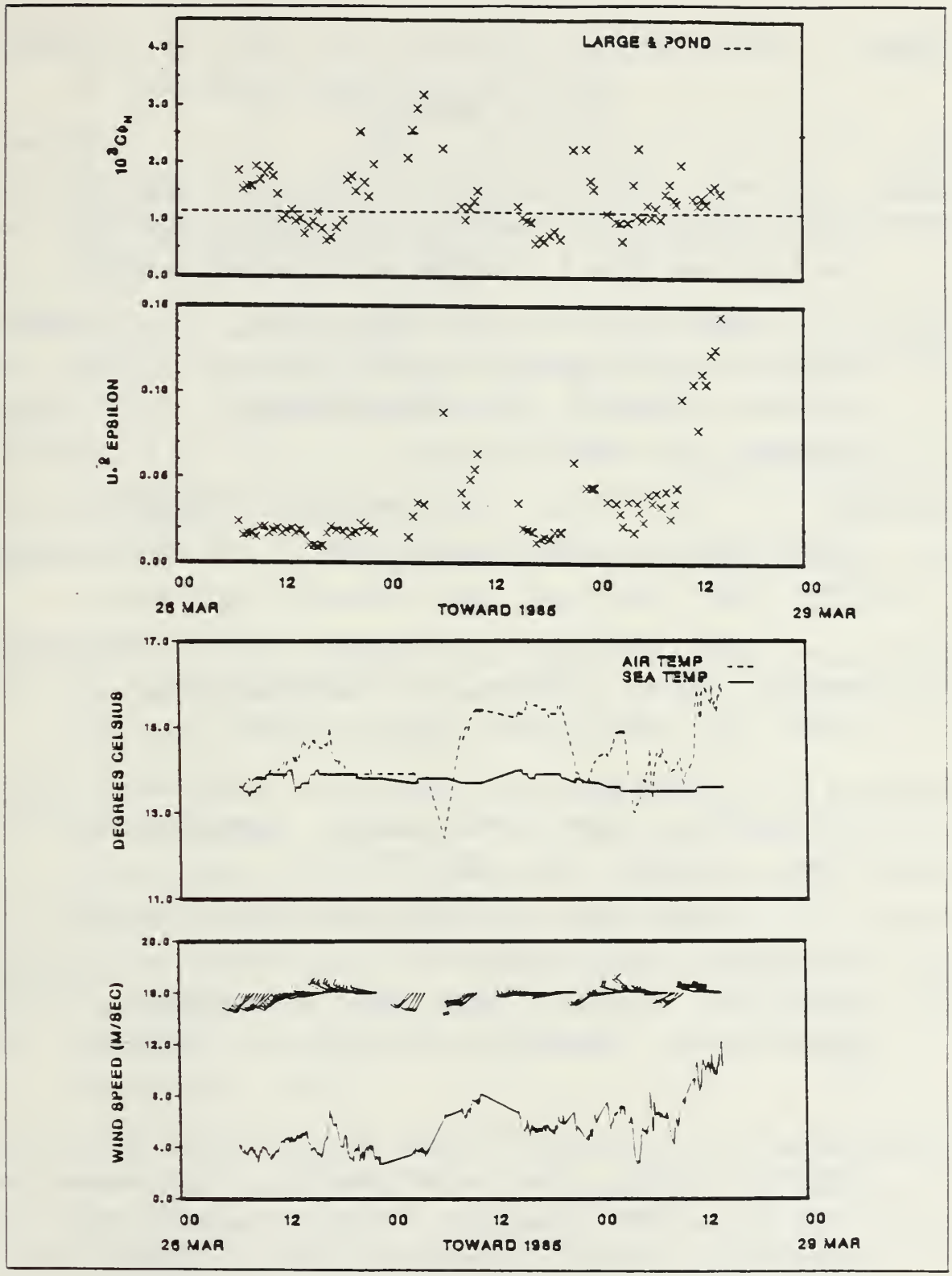

Figure A.32 26 to 29 March 1985.

LIST OF REFERENCES

Blanc, T. V., 1981: Report on analysis of the May 1979 marine surface layer micrometeorological experiment at San Nicholas Island, California. NRL Report 8363.

_____, 1985: Variation of bulk derived surface flux, stability and roughness results due to the use of different transfer coefficient schemes. J. Phys. Oceanogr., 15, 650-669.

Businger, J. A., 1972: The atmospheric boundary layer. Remote Sensing in the Troposphere, V. E. Derr, Ed., NOAA, 51 pp.

_____, 1973: Turbulent transfers in the atmospheric surface layer. Workshop on Micrometeorology, D. H. Haugen, Ed., Amer. Meteor. Soc., 392 pp.

_____, J. C. Wyngaard, Y. Izumi and E. F. Bradley, 1971: Flux profile relationships in the atmospheric surface layer. J. Atmos. Sci., 28, 181-189.

Byrne, H. M., 1982: The variation of the drag coefficient in the marine surface layer due to temporal and spatial variations in the wind and sea state, Ph.D. dissertation, University of Washington, Seattle, 126 pp.

Champagne, F. H., C. A. Friehe, J. C. LaRue and J. C. Wyngaard, 1977: Flux measurements, flux estimation techniques, and fine-scale turbulence measurements in the unstable surface layer over land. J. Atmos. Sci., 34, 515-530.

Charnock, H., 1955: Wind stress on a water surface. Quart. J. Roy. Meteor. Soc., 81, 639-640.

Davidson, K. L., 1974: Observational results on the influence of stability and wind-wave coupling on the momentum transfer and turbulent fluctuations over ocean waves. Bound.-Layer Meteor., 6, 305-331.

Denman, K. L. and M. Miyake, 1973: Behavior of the mean wind, drag coefficient and the wave field in the open ocean. J. Geophys. Res., 78, 1917-1931.

Fleagle, R. W. and J. A. Businger, 1980: An Introduction to Atmospheric Physics, 2nd ed., Academic Press, 432 pp.

Garratt, J. R., 1977: Review of drag coefficients over oceans and continents, Mon. Wea. Rev., 105: 915-929.

Geernaert, G. L., 1983: Variation of the drag coefficient and its dependence on sea state, Ph.D. dissertation, University of Washington, Seattle, 186 pp.

_____, 1985a: A model for the drag coefficient based on environmental parameters for the near coastal zone. Unpublished report: Department of Meteorology, Naval Postgraduate School, Monterey, California, 93943.

_____, 1985b: On the derivation of the neutral drag coefficient. Unpublished report: Department of Meteorology, Naval Postgraduate School, Monterey, California, 93943.

_____, K. L. Katsaros and K. Richter, 1985: Variation of the drag coefficient and its dependence on sea state. Unpublished report: Department of Meteorology, Naval Postgraduate School, Monterey, California, 93943.

Haltiner, G. J. and R. T. Williams, 1980: Numerical Prediction and Dynamic Meteorology, 2nd ed., John Wiley and Sons, 477 pp.

Hess, S. L, 1979: Introduction to Theoretical Meteorology, 2nd ed., Robert E. Krieger Publishing Co., 362 pp.

Hicks, B. B., 1972: Some evaluations of drag and bulk transfer coefficients over water bodies of different sizes. Bound.-Layer Meteor., 3, 201-213.

Holton, J. R. 1979: An Introduction to Dynamic Meteorology, 2nd ed., Academic Press, 388 pp.

Hsu, S. A., 1974: A dynamic roughness equation and its application to wind stress determination at the air-sea interface. J. Phys. Oceanogr., 4, 116-120.

_____, 1985: A mechanism for the increase of wind stress (drag) coefficients with wind speed over water surfaces: A parametric model. Unpublished report: Coastal Studies Institute, Louisiana State University, Baton Rouge, 70803, 9 pp.

Kitaigorodskii, S. A., 1973: The Physics of Air-Sea Interaction, Israel Program for Scientific Translations, 415 pp.

Kraus, E. B., 1972: Atmosphere Ocean Interaction, Oxford University Press, 275 pp.

Large, W. G. and S. Pond, 1981: Open ocean momentum flux measurements in moderate to strong winds. J. Phys. Oceanogr., 11 324-336.

Lo, A. K. and G. A. McBean, 1978: On the relative errors in methods of flux calculations. J. Appl. Meteor., 17 1704-1711.

Monin, A. S. and A. M. Obukhov, 1954: Basic laws of turbulent mixing in the ground layer of the atmosphere. Trans. Geophys. Inst. Akad., 151, 163-187.

National Oceanic and Atmospheric Administration, 1983: Local Climatological Data: Annual Summaries for 1982, Part I.

Panofsky, H. A. and J. A. Dutton, 1984: Atmospheric Turbulence, John Wiley and Sons, 397 pp.

Paulson, C. A., 1970: The mathematical representation of windspeed and temperature profiles in the unstable atmospheric surface layer. J. Appl. Meteor., 9, 857-861.

Phillips, O. M., 1980: The Dynamics of the Upper Ocean, Cambridge University Press, 398 pp.

Roll, H. U., 1965: Physics of the Marine Atmosphere, Academic Press, 426 pp.

Schacher, G. E., K. L. Davidson, T. Houlihan and C. W. Fairall, 1981: Measurements of the rate of dissipation of turbulent kinetic energy over the ocean. Bound.-Layer Meteor., 20, 321-330 pp.

Smith, S. D., 1980: Wind stress and heat flux over the ocean in gale force winds. J. Phys. Oceanogr., 10, 709-726.

Wu, J., 1985: Parameterization of wind stress coefficients over water surfaces: Unpublished report, College of Marine Studies, University of Delaware, Newark, 19716, 15 pp.

Wyngaard, J. C. and O. R. Cote', 1971: The budgets of turbulent kinetic energy and temperature variance in the atmospheric surface layer. J. Atmos. Sci., 28, 190-201.

Yaglom, A. M., 1977: Comments on wind and temperature flux-profile relationships. Bound.-Layer Meteor., 11, 89-102.

INITIAL DISTRIBUTION LIST

		No. Copies
1.	Defense Technical Information Center Cameron Station Alexandria, VA 22304-6145	2
2.	Library, Code 0142 Naval Postgraduate School Monterey, CA 93943-5100	2
3.	Professor R.J. Renard, Code 63Rd Naval Postgraduate School Monterey, CA 93943-5100	1
4.	Professor C.N.K. Mooers, Code 68Mr Naval Postgraduate School Monterey, CA 93943-5100	1
5.	Professor K.L. Davidson, Code 63Ds Naval Postgraduate School Monterey, CA 93943-5100	5
6.	Director Naval Oceanography Division Naval Observatory 24TH and Massachusetts Ave., NW Washington, D.C. 20390	1
7.	Commander Naval Oceanography Command NSTL Station Bay St. Louis, MS 39522	1
8.	Commanding Officer Naval Oceanographic Office NSTL Station Bay St. Louis, MS 39522	1
9.	Commanding Officer Fleet Numerical Oceanography Center Monterey, CA 93940	1
10.	Commanding Officer Naval Ocean Research and Development Activity NSTL Station Bay St. Louis, MS 39522	1
11.	Commanding Officer Naval Environmental Prediction Research Facility Monterey, CA 93940	1
12.	Chairman Meteorology Department U.S. Naval Academy Anapolis, MD 21402	1
13.	Chief of Naval Research 800 N. Quincy Street Arlington, VA 22217	1

14. Office of Naval Research (Code 480) 1
Naval Oceanography Research and Development Activity
NSTL Station
Bay St. Louis, MS 39522

15. Scientific Liaison Office 1
Office of Naval Research
Scripps Institute of Oceanography
La Jolla, CA 92037

16. Dr. G.L. Geernaert 2
Space Sensing
Naval Research Laboratory
Washington, D.C. 20390

17. Dr. Torben Mikkelsen, Code 63Ds 1
Naval Postgraduate School
Monterey, CA 93943-5100

18. Stephan Borrmann, Code 63Ds 1
Naval Postgraduate School
Monterey, CA 93943-5100

19. LCDR Beverly J. Byars 2
Naval Oceanography Command Center, Guam
COMNAVMARIANAS, Box 12
FPO San Francisco, 96630

216171

Thesis
B95193 Byars
c.1 Variation of the
drag coefficient with
wind and wave state.